DISCRIMINATING CLEAR-SKY FROM CLOUD WITH MODIS
ALGORITHM THEORETICAL BASIS DOCUMENT (MOD35)

MODIS Cloud Mask Team

Steve Ackerman[1], Kathleen Strabala[1], Paul Menzel[1,2], Richard Frey[1], Chris Moeller[1], Liam Gumley[1], Bryan Baum[3], Suzanne Wetzel Seemann[1], and Hong Zhang[1]

[1]Cooperative Institute for Meteorological Satellite Studies, University of Wisconsin - Madison

[2]NOAA/NESDIS

[3]NASA/LaRC, Hampton, VA

Version 5.0

October 2006

TABLE OF CONTENTS

APPENDIX A. EXAMPLE CODE FOR READING CLOUD MASK OUTPUT 100

1.0 Introduction

Clouds are generally characterized by higher reflectance and lower temperature than the underlying earth surface. As such, simple visible and infrared window threshold approaches offer considerable skill in cloud detection. However, there are many surface conditions when this characterization of clouds is inappropriate, most notably over snow and ice. Additionally, some cloud types such as thin cirrus, low stratus at night, and small cumulus are difficult to detect because of insufficient contrast with the surface radiance. Cloud edges cause further difficulty since the instrument field of view will not always be completely cloudy or clear.

The 36 channel Moderate Resolution Imaging Spectroradiometer (MODIS) offers the opportunity for multispectral approaches to cloud detection so that many of these concerns can be mitigated; additionally, spatial and temporal uniformity tests offer confirmation of cloudy or clear-sky conditions. This document describes the approach and algorithms for detecting clouds using MODIS observations, developed in collaboration with members of the MODIS Science Teams. The MODIS cloud screening approach includes new spectral techniques and incorporates many of the existing techniques to detect obstructed fields of view. Section 2 gives an overview of the masking approach. The individual spectral tests are discussed in Section 3. Examples of results and how to interpret the cloud mask output are included in Section 4 along with validation activities. Appendix A includes an example FORTRAN, Matlab and IDL code for reading the cloud mask.

2.0 Overview

2.1 Objective

The MODIS cloud mask indicates whether a given view of the earth surface is unobstructed by clouds or optically thick aerosol. The cloud mask is generated at 250 and 1000-meter resolutions. Input to the cloud mask algorithm is assumed to be calibrated and navigated level 1B radiance data. Additionally, the MODIS data are assumed to meet instrument specifications so that

no accommodation for striping or poor navigation is required (Examples of the impact of striping on the cloud mask are given in Section 4). The cloud mask is determined for good data only (i.e., fields of view where data in MODIS bands 1, 2, 4, 5, 6, 7, 17, 18, 19, 20, 22, 26, 27, 28, 29, 31, 32, 33, and 35 have radiometric integrity). Incomplete or bad radiometric data creates holes in the cloud mask.

Several points need to be made regarding the approach to the MODIS cloud mask presented in this Algorithm Theoretical Basis Document (ATBD).

(1) The cloud mask is not the final cloud product from MODIS; several Principal Investigators have the responsibility to deliver algorithms for various additional cloud parameters, such as water phase and altitude.

(2) The cloud mask ATBD assumes that calibrated, quality controlled data are the input and a cloud mask is the output. The overall template for the MODIS data processing was planned at the project level and coordinated with activities that produced calibrated level 1B data.

(3) The snow/ice bit in the cloud mask output indicates the chosen processing path in the algorithm and should not be considered as confirmation of snow or ice scene. This is the first step in distinguishing cloud from snow.

(4) In certain heavy aerosol loading situations (e.g., dust storms, volcanic eruptions and forest fires) particular tests may flag the aerosol-laden atmosphere as cloudy. An aerosol bit has been included in the mask to indicate fields-of-view that are potentially contaminated with optically thick aerosol.

(5) Thin cirrus detection is conveyed through a separate thin cirrus bit. The bit is designed to caution the user that thin cirrus may be present, though the cloud mask final result may indicate no obstruction. This cirrus is defined in Section 3.2.4.

There are operational constraints to consider in the cloud mask algorithm for MODIS. These constraints are driven by the need to process MODIS data in a timely fashion.

- CPU Constraint: Many algorithms must first determine if the pixel is cloudy or clear. Thus, the cloud mask algorithm lies at the top of the data processing chain and must be versatile

enough to satisfy the needs of many applications. The clear-sky determination algorithm must run in near-real time, limiting the use of CPU-intensive algorithms.

- Output File Size Constraint: Storage requirements are also a concern. The current cloud mask is more than a yes/no decision. The 48 bits of the mask include an indication of the likelihood that the pixel is contaminated with cloud. It also includes ancillary information regarding the processing path and the results from individual tests. In processing applications, one need not process all the bits of the mask. An algorithm can make use of only the first 8 bits of the mask if that is appropriate. The current 48-bit cloud mask requires 4.8 gigabytes of storage per day.
- Comprehension: Because there are many users of the cloud mask, it is important that the mask not only provides enough information to be widely used, but also that it be easily understood. To intelligently interpret the output from this algorithm, it is important to have the algorithm simple in concept but effective in its application.

In summary, our approach to the MODIS cloud mask is, in its simplest form, to provide a confidence flag indicating certainty of clear sky for each pixel; and beyond that, to provide additional background information designed to help the user interpret the cloud mask result for his or her particular application. The cloud masking algorithm must operate under the following restrictions: near-real time execution, limited computer storage, and simplicity so that many users can follow the algorithm path.

2.2 Background

Development of the MODIS cloud mask algorithm benefits from previous work to characterize global cloud cover using satellite observations. The International Satellite Cloud Climatology Project (ISCCP) has developed cloud detection schemes using visible and infrared window radiances. The AVHRR (Advanced Very High Resolution Radiometer) Processing scheme Over cLoud Land and Ocean (APOLLO) cloud detection algorithm uses the five visible and infrared channels of the AVHRR. The NOAA Cloud Advanced Very High Resolution Radiometer

(CLAVR) also uses a series of spectral and spatial variability tests to detect a cloud. CO_2 slicing characterizes global high cloud cover, including thin cirrus, using infrared radiances in the carbon dioxide sensitive portion of the spectrum. Additionally, spatial coherence of infrared radiances in cloudy and clear skies has been used successfully in regional cloud studies. The following paragraphs briefly summarize some of these prior approaches to cloud detection.

The ISCCP cloud masking algorithm described by Rossow (1989, 1993), Rossow et al. (1989), Sèze and Rossow (1991a) and Rossow and Garder (1993) utilizes the narrowband visible (0.6 μm) and the infrared window (11 μm) channels on geostationary platform. Each observed radiance value is compared with its corresponding clear-sky composite value. Clouds are detected only when they alter the clear-sky radiances by more than the uncertainty in the clear values. In this way the "threshold" for cloud detection is the magnitude of the uncertainty in the clear radiance estimates.

The ISCCP algorithm is based on the premise that the observed visible and infrared radiances are caused by only two types of conditions, *cloudy* and *clear*, and that the ranges of radiances and their variability associated with these two conditions do not overlap (Rossow and Garder 1993). As a result, the algorithm is based upon thresholds; a pixel is classified as cloudy only if at least one radiance value is distinct from the inferred clear value by an amount larger than the uncertainty in that clear threshold value. The uncertainty can be caused both by measurement errors and by natural variability. This algorithm is constructed to be cloud-conservative, minimizing false cloud detections but missing clouds that resemble clear conditions.

The ISCCP cloud-detection algorithm consists of five steps (Rossow and Garder 1993): (1) space contrast test on a single infrared image; (2) time contrast test on three consecutive infrared images at constant diurnal phase; (3) accumulation of space/time statistics for infrared and visible images; (4) construction of clear-sky composites for infrared and visible every 5 days at each diurnal phase and location; and (5) radiance threshold for infrared and visible for each pixel.

APOLLO is discussed in detail by Saunders and Kriebel (1988), Kriebel et al. (1989) and Gesell (1989). The scheme uses AVHRR channels 1 through 5 at full spatial resolution, nomi-

nally 1.1 km at nadir. The 5 spectral bandpasses are approximately 0.58-0.68 μm, 0.72-1.10 μm, 3.55-3.93 μm, 10.3-11.3 μm, and 11.5-12.5 μm. The technique is based on 5 threshold tests. A pixel is called cloudy if it is brighter or colder than a threshold, if the reflectance ratio of channels 2 to 1 is between 0.7 and 1.1, if the temperature difference between channels 4 and 5 is above a threshold, and if the spatial uniformity over ocean is greater than a threshold (Saunders and Kriebel 1988). These tests distinguish between cloud free and cloudy pixels. A pixel is defined as cloud free if the multispectral data have values below the threshold for each test. The pixel is defined as cloud contaminated if it fails any single test, thus it is clear-sky conservative. Two of those tests are then used with different thresholds to identify cloud-filled pixels from the sub pixel clouds.

The NOAA CLAVR algorithm (Phase I) uses all five channels of AVHRR to derive a global cloud mask (Stowe et al. 1991). It examines multispectral information, channel differences, and spatial differences and then employs a series of sequential decision tree tests. Cloud free, mixed (sub pixel cloud), and cloudy regions are identified for 2×2 global area coverage (GAC) pixel (4 km resolution) arrays. If all four pixels in the array fail all the cloud tests, then the array is labeled as cloud-free (0% cloudy). If all four pixels satisfy just one of the cloud tests, then the array is labeled as 100% cloudy. If 1 to 3 pixels satisfy a cloud test, then the array is labeled as mixed and assigned an arbitrary value of 50% cloudy. If all four pixels of a mixed or cloudy array satisfy a clear-restorer test (required for snow or ice, ocean specular reflection, and bright desert surfaces) then the pixel array is re-classified as "restored-clear" (0% cloudy). The set of cloud tests is subdivided into daytime ocean scenes, daytime land scenes, nighttime ocean scenes and nighttime land scenes.

Subsequent versions of CLAVR use dynamic thresholds predicted from the angular pattern observed from the clear-sky radiance statistics of the previous 9-day repeat cycle of the NOAA satellite for a mapped one degree equal area grid cell (Stowe et al. 1994). As a further modification, CLAVR will include pixel by pixel classification based upon different threshold tests to separate clear from cloud contaminated pixels and to separate cloud contaminated pixels into

partial and overcast cover. Cloud contaminated pixels are radiatively "typed" as belonging to low stratus, thin cirrus, and deep convective cloud systems. A fourth type indicates all other clouds, including mixed level clouds.

The Cloud and Surface Parameter Retrieval (CASPR) system is a toolkit for the analysis of data from the Advanced Very High Resolution Radiometer (AVHRR) satellite sensor carried on NOAA polar-orbiting satellites (Key 2000). The toolkit is a collection of algorithms that can be used to retrieve a variety of surface and cloud parameters.

CO_2 slicing (Wylie et al. 1994) has been used to distinguish transmissive clouds from opaque clouds and clear-sky using High resolution Infrared Radiation Sounder (HIRS) multispectral observations. Using radiances within the broad CO_2 absorption band centered at 15 μm, clouds at various levels of the atmosphere can be detected. Radiances near the center of the absorption band are sensitive to the upper troposphere while radiances from the wings of the band (away from the band center) see successively lower into the atmosphere. The CO_2 slicing algorithm determines both cloud level and effective cloud amount from radiative transfer principles. It is especially effective for detecting thin cirrus clouds that are often missed by simple infrared window and visible broad-based approaches. Difficulties arise when the clear minus cloudy radiance for a spectral band is less than the instrument noise. Li et al (2000) use a 1DVAR method to retrieve the cloud top height and effective cloud amount using the CO2-slicing technique as a first guess.

Many algorithms have also been developed for cloud clearing of the TIROS-N Operational Vertical Sounder (TOVS). For example, the fifth version of the International TOVS Processing Package (ITPP-5, Smith et al. 1993) uses collocated AVHRR and HIRS/2 to cloud clear the HIRS/2 footprints. A 3×3 retrieval box of collocated AVHRR and HIRS/2 is interrogated to determine the warm, average and cold scene temperatures. A scene, or HIRS/2 field of view, is classified as cloudy if any of the following conditions are meet:

(1) The average AVHRR $BT_{3.7}$ or the warm signal exceeds the average AVHRR BT_{11} warm signal;

(2) The skin temperature as derived from the AVHRR is more than 10°C colder than the initial guess surface temperature;

(3) The average albedo for the warm HIRS/2 footprint in either of the AVHRR solar channels is greater than 25% (day tests);

(4) The albedo in the HIRS visible channel (channel 20) is larger than 25% (day test);

(5) The average AVHRR $BT_{3.7}$ for the warm scene is more than 4°C warmer than the skin temperature as derived by the AVHRR (night test);

(6) The average HIRS/2 $BT_{3.7}$ for the warm scene is more than 4°C warmer than the skin temperature as derived by the HIRS/2 (night test); or

(7) Skin temperatures derived from the AVHRRR and HIRS/2 differ by more than 2°C.

If a HIRS/2 footprint is determined to be cloudy, further tests are executed to determine the nature of the cloud cover. Other TOVS cloud clearing approaches (Rizzi et al. 1994) are based on the N* approach developed by Smith (1968). Frey et al (1995 used collocated AVHRR and HIRS/2 observations to provide global cloud estimates using combined AVHRR and HIRS/2 cloud detection tests.

Operational GOES products by NESDIS also require cloud detection, an algorithm referred to as "cloud clearing." In this application, an array of $n \times n$ contiguous pixels is categorized as *clear*, *cloudy* or *unusable*. The *clear* arrays are subcategorized as *truly clear* and *clear/cloudy*. In an approach similar to the ITPP-5 method, clear conditions are determined based on brightness thresholds, difference thresholds, and comparison of observations with first guess profiles. NASA also processes GOES data in near real-time for cloud property retrieval (e.g. Minnis et al 1995)

The above algorithms are noted as they have been incorporated into existing global cloud climatologies or have been run in an operational mode over long time periods, and thus faced some of the constraints of the MODIS cloud mask algorithm. Many other studies (see the reference list) of cloud detection influenced this ATBD. The MODIS cloud mask algorithm builds on this work, benefiting from an extended multispectral complement coupled with high spatial reso-

lution and high radiometric accuracy. MODIS has 250 m resolution in two of the visible bands, 500 m resolution in five visible and near-infrared bands, and 1000 m resolution in the remaining bands. Of the 36 spectral bands available, 19 visible and infrared radiances will be used to mitigate some of the difficulties experienced by the previous algorithms.

Table 1 lists many of the threshold tests used to detect different cloud types over ocean, vegetated and desert surfaces in various studies. Many of these tests were included in the

Table 1. General approaches to cloud detection over different land types using satellite observations that rely on thresholds for reflected and emitted energy.

Scene	Solar/Reflectance	Thermal	Comments
Low cloud over water	$R_{0.87}$, $R_{0.67}/R_{0.87}$, BT_{11}-$BT_{3.7}$	Difficult. Compare BT_{11} to daytime mean clear-sky values of BT_{11}; BT_{11} in combination with brightness temperature difference tests; Over oceans, expect a relationship between BT_{11}-$BT_{8.6}$, BT_{11}-BT_{12} due to water vapor amount being correlated to SST	Spatial and temporal uniformity tests sometimes used over water scenes; Sun-glint regions over water present a problem.
High Thick cloud over water	$R_{1.38}$, $R_{0.87}$, $R_{0.67}/R_{0.87}$,	BT_{11}; $BT_{13.9}$; $BT_{6.7}$ BT_{11}-$BT_{8.6}$, BT_{11}-BT_{12}	
High Thin cloud over water	$R_{1.38}$	$BT_{6.7}$; $BT_{13.9}$ BT_{11}-BT_{12}, $BT_{3.7}$-BT_{12}	For $R_{1.38}$, surface reflectance for atmospheres with low total water vapor amounts can be a problem.
Low cloud over snow	$(R_{0.55} - R_{1.6}) / (R_{0.55} + R_{1.6})$; BT_{11}-$BT_{3.7}$	BT_{11} -$BT_{6.7}$, BT_{13}-BT_{11} Difficult, look for inversions	Ratio test is called, NDSI (Normalized Difference Snow Index). $R_{2.1}$ is also dark over snow and bright for low cloud.
High thick cloud over snow	$R_{1.38}$; $(R_{0.55} - R_{1.6}) / (R_{0.55} + R_{1.6})$;	$BT_{13.6}$; BT_{11} -$BT_{6.7}$, BT_{13}-BT_{11} Look for inversions, suggesting cloud-free.	

Table 1. Continued.

Scene	Solar/Reflectance	Thermal	Comments
High thin cloud over snow	$R_{1.38}$; $(R_{0.55} - R_{1.6}) / (R_{0.55} + R_{1.6})$;	$BT_{13.6}$; BT_{11}-$BT_{6.7}$, BT_{13} - BT_{11}	Look for inversions, suggesting cloud-free region.
High Thick cloud over vegetation	$R_{1.38}$, $R_{0.87}$, $R_{0.67}/R_{0.87}$, $(R_{0.87} - R_{0.65}) / (R_{0.87} + R_{0.65})$;	BT_{11}; $BT_{13.9}$; $BT_{6.7}$ BT_{11}-$BT_{8.6}$, BT_{11}-BT_{12}	
High Thin cloud over vegetation	$R_{1.38}$, $R_{0.87}$, $R_{0.67}/R_{0.87}$, $(R_{0.87} - R_{0.65}) / (R_{0.87} + R_{0.65})$;	$BT_{13.9}$; $BT_{6.7}$ BT_{11}-$BT_{8.6}$, BT_{11}-BT_{12}	Tests a function of ecosystem to account for variations in surface emittance and reflectance.
Low cloud over bare soil	$R_{0.87}$, $R_{0.67}/R_{0.87}$, BT_{11}-$BT_{3.7}$; $BT_{3.7}$-$BT_{3.9}$	BT_{11} in combination with brightness temperature difference tests. $BT_{3.7}$-$BT_{3.9}$ BT_{11}-$BT_{3.7}$	Difficult due to brightness and spectral variation in surface emissivity. Surface reflectance at 3.7 and 3.9 μm is similar and therefore thermal test is useful.
High Thick cloud over bare soil	$R_{1.38}$, $R_{0.87}$, $R_{0.67}/R_{0.87}$	$BT_{13.9}$; $BT_{6.7}$ BT_{11} in combination with brightness temperature difference tests.	
High Thin cloud over bare soil	$R_{1.38}$, $R_{0.87}$, $R_{0.67}/R_{0.87}$, BT_{11}-$BT_{3.7}$;	$BT_{13.9}$; $BT_{6.7}$ BT_{11} in combination with brightness temperature difference tests, for example $BT_{3.7}$-$BT_{3.9}$	Difficult for global applications. Surface reflectance at 1.38 μm can sometimes cause a problem for high altitude deserts. For BT difference tests, variations in surface emissivity can cause false cloud screening.

MODIS cloud mask algorithm. Some comments associated with these tests are given in the last column of the table.

2.3 MODIS Characteristics

The MODIS bands used in the cloud mask algorithm are identified in Table 2.

Table 2. MODIS bands used in the MODIS cloud mask algorithm.

Band	Wavelength (μm)		Comment
1 (250 m)	0.659	Y	(250 m and 1 km) clouds, shadow
2 (250 m)	0.865	Y	(250 m and 1 km) low clouds
3 (500 m)	0.470	N	
4 (500 m)	0.555	Y	
5 (500 m)	1.240	Y	Snow
6 (500 m)	1.640	Y	snow, shadow
7 (500 m)	2.130	Y	
8	0.415	N	
9	0.443	N	
10	0.490	N	
11	0.531	N	
12	0.565	N	
13	0.653	N	
14	0.681	N	
15	0.750	N	
16	0.865	N	
17	0.905	Y	
18	0.936	Y	low cloud detection
19	0.940	Y	
26	1.375	Y	thin cirrus, high cloud
20	3.750	Y	shadow
21/22	3.959	N(21)/Y(22)	window, shadow
23	4.050	Y	
24	4.465	N	
25	4.515	N	
27	6.715	Y	high cloud, polar inversions
28	7.325	Y	cloud at night over land with B31
29	8.550	Y	brightness temperature difference
30	9.730	N	
31	11.030	Y	window threshold
32	12.020	Y	brightness temperature difference
33	13.335	Y	polar regions, used with B31
34	13.635	N	
35	13.935	Y	high cloud test
36	14.235	N	

In preparation for a MODIS day-1 cloud mask product, observations from the MODIS Airborne Simulator (MAS) (King et al. 1996), AVHRR, and the HIRS/2 were used to develop the multispectral cloud mask algorithm. The AVHRR and HIRS/2 instruments fly on the NOAA

polar orbiting satellites, while the MAS flies onboard NASA's high altitude ER-2 aircraft collecting 50 m resolution data across a 37 km swath. Thresholds developed with these instruments were modified once MODIS data became available. This document lists these changes and the thresholds used in the algorithm. Ackerman et al (1998) discuss the cloud masking approach and provide examples with MAS and AVHRR data.

2.4 Cloud Mask Inputs and Outputs

The following paragraphs summarize the input and output of the MODIS cloud algorithm. Details on the multispectral single field-of-view (FOV) and spatial variability algorithms are found in the algorithm description section. As indicated earlier, input to the cloud mask algorithm is assumed to be calibrated and navigated level 1B radiance data in channels 1, 2, 4, 5, 6, 7, 17, 18, 19, 20, 22, 26, 27, 28, 29, 31, 32, 33, and 35. Incomplete or bad radiometric data will create holes in the cloud mask. Additionally, the cloud mask requires several ancillary data inputs:

- sun angle, azimuthal angle, and viewing angle: obtained from MOD03 (geolocation fields);
- land/water map at 1 km resolution: obtained from MODIS geolocation data (MOD03);
- topography: elevation above mean sea level from geolocation data (MOD03);
- ecosystems: global 1 km map of ecosystems based on the Olson classification system;
- Daily NISE snow/ice map provided by NSIDC (National Snow and Ice Data Center);
- Daily sea ice concentration product from NOAA;

The best available ancillary data are used for the MODIS cloud mask. However, it is expected that several MODIS investigator products will improve upon these ancillary data, so an evolutionary development of the cloud mask is envisioned.

The output of the MODIS cloud mask algorithm is a 48-bit word for each FOV (Table 3). The mask includes information about the processing path the algorithm followed (e.g., land or ocean) and whether a view of the surface is obstructed. We recognize that a potentially large number of applications will use the cloud mask. Some algorithms will be more tolerant of cloud

contamination than others. For example, some algorithms may apply a correction to account for the radiative effects of a thin cloud, while other applications will avoid all cloud contaminated scenes. In addition, certain algorithms may use spectral channels that are more sensitive to the presence of clouds than others. For this reason, the cloud mask output also includes results from particular cloud detection tests.

The boundary between defining a pixel as cloudy or clear is sometimes ambiguous. For example, a pixel may be partly cloudy, or a pixel may appear as cloudy in one spectral channel and appear cloud-free at a different wavelength. Figure 1 shows three spectral images of a subvisual contrails and thin cirrus taken from the Terra MODIS over Europe in June 2001. The top-left most panel is a MODIS image in the 0.86 μm channel, a spectral channel typical of many satellites and commonly used for land surface classifications such as the NDVI. The contrails are not

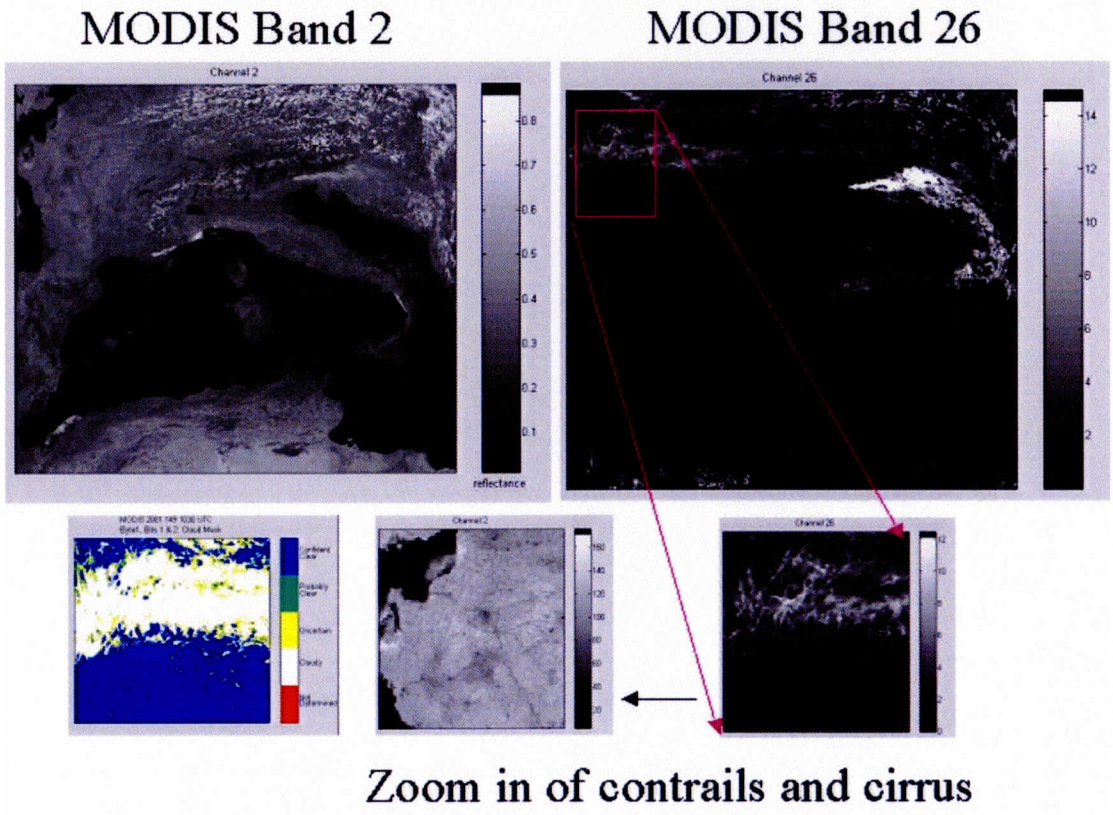

Figure 1. Two MODIS spectral images (0.86, 1.38) taken over Europe in June 2001. The lower image to the left represents the results of the MODIS cloud mask algorithm.

discernible in this image and scattering effects of the radiation may be accounted for in an appropriate atmospheric correction algorithm. The top-right most panel is a MODIS 1.38 μm image. The 1.38 μm spectral channel is near a strong water vapor absorption band and, during the day, is extremely sensitive to the presence of high-level clouds. While the contrail seems to have little impact on visible reflectances, it is very apparent in the 1.38 μm channel. In this type of scene, the cloud mask needs to provide enough information to be useful for a variety of applications.

To accommodate a wide variety of applications, the mask is more than a simple yes/no decision (though bit 1 alone could be used to represent a single bit cloud mask). The cloud mask includes 4 levels of 'confidence' with regard to whether a pixel is thought to be clear (bits 1 and 2)[1] as well as the results from different spectral tests. The bit structure of the cloud mask is:

[1] In this document, representations of bit fields are ordered from right to left. Bit 0, or the right-most bit, is the least significant.

Table 3. File specification for the 48-bit MODIS cloud mask. A '0' for tests 13-47 may mean the test was not run.

BIT FIELD	DESCRIPTION KEY	RESULT
0	Cloud Mask Flag	0 = not determined 1 = determined
1-2	Unobstructed FOV Confidence Flag	00 = cloudy 01 = uncertain 10 = probably clear 11 = confident clear
PROCESSING PATH FLAGS		
3	Day / Night Flag	0 = Night / 1 = Day
4	Sun glint Flag	0 = Yes / 1 = No
5	Snow / Ice Background Flag	0 = Yes/ 1 = No
6-7	Land / Water Flag	00 = Water 01 = Coastal 10 = Desert 11 = Land
ADDITIONAL INFORMATION		
8	Non-cloud obstruction Flag (heavy aerosol)	0 = Yes / 1 = No
9	Thin Cirrus Detected (solar)	0 = Yes / 1 = No
BIT FIELD	**DESCRIPTION KEY**	**RESULT**
10	Shadow Found	0 = Yes / 1 = No
11	Thin Cirrus Detected (infrared)	0 = Yes / 1 = No
12	Spare (Cloud adjacency)	(post launch)
	1-km CLOUD FLAGS	
13	Cloud Flag - simple IR Threshold Test	0 = Yes / 1 = No
14	High Cloud Flag - CO_2 Threshold Test	0 = Yes / 1 = No
15	High Cloud Flag - 6.7 μm Test	0 = Yes / 1 = No
16	High Cloud Flag - 1.38 μm Test	0 = Yes / 1 = No
17	High Cloud Flag - 3.7-12 μm Test	0 = Yes / 1 = No
18	Cloud Flag - IR Temperature Difference	0 = Yes / 1 = No
19	Cloud Flag - 3.9-11 μm Test	0 = Yes / 1 = No
20	Cloud Flag - Visible Reflectance Test	0 = Yes / 1 = No
21	Cloud Flag - Visible Ratio Test	0 = Yes / 1 = No
22	Clear-sky Restoral Test- NDVI in Coastal Areas	0 = Yes / 1 = No
23	Cloud Flag - 7.3-11 μm Test	0 = Yes / 1 = No
ADDITIONAL TESTS		
24	Cloud Flag - Temporal Consistency	0 = Yes / 1 = No
25	Cloud Flag - Spatial Consistency	0 = Yes / 1 = No
26	Clear-sky Restoral Tests	0 = Yes / 1 = No
27	Cloud Test - Night Ocean Variability Test	0 = Yes / 1 = No
28	Suspended Dust Flag	0 = Yes / 1 = No
29-31	Spares	
	250-m CLOUD FLAG - AISIBLE TESTS	
32	Element (1,1)	0 = Yes / 1 = No
33	Element (1,2)	0 = Yes / 1 = No
34	Element (1,3)	0 = Yes / 1 = No
35	Element (1,4)	0 = Yes / 1 = No
36	Element (2,1)	0 = Yes / 1 = No
37	Element (2,2)	0 = Yes / 1 = No
38	Element (2,3)	0 = Yes / 1 = No
39	Element (2,4)	0 = Yes / 1 = No
40	Element (3,1)	0 = Yes / 1 = No
41	Element (3,2)	0 = Yes / 1 = No
42	Element (3,3)	0 = Yes / 1 = No
43	Element (3,4)	0 = Yes / 1 = No
44	Element (4,1)	0 = Yes / 1 = No
45	Element (4,2)	0 = Yes / 1 = No
46	Element (4,3)	0 = Yes / 1 = No
47	Element (4,4)	0 = Yes / 1 = No

2.4.1 INPUT (BITS 3-7)

These input bits describe the processing path taken by the cloud mask algorithm. The num-

ber of test executed, and the thresholds are a function of the processing path.

BIT 3 - DAY / NIGHT FLAG

A combination of solar zenith angle and instrument mode (day or night mode) at the pixel latitude and longitude at the time of the observations is used to determine if a daytime or nighttime cloud masking algorithm should be applied. Daytime algorithms, which include solar reflectance data, are constrained to solar zenith angles less than 85°. If this bit is set to 1, daytime algorithms were executed.

BIT 4 - SUN GLINT FLAG

Sun glint processing path is taken when the reflected sun angle, θ_r, lies between 0° and approximately 36°, where

$$\cos\theta_r = \sin\theta \sin\theta_0 \cos\phi + \cos\theta \cos\theta_0, \quad (1)$$

where θ_0 is the solar zenith angle, θ is the viewing zenith angle, and ϕ is the azimuthal angle. Sun glint is also a function of surface wind and sea state, though that dependence is not directly included in the algorithm. Certain tests (e.g. visible reflectance over water) consist of thresholds that are a function of this sunglint angle.

BIT 5 - SNOW / ICE BACKGROUND FLAG

Certain cloud detection tests (e.g., visible reflectance tests) are applied differently in the presence of snow or ice. This bit is set to a value of 0 when the cloud mask algorithm finds that snow is present. The bit is set based on an abbreviated snow index (NDSI, Hall et al. 1995) incorporated into the cloud mask. The NDSI uses the MODIS 0.55 and 1.6 μm channels to form a ratio where values greater than a predetermined threshold are deemed snow or ice covered. The normalized snow difference index, is defined as

$$\mathrm{NSDI} = \frac{R_{.55} - R_{1.6}}{R_{.55} + R_{1.6}}.$$

In warmer parts of the globe, the NSIDC and/or NOAA ancillary snow and ice data sets are

used as a check on the NDSI algorithm. At night, only the ancillary data are used to indicate the presence of surface ice.

Note that this bit indicates a processing path only and does not necessarily indicate that surface ice was detected, implying clear skies. Users interested in snow detection should access MODIS Level 2 Product MOD10.

BITS 6 AND 7 - LAND / WATER BACKGROUND FLAG

Bits 6 and 7 of the cloud mask output file contain information concerning the processing path taken through the algorithm. There are four possible surface-type processing paths: land, water, desert, or coast. Naturally, there are times when more than one of these flags could apply to a pixel. For example, the northwest coast of the African continent could be simultaneously characterized as coast, land, and desert. In such cases, we choose to output the flag that indicates the most important characteristic for the cloud masking process. The flag precedence will be as follows: coast, desert, land or water.

Thresholds for the spectral tests are a function of surface background, land and water being the two most obvious. Therefore, each pixel will be tagged as being land or water. The 1 km United States Geological Survey (USGS) global land/water mask is currently used for this determination , which has been included in MODIS geolocation data (MOD03 files).

Some cloud detection algorithms are also ecosystem dependent. Thus, an ecosystem will be determined for each land pixel. The cloud mask uses the 1 km ecosystem map of Loveland, available from EDC.

2.4.2 OUTPUT (BITS 0, 1, 2 AND 8-47)

This section gives a brief description of the meaning of the output bits. More discussion is given in the following sections.

Bit 0 - Execution Flag

There are conditions for which the cloud mask algorithm will not be executed. For exam-

ple, if all the radiance values used in the cloud masking are deemed bad, then masking cannot be undertaken. If bit 0 is set to 0, then the cloud mask algorithm was not executed. Conditions for which the cloud mask algorithm will not be executed include: no valid radiance data, no valid geolocation data, or any missing or invalid required radiance data when processing in sun-glint regions.

Bits 1-2 - Unobstructed FOV Confidence Flag

Confidence flags convey certainty in the outcome of the cloud mask algorithm tests for a given FOV. When performing spectral tests, as one approaches a threshold limit, the certainty or confidence in the outcome is reduced. Therefore, a confidence flag for each individual test, based upon proximity to the threshold value, is assigned and used to work towards a final confidence flag determination for the FOV. The current scheme applies a linear interpolation between a low confidence clear threshold (0% confidence of clear) and high confidence clear threshold (100% confidence clear) for each spectral test.

A combination of the confidences of all applied tests dictates whether additional testing (using spatial variability tests) is warranted to improve the confidence. The final cloud mask determination is clear or cloudy with a confidence level associated with it. This approach quantifies our confidence in the derived cloud mask for a given pixel. For MODIS applications, spatial and temporal consistency tests are invoked as a final check for some scene types. The planned temporal consistency test compares composite clear-sky radiances with the current clear-sky single pixel results. Spatial consistency checks neighboring pixel radiances (within the same ecosystem). If all consistency tests pass, the confidence in the final cloud/no cloud determination is increased.

Bit 8 - Non-cloud Obstruction

Smoke from forest fires, dust storms over deserts, and other aerosols between the surface and the satellite that result in obstruction of the FOV may be flagged as "cloud." The aerosol obstruction bit will be set to on (a value of 0) if simple spectral tests indicate the possible presence

of aerosols. This bit is not an aerosol product; rather, if the bit is set to zero, then the instrument may be viewing an aerosol-laden atmosphere. An example of such an aerosol test is presented in section 3.2.3.

Bit 9 - Thin Cirrus (near-infrared)

MODIS includes a unique spectral channel—1.38 μm—specifically included for the detection of thin cirrus. Land and sea surface retrieval algorithms may attempt to correct the observed radiances for the effects of thin cirrus. This test is discussed in Section 3.2.4. If this bit is set to 0, thin cirrus was detected using this channel.

Bit 10 - Shadow bit

Some land retrieval products are as sensitive to the presence of shadows as they are to contamination by thin clouds. The MODIS cloud masking algorithm checks for the presence of a shadow whenever bits 1 and 2 are greater than 00. Though much work remains, section 3.2.6 discusses the shadow detection algorithm. If bit 10 is set to zero, a shadow was detected using spectral tests.

Bits 11 - Thin Cirrus (infrared)

This second thin cirrus bit indicates that IR tests detect a thin cirrus cloud. The results are independent of the results of bit 9, which makes use of the 1.38 μm channel. This test is discussed in Section 3.2.5. If this bit is set to 0, thin cirrus was detected using infrared channels.

Bits 12 - Spare Bit (Post Launch Cloud Adjacency Bit)

This bit was added for potential use later if additional information is required. If a pixel is clear, adjacent pixels will be searched to determine if any are low confidence clear. If so, this bit will be set to 0. This algorithm will be implemented post-launch.

Bits 13 through 23 - 1 km Cloud Mask

These 11 bits represent the results of tests that make use of the 1 km observations. Each in-

dividual test is discussed in the next section. Some tests make use of channels with a 500 m resolution; these channels are averaged up to the 1 km FOV. The number of spectral tests applied is a function of the processing path. Table 4 lists the tests applied for each path. It is important to refer to this table (or the QA flag) when interpreting the meaning of bits 13 through 23, as a value of 0 can mean the pixel is clear, or that the test was not performed. An exception is bit 22, a clear-sky restoral test in coastal regions added after the Aqua launch.

Bits 24 and 25 - Consistency Tests

These 2 bits represent the results from temporal and spatial constancy tests.

Bits 26 Through 28 - Additional Tests

These tests were added after launch and are described below.

Bits 28 Through 31 - Spare Bits

These spare bits are reserved for future tests.

Bits 32 Through 47 - 250 Meter Resolution Flags

The 250-m cloud mask is collocated within the 1000 m cloud mask in a fixed way; of the twenty-eight 250-m pixels that can be considered located within a 1000 m pixel, the most centered sixteen are processed for the cloud mask. Of the four rows of 250 m pixels, 1 through 7 that fall into a 1000-m pixel, four rows of pixels 3 through 6 will be selected. The relationship between the sixteen 250-m fov's and the 1 km footprint in the cloud mask is defined as:

250-m beginning element number = (1 km element number - 1) * 4 + 1

250-m beginning line number = (1 km line number - 1) * 4 + 1

where the first line and element are 1,1. From this beginning location, the 4×4 array of lines and elements can be identified. The indexing order of the sixteen 250-m pixels in the cloud mask file is lines, elements. Bit 3 must be set to 1 for the 250-m mask to have any meaning (e.g., ignore the last 16 bits if nighttime).

It is possible to infer cloud fraction in the 1000-m field of view from the 16 visible pixels

within the 1 km footprint. The cloud fraction would be the number of zeros divided by 16. This would be inadvisable in particular situations, such as over snow.

Initially, the results from the 1 km cloud mask are copied into the 16 250-meter cloud bits, where a confidence is less than 0.66 is considered cloudy. The final results can be changed based on the tests described in sections 3.2.7 and 3.2.8.

Table 4. MODIS cloud mask tests executed for a given processing path. The red check (✓) indicates that the test has been implemented, and the blue circle (○) indicates that the test is not yet fully tested on MODIS data.

	Daytime Ocean	Nighttime Ocean	Daytime Land	Nighttime Land	Daytime Snow/ice	Nighttime Snow/ice	Daytime Coastline	Nighttime Coastline	Daytime Desert	Nighttime Desert
BT_{11} (Bit 13)	✓	✓								
$BT_{13.9}$ (Bit 14)	✓	✓	✓	✓	✓	✓	✓	✓	✓	✓
$BT_{6.7}$ & $BT_{11} - BT_{6.7}$ (Bit 15)	✓	✓	✓	✓	✓	✓	✓	✓	✓	○
$R_{1.38}$ (Bit 16)	✓		✓		✓		✓		✓	
$BT_{3.7} - BT_{12}$ (Bit 17)				✓		✓				✓
$BT_{8.6} - BT_{11}$ & $BT_{11} - BT_{12}$ (Bit 18)	✓	✓	✓	✓			✓	✓	✓	✓
$BT_{11} - BT_{3.9}$ (Bit 19)	✓	✓	✓	✓	✓	✓	✓	✓	✓	✓
$R_{0.66}$ or $R_{0.87}$ (Bit 20)	✓		✓		✓		✓		✓	
$R_{0.87}/R_{0.66}$ (Bit 21)	✓		✓				✓			
Delete this row.										
$BT_{7.3} - BT_{11}$ (Bit 23)				○				○		○
Temporal Consistency (Bit 24)	○	○								○
Spatial Variability (Bit 25)	✓	✓								

3.0 Algorithm Description

The theoretical basis of the algorithms and practical considerations are contained in this section. For nomenclature, we shall denote the satellite measured solar reflectance as R, and refer to the infrared radiance as brightness temperature (equivalent blackbody temperature determined using the Planck function) denoted as BT. Subscripts refer to the wavelength at which the measurement is made. The strategy for this cloud mask algorithm is to start with single pixel (1000 m field of view) tests. Cloud detection using automated textural classification techniques were considered for difficult scenes (e.g., polar conditions); however, it is anticipated that the many spectral channels of MODIS may negate the use of textural applications. The disadvantage of textural methods is the required CPU, an extreme disadvantage when operating a real-time cloud mask. When confidence levels are below 95%, spatial uniformity tests are then applied. Over water the clear pixel results are measured for spatial and temporal consistency.

Many of the single pixel tests rely on radiance (temperature) thresholds in the infrared and reflectance thresholds in the solar. These thresholds vary with surface emissivity, with atmospheric moisture and aerosol content, and with MODIS viewing scan angle. This section describes these spectral tests.

3.1 Confidence Flags

Most of the single pixel tests that are discussed in Section 3.2 rely on thresholds. Thresholds are never global. There are always exceptions. For example, the ratio of reflectance at 0.86 to 0.66 μm identifies cloud for values in the range $0.9 < R_{0.87}/R_{0.66} < 1.1$. It seems unrealistic to label a pixel with $R_{0.87}/R_{0.66} = 1.09$ as cloudy, and a neighboring pixel with the ratio of 1.11 as non-cloudy. Rather, as one approaches the threshold limits, the certainty or confidence in the labeling becomes more and more uncertain. An individual confidence flag is assigned to each single pixel test and is a function of how close the observation is to the thresholds. The individual confidence flags are combined to produce the final cloud mask flag for the output file (bits 1

and 2).

The uncertainty is a function of instrument noise in that channel and the magnitude of the correction that was necessary due to surface spectral radiative properties, as well as atmospheric moisture and/or aerosol reflection contributions. The individual confidence flag indicates a confidence level for each single pixel test result. The initial FOV obstruction determination is an amalgamation of all confidence flags and single pixel test results (Section 3.2.11). This determination dictates whether additional testing (e.g., spatial uniformity tests) is warranted to improve the confidence. The final cloud mask determination (bits 1 and 2) is a clear-sky confidence with one of four levels associated with it: *clear*, *probably clear*, *uncertain* and *cloudy*. This approach quantifies our confidence in the derived cloud mask for a given pixel. This section describes the method of assigning a confidence to a given spectral test.

Many cloud detection schemes have a single threshold for a given test. For example, if the visible reflectance over the ocean is greater than 6% then the pixel is set to cloudy. The MODIS cloud masking algorithm is designed to provide information on how much confidence a user can place on the result. Each test is assigned a value between 0 and 1 representing increasing confidence in clear-sky conditions. Figure 2 is a graphical representation of how a confidence level is

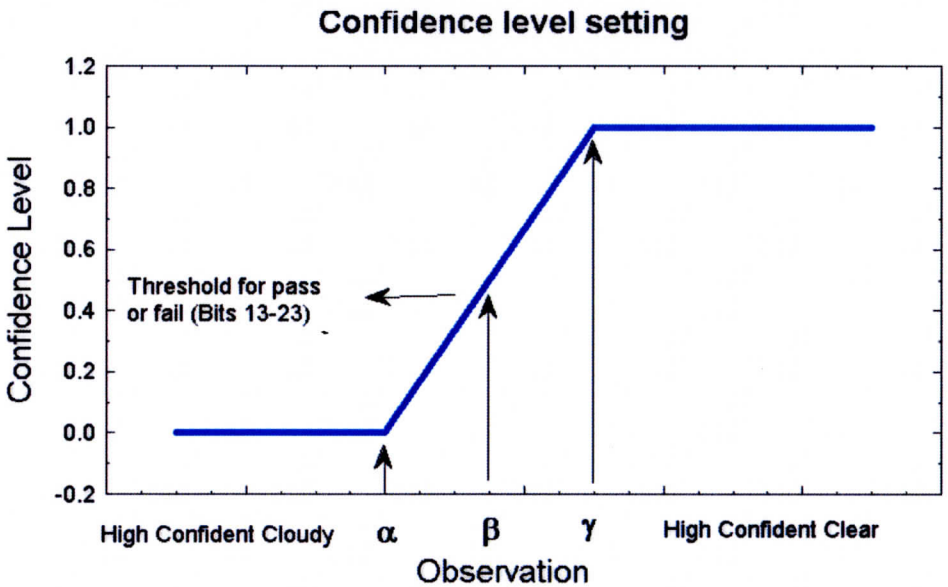

Figure 2. A graphical depiction of three thresholds used in cloud screening.

assigned for a spectral test. The abscissa represents the observation and the ordinate the clear-sky confidence level. In this test, an observation greater than a value of γ is determined to be a high confidence clear scene and assigned a value of 1. An observation with a value less than α is cloudy and assigned a confidence level of 0. These high confidence clear and cloud thresholds, γ and α respectively, are determined from observations and/or theoretical simulations. Values between α and γ are assigned a value between 0 and 1 (or 1 and 0). Assignment is based on a linear function.

In the final cloud mask only four levels of confidence are provided. Numerical values are assigned to each of these four confidence levels, 0.99 confidence of clear, 0.95, 0.66 and less than 0.66. These numerical values are set based on how close the observed value is to a set of thresholds. A description of how the final confidence level is determined is given in section 3.2.11.

With the exception of bit 22, a clear-sky restoral test, bits 13 through 23 represent the results from independent cloud tests, with no confidence associated with the output. The β value in Figure 2 is the pass/fail threshold for a given test. Thus, each test therefore has a minimum of three thresholds value for pass/fail, high confidence pass and high confidence fail. Some tests, such as the visible ratio test, identify cloud if the observations fall within a given range (e.g., $0.9 < R_{0.87}/R_{0.66} < 1.1$). For these range tests there are six thresholds, three for each end.

3.2 Theoretical Description of Cloud Detection

This section discusses the physics of detecting clouds using multispectral radiances from a given field of view (FOV) or an array of FOVs, presents the application with MODIS data, and indicates various problem areas.

3.2.1 Infrared Brightness Temperature Thresholds and Difference (BTD) Tests

The azimuthally averaged form of the infrared radiative transfer equation is given by

$$\mu \frac{dI(\delta,\mu)}{d\delta} = I(\delta, \mu) - (1-\omega_0)B(T) - \frac{\omega_0}{2}\int_{-1}^{1} P(\delta, \mu, \mu')\, I(\delta, \mu')\, d\mu'. \quad (3)$$

In addition to atmospheric structure, which determines $B(T)$, the parameters describing the transfer of radiation through the atmosphere are the single scattering albedo, $\omega_0 = \sigma_{sca}/\sigma_{ext}$, which ranges between 1 for a non-absorbing medium and 0 for a medium that absorbs and does not scatter energy, the optical depth, δ, and the Phase function, $P(\mu, \mu')$, which describes the direction of the scattered energy.

To gain insight on the issue of detecting clouds using IR observations from satellites, it is useful to first consider the two-stream solution to Eq. (3). Using the discrete-ordinates approach (Liou 1973; Stamnes and Swanson 1981), the solution for the upward radiance from the top of a uniform single cloud layer is:

$$I_{obs} = M\_L\_\exp(-k\delta) + M_+L_+ + B(T_c), \quad (4)$$

where

$$L_+ = \frac{1}{2}\left[\frac{I\downarrow + I\uparrow - 2B(T_c)}{M_+ e^{-k\delta} + M_-} + \frac{I\downarrow + I\uparrow}{M_+ e^{-k\delta} + M_-}\right], \quad (5)$$

$$L_- = \frac{1}{2}\left[\frac{I\downarrow + I\uparrow - 2B(T_c)}{M_+ e^{-k\delta} + M_-} + \frac{I\downarrow - I\uparrow}{M_+ e^{-k\delta} - M_-}\right], \quad (6)$$

$$M_\pm = \frac{1}{1 \pm k}\left(\omega_0 \mp \omega_0 g(1-\omega_0)\frac{1}{k}\right), \quad (7)$$

$$k = \left[(1-\omega_0)(1-\omega_0 g)\right]^{\frac{1}{2}}. \quad (8)$$

$I\downarrow$ is the downward radiance (assumed isotropic) incident on the top of the cloud layer, $I\uparrow$ the upward radiance at the base of the layer, and g the asymmetry parameter. T_c is a representative temperature of the cloud layer.

A challenge in cloud masking is detecting thin clouds. Assuming a thin cloud layer, the effective transmittance (ratio of the radiance exiting the layer to that incident on the base) is derived from equation (4) by expanding the exponential. The effective transmittance is a function of the ratio of $I\downarrow/I\uparrow$ and $B(T_c)/I\uparrow$. Using atmospheric window regions for cloud detection mini-

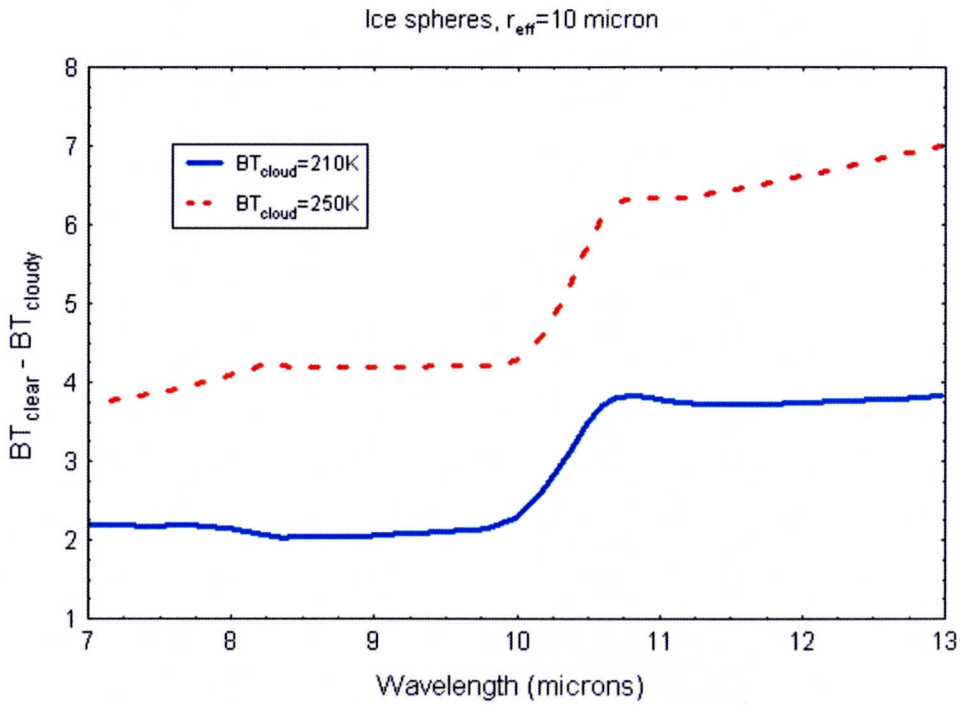

Figure 3. A simple simulation of the brightness temperature differences between a "clear" and cloudy sky as a function of wavelength. The underlying temperature is 290 K and the cloud optical depth is 0.1. All computations assume ice spheres with r_e = 10 μm.

mizes the $I\downarrow/I\uparrow$ term and maximizes the $B(T_c)/I\uparrow$ term. Figure 3 is a simulation of differences in brightness temperature between clear and cloudy sky conditions using the simplified set of equations (4)-(8). In these simulations, there is no atmosphere, the surface is emitting at a blackbody temperature of 290 K, the cloud particles are ice spheres with a gamma size distribution assuming an effective radius of 10 μm, and the cloud optical depth $\delta = 0.1$. Two cloud temperatures are simulated (210 K and 250 K). Brightness temperature differences between the clear and cloudy sky are caused by non-linearity of the Planck function and spectral variation in the single scattering properties of the cloud. This figure does not include the absorption and emission of atmospheric gases, which would also contribute to brightness temperature differences. Observations of brightness temperature differences at two or more wavelengths can help separate the atmospheric signal from the cloud effect.

The infrared threshold technique is sensitive to thin clouds given the appropriate characterization of surface emissivity and temperature. For example, with a surface at 300 K and a cloud

at 220 K, a cloud with an emissivity of 0.01 affects the top-of-atmosphere brightness temperature by 0.5 K. Since the expected noise equivalent temperature of MODIS infrared window channel 31 is 0.05 K, the cloud detecting potential of MODIS is obviously very good. The presence of a cloud modifies the spectral structure of the radiance of a clear-sky scene depending on cloud microphysical properties (e.g., particle size distribution and shape). This spectral signature, as demonstrated in Figure 3, is the physical basis behind the brightness temperature difference tests.

Simple *BT* threshold Test (Bit 13)

Several infrared window threshold and temperature difference techniques have been developed. These algorithms are most effective for cold clouds over water and must be used with caution in other situations. The first infrared test to apply over the oceans is a simple threshold test. Over open ocean when the brightness temperature in the 11 μm (BT_{11}) channel (band 31) is less than 270 K, we assume the pixel to fail the clear-sky condition. With reference to Figure 2, the three thresholds over ocean are 267, 270, and 273 K, respectively, as shown in Figure 4.

Cloud masking over land surface from thermal infrared bands is more difficult than over ocean due to potentially larger variations in surface emittance. Nonetheless, simple thresholds

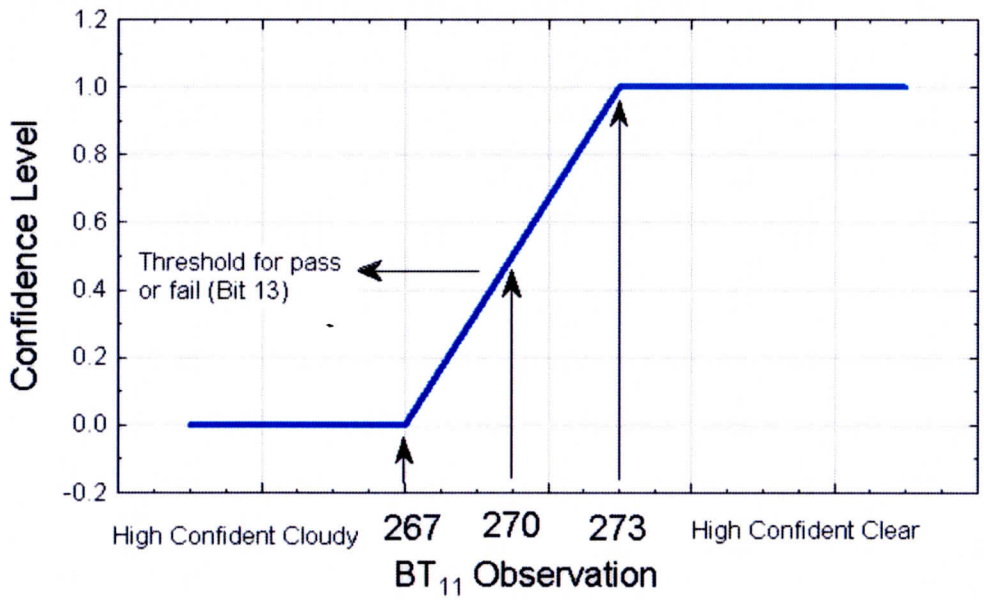

Figure 4. Thresholds for the simple IR window cold cloud test.

Table 5. Thresholds used for BT_{11} threshold test in the MODIS cloud mask algorithm.

Scene Type	Threshold	High confidence clear	Low confidence clear
Day ocean	270 K	273 K	267 K
Night ocean	270 K	273 K	267 K
Day land*	297.5 K	302.5 K	NA
Night land*	292.5 K	297.5 K	NA
Day snow/ice	NA		NA
Night snow/ice	NA	NA	NA
Night desert*	292.5 K	297.5 K	NA
Day Desert*	292.5 K	302.5 K	NA
Coastal	NA	NA	NA

* Restoral test at sea level

are useful over certain land features. Over land, the BT_{11} is used as a clear-sky restoral test. If the result of the initial cloud mask is uncertain, the pixel is set to clear if the observed BT_{11} exceeds a threshold defined as a function of elevation and ecosystem. The sea level, vegetated land value is 297.5K (cf Table 5).

BT_{11} - BT_{12} and $BT_{8.6}$ - BT_{11} Test (Bit 18)

As a result of the relative spectral uniformity of surface emittance in the IR, spectral tests within various atmospheric windows (such as MODIS bands 29, 31, 32 at 8.6, 11, and 12 μm, respectively) can be used to detect the presence of cloud. Differences between BT_{11} and BT_{12} are widely used for cloud screening with AVHRR and GOES measurements, and this technique is often referred to as the split window technique. Saunders and Kriebel (1988) used BT_{11} - BT_{12} differences to detect cirrus clouds—brightness temperature differences are larger over thin clouds than over clear or overcast conditions. Cloud thresholds were set as a function of satellite zenith angle and the BT_{11} brightness temperature. Inoue (1987) also used BT_{11} - BT_{12} versus BT_{11} to separate clear from cloudy conditions.

In difference techniques, the measured radiances at two wavelengths are converted to brightness temperatures and subtracted. Because of the wavelength dependence of optical thickness and the non-linear nature of the Planck function (B_λ), the two brightness temperatures are often different. Figure 5 is an example of a theoretical simulation of the brightness temperature

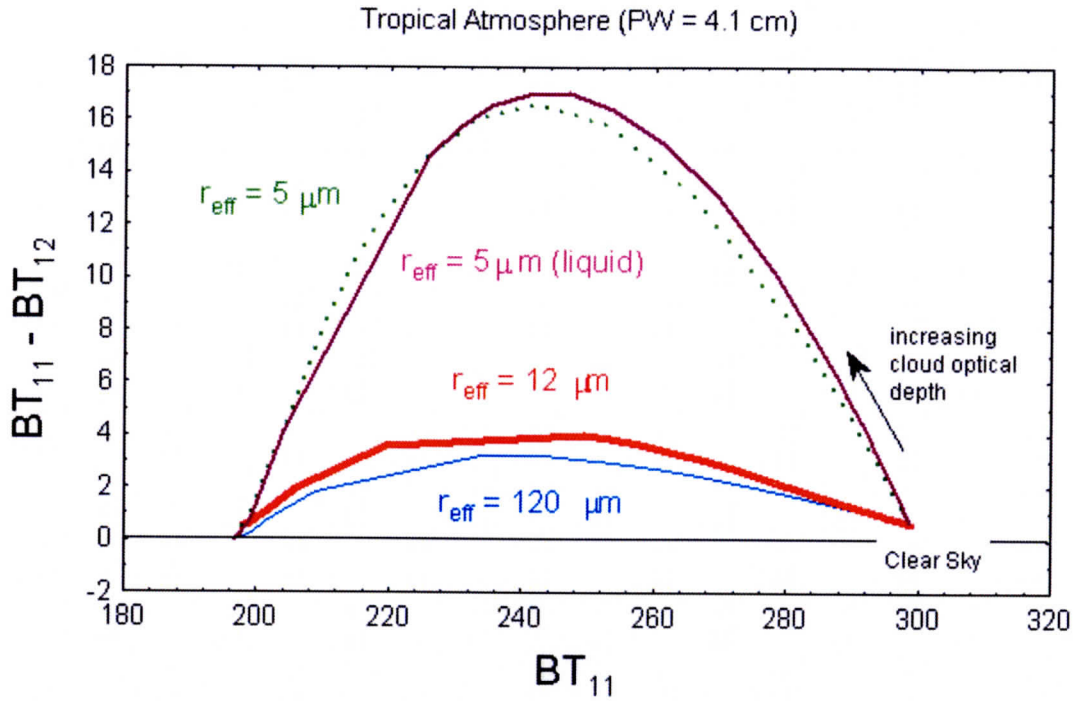

Figure 5. Theoretical simulations of the brightness temperature difference as a function of BT_{11} for a cirrus cloud of varying cloud microphysical properties.

difference between 11 and 12 μm versus the brightness temperature at 11 μm, assuming a standard tropical atmosphere. The difference is a function of cloud optical thickness, the cloud temperature, and the cloud particle size distribution. The difficulty in using these tests for cloud detection is often defining the clear-sky value on this type of diagram.

The basis of the split window and tri-spectral technique for cloud detection lies in the differential water vapor absorption that exists between different window channel (8.6 and 11 μm and 11 and 12 μm) bands. These spectral regions are considered to be part of the atmospheric window, where absorption is relatively weak. Most of the absorption lines are a result of water vapor molecules, with a minimum occurring around 11 μm. Since the absorption is weak, BT_{11} can be corrected for moisture absorption by adding the scaled brightness temperature difference of two spectrally close channels with different water vapor absorption coefficients; the scaling coefficient is a function of the differential water vapor absorption between the two channels.

The surface temperature, T_s, can be determined using remote sensing instruments if observations are corrected for water vapor absorption effects,

$$T_s = BT_{11} + \Delta BT, \tag{9}$$

where BT_{11} is a window channel brightness temperature. To begin, the radiative transfer equation for a clear atmosphere can be written

$$I_{\lambda,\mathrm{clr}} = B_\lambda(T(p_s))\tau_\lambda(p_s) + \int_{p_s}^{p_0} B_\lambda(T(p))\frac{\mathrm{d}\tau_\lambda(p)}{\mathrm{d}p}\mathrm{d}p\,. \tag{10}$$

As noted above, absorption is relatively weak across the window region so that a linear approximation is made to the transmittance

$$\tau \approx 1 - k_\lambda u, \tag{11}$$

Here k_λ is the absorption coefficient of water vapor and u is the path length. The differential transmittance then becomes

$$\mathrm{d}\tau_\lambda = -k_\lambda \mathrm{d}u. \tag{12}$$

Inserting this approximation into the window region radiative transfer equation will lead to

$$I_{\lambda,\mathrm{clr}} = B_{\lambda,s}(1 - k_\lambda u) + k_\lambda \int_0^{u_s} \overline{B}_\lambda \,\mathrm{d}\,u\,. \tag{13}$$

Here, $\overline{B_\lambda}$ is the atmospheric mean Planck radiance. Since $B_{\lambda,s}$ will be close to both $I_{\lambda,\mathrm{clr}}$ and $\overline{B_\lambda}$, we can linearize the radiative transfer equation with respect to T_s

$$BT_{b\lambda} = T_s(1 - k_\lambda u_s) + k_\lambda u_s \overline{BT_\lambda}\,, \tag{14}$$

where $\overline{BT_\lambda}$ is the mean atmospheric temperature corresponding to $\overline{B_\lambda}$. Using observations from two window channels, one may ratio this equation, cancel out common factors and rearrange to end up with the following approximation

$$\frac{T_s - BT_{\lambda,1}}{T_s - BT_{\lambda,2}} = \frac{k_{\lambda,1}}{k_{\lambda,2}}\,. \tag{15}$$

Solving the equation for T_s yields

$$T_s = BT_{\lambda,1} + \frac{k_{\lambda,1}}{k_{\lambda,2} - k_{\lambda,1}}(BT_{\lambda,1} - BT_{\lambda,2}). \tag{16}$$

Thus, with a reasonable estimate of the sea surface temperature and total precipitable water

(on which k_λ is dependent), one can develop appropriate thresholds for cloudy sky detection. For example,

$$BT_{11} + a_{PW}(BT_{11} - BT_{12}) < \text{SST}, \tag{17}$$

or

$$BT_{11} + b_{PW}(BT_{11} - BT_{8.6}) < \text{SST}, \tag{18}$$

where a_{PW} and b_{PW} are determined from a lookup table as a function of total precipitable water vapor (PW). This approach has been used operationally using 8.6 and 11 μm bandwidths from NOAA satellites, with a coefficient independent of PW (Menzel et al. 1993, Wylie et al. 1994).

Ackerman et al. (1990) proposed a tri-spectral combination of observations at 8.6, 11 and 12 μm for detecting cloud properties. Strabala et al. (1994) further explored this technique by utilizing very high spatial-resolution data from MAS. The physical premise of the technique is that ice and water vapor absorption peak in opposite halves of the window region; so that positive 8.6 minus 11 μm brightness temperature differences indicate cloud while negative differences, over oceans, indicate clear regions. The relationship between the two brightness temperature differences and clear-sky have also been examined using collocated HIRS and AVHRR GAC global ocean data sets. As the atmospheric moisture increases, $BT_{8.6} - BT_{11}$ decreases while $BT_{11} - BT_{12}$ increases.

Based on these observations, a threshold is set for clear-sky conditions. The clear-sky threshold is set for both differences:

$$\text{T8M11} = -3.19767 - 1.64805 \ln (\text{PW}), \tag{18}$$

$$\text{T11M12} = -0.456924 + 0.488198\ \text{PW}. \tag{19}$$

If $BT_{8.6} - BT_{11} > \text{T8M11}$ and $BT_{11} - BT_{12} > \text{T11M12}$, then a cloud is assumed.

High confidence clear conditions are

$$BT_{8.6} - BT_{11} < \text{T8M11} - 0.5 \text{ and } BT_{11} - BT_{12} > \text{T11M12} - 0.5, \tag{20}$$

and low confidence clear conditions are

$$BT_{8.6} - BT_{11} < \text{T8M11} + 0.5 \text{ and } BT_{11} - BT_{12} > \text{T11M12} + 0.5. \tag{21}$$

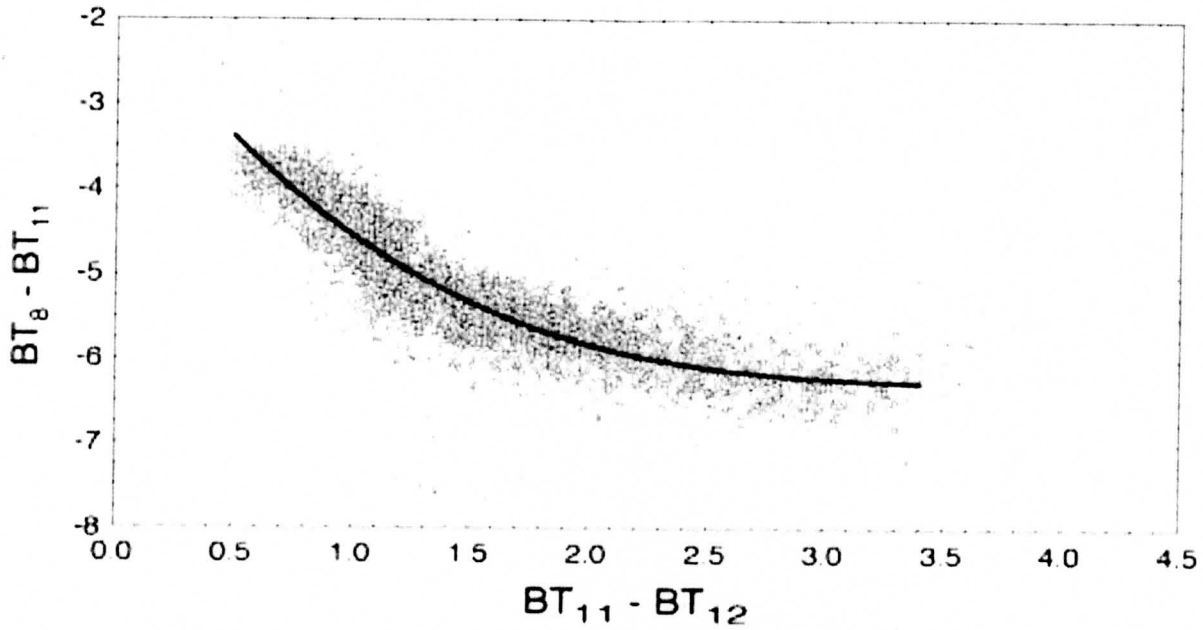

Figure 6. The tri-spectral diagram for clear-sky ocean scenes.

The above conditions assume an estimate of the precipitable water is available. These equations demonstrate that a relationship between T8M11 and T11M12 exists and thus a PW value is not needed, but rather given a value of T8M11, to be a clear pixel requires T11M12 to fall within a certain range of values. This is demonstrated in Figure 6 using collocated AVHRR and HIRS/2 observations.

Brightness temperature difference testing can also be applied over land with careful consideration of variation in spectral emittance. For example, $BT_{11} - BT_{8.6}$ has large negative values over daytime desert and is driven to positive differences in the presence of cirrus. Some land regions have an advantage over ocean regions because of the larger number of surface observations, including air temperature and vertical profiles of moisture and temperature.

BT_{11} - $BT_{3.9}$ Test (Bit 19)

MODIS band 22 (3.9 μm) measures radiances in the window region near 3.5-4 μm so that the difference between BT_{11} and $BT_{3.9}$ can be used to detect the presence of clouds. At night the difference between the brightness temperatures measured in the shortwave (3.9 μm) and in the longwave (11 μm) window regions ($BT_{11} - BT_{3.9}$) can be used to detect partial cloud or thin

cloud within the MODIS field of view. Small or negative differences are observed only for the case where an opaque scene (such as thick cloud or the surface) fills the field of view of the sensor. Negative differences occur at night over extended clouds due to the lower cloud emissivity at 3.9 μm.

During the daylight hours the difference between BT_{11} and $BT_{3.9}$ is large and negative because of reflection of solar energy at 3.9 μm. This technique is very successful at detecting low-level water clouds.

Moderate to large differences between BT_{11} and $BT_{3.9}$ result when a non-uniform scene (e.g., broken cloud) is observed. The different spectral response to a scene of non-uniform temperature is a result of Planck's law. The brightness temperature dependence on the warmer portion of the scene increasing with decreasing wavelength (the shortwave window Planck radiance is proportional to temperature to the thirteenth power, while the longwave dependence is to the fourth power). Differences in the brightness temperatures of the longwave and shortwave channels are small when viewing mostly clear or mostly cloudy scenes; however, for intermediate situations the differences become large (greater than 3°C). Table 6 lists examples of the thresholds used in MODIS collection 4 algorithm.

The application of $BT_{11} - BT_{3.9}$ is difficult in deserts during daytime. Bright desert regions with highly variable emissivities tend to be incorrectly classified as cloudy with this test. The problem is mitigated somewhat in the MODIS cloud mask by making use of a double-sided test where brightness temperature differences greater than a "low" threshold but less than a "high" threshold are labeled clear while values outside this range are called cloudy. The thresholds are listed in Table 6. This threshold strategy along with the use of clear-sky restoral tests is effective for detecting low-level clouds over deserts.

Detecting clouds at high latitudes using infrared window is a challenging problem due to the cold surface temperatures. Yamanouchi et al. (1987) describe a nighttime polar (Antarctic) cloud/surface discrimination algorithm based upon brightness temperature differences between the AVHRR 3.7 and 11 μm channels and between the 11 and 12 μm channels. Their

Table 6. Thresholds used for $BT_{11} - BT_{3.9}$ test for low cloud in the MODIS cloud mask algorithm.

Scene Type	Threshold	High confidence clear	Low confidence clear
Day ocean	-8 .0 K	-6.0 K	-1 0.0 K
Night ocean	0.0 K	-1.0 K	1.0 K
Day land	-12.0 K	-10.0 K	-14. 0 K
Night land (fn. of BT 11-12)			
Day snow/ice	-7.0 K	-4.0 K	-10.0 K
Polar night snow (fn. of BT 11)			
Antarctic day	10.0K	6.0K	14.0K
Night snow/ice	0.60 K	0.50 K	0.70 K
Day desert	-18.0, 0 K	>-16, <-2 K	<-20, >2 K

cloud/surface discrimination algorithm was more effective over water surfaces than over inland snow-covered surfaces. Note that the thresholds for Antarctica are significantly different than other regions. Also, the thresholds for land at night are calculated as a function of BT_{11} - BT_{12} and those for polar night conditions are a function of BT_{11}.

$BT_{3.7}$ - BT_{12} Test (Bit 17)

This window brightness temperature difference test is applied during the nighttime over some, but not all, surfaces. This difference is useful for separating thin cirrus and cloud free condition and is relatively insensitive to the amount of water vapor in the atmosphere (Hutchison and Hardy 1995). This test is executed over land at night. The three thresholds for are 15, 10, and 5 K, for low confidence, mid-point, and high confidence, respectively. Over snow-covered surfaces, the thresholds are 4.50, 4.00, and 3.50K.

$BT_{7.3}$ - BT_{11} Test (Bit 23)

A test for identifying high and mid-level clouds over land at night uses the brightness temperature difference between 7.3 and 11 μm. Under clear-sky conditions, $BT_{7.3}$ is sensitive to temperature and moisture in middle levels of the atmosphere while BT_{11} measures radiation mainly from the warmer surface. Clouds reduce the absolute value of this difference. The thresholds used are -8K, -10K, and -11K for low, mid-point, and high confidences, respectively.

High Cloud Test (Bit 15)

In clear-sky situations, the 6.7 μm radiation measured by satellite instruments is emitted by water vapor in the atmospheric layer between approximately 200 and 500 hPa (Soden and Bretherton 1993; Wu et al. 1993) and has a brightness temperature ($BT_{6.7}$) related to the temperature and moisture in that layer. The 6.7 μm radiation emitted by the surface or low clouds is absorbed in the atmosphere above and is generally not sensed by the satellite instruments. Therefore, thick clouds found above or near the top of this layer have colder brightness temperatures than surrounding pixels containing clear skies or lower clouds. The 6.7 μm thresholds for this test are 215K, 220K, and 225K for low confidence, mid-point, and high confidence, respectively. This test is performed on all scenes.

Detection of clouds over polar regions during winter is difficult. Under clear-sky conditions, strong surface radiative temperature inversions often exist. Thus, IR channels whose weighting function peaks low in the atmosphere will often have a larger BT than a window channel. For example, $BT_{8.6} > BT_{11}$ in the presence of an inversion. The surface inversion can also be confused with thick cirrus cloud; this can be mitigated by other tests (e.g., the magnitude of BT_{11} or the BT_{11} - BT_{12}). Analysis of BT_{11} - $BT_{6.7}$ has shown large negative differences in winter over the Antarctic Plateau and Greenland, which may be indicative of a strong surface inversion and thus clear skies (Ackerman 1996a). Under clear-sky conditions, the measured 11 μm radiation originates primarily at the surface, with a small contribution by the near-surface atmosphere. Because the surface is normally warmer than the upper troposphere, BT_{11} is normally warmer than the 6.7 μm brightness temperature; thus the difference, BT_{11} - $BT_{6.7}$, is normally greater than zero. Large negative differences in BT_{11} - $BT_{6.7}$ (less than -10 K) exist over the Antarctic Plateau and Greenland during their respective winters and are indicative of clear-sky conditions and the existence of strong low-level temperature inversions.

In polar regions, strong surface radiation inversions can develop as a result of longwave energy loss at the surface due to clear-skies and a dry atmosphere. Figure 7 is a temperature (solid-line) and dew point temperature (dashed-line) profile measured over the South Pole at 0000 UTC on 13 September 1995 and illustrates this surface inversion. On this day the temperature inversion was approximately 20 K over the lowest 100 m of the atmosphere. The surface temperature was more than 25 K colder than the temperature at 600 hPa. Temperatures over Antarctica near the surface can reach 200 K (Stearns et al. 1993), while the middle troposphere is ~235 K. Under such conditions, satellite channels located in strong water vapor absorption bands, such as the 6.7 μm channel, have a warmer equivalent brightness temperature than the 11 μm window channel. A simulation of the HIRS/2 BT_{11} - $BT_{6.7}$ difference using Figure 7 temperature and moisture profile was -14 K. This brightness temperature difference between 11 and 6.7 μm is an asset for detecting cloud-free conditions over elevated surfaces in the polar night (Ackerman 1996a). Clouds inhibit the formation of the inversion and obscure the inversion from satellite detection if the IWP is greater than approximately 20 g m^{-2}. In the cloud mask, under polar night conditions, pixels with differences < -10°C are labeled clear and reported in bit 26 (bit set to 1).

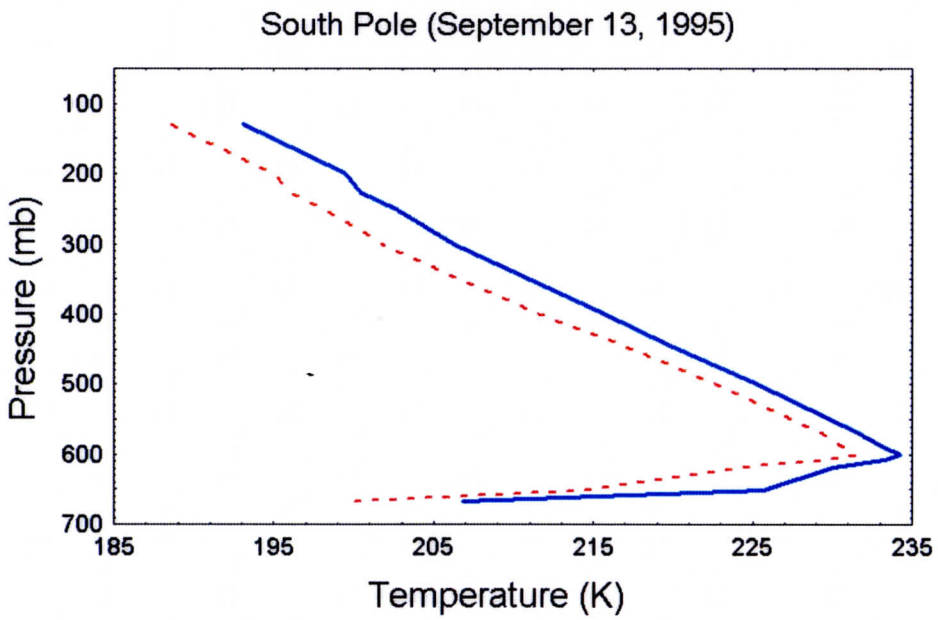

Figure 7. Vertical profile of atmospheric temperature and dew point temperature over the South Pole on 13 September 1995. The deep surface radiation inversion is useful for clear-sky detection.

3.2.2 CO_2 Channel Test for High Clouds (Bit 14)

CO_2 slicing (Smith et al. 1974; Wylie and Menzel 1989) is a useful method for sensing cloud amount and the height of clouds. CO_2 slicing is not a simple test and therefore is not incorporated into the cloud mask algorithm. A separate product, MOD06, includes results from CO_2 slicing. Simple tests using the CO_2 channels are useful for cloud detection, particularly high clouds. Whether a cloud is sensed by observations at these wavelengths (MODIS bands 33-36) is a function of the weighting function of the particular channel and the altitude of the cloud.

MODIS band 35 (13.9 μm) provides good sensitivity to the relatively cold regions of the upper troposphere. Only clouds above 500 hPa have strong contributions to the radiance to space observed at 13.9 μm; negligible contributions come from the earth's surface. Thus, a threshold test for cloud versus ambient atmosphere and a histogram test should reveal clouds above 500 hPa.

Figure 8 depicts a histogram of brightness temperature at 14.0 and 13.6 μm derived from the HIRS/2 instrument (channels 5 and 6 respectively) using the CHAPS data set. The narrow peaks at the warm end are associated with clear-sky conditions, or with clouds that reside low in the

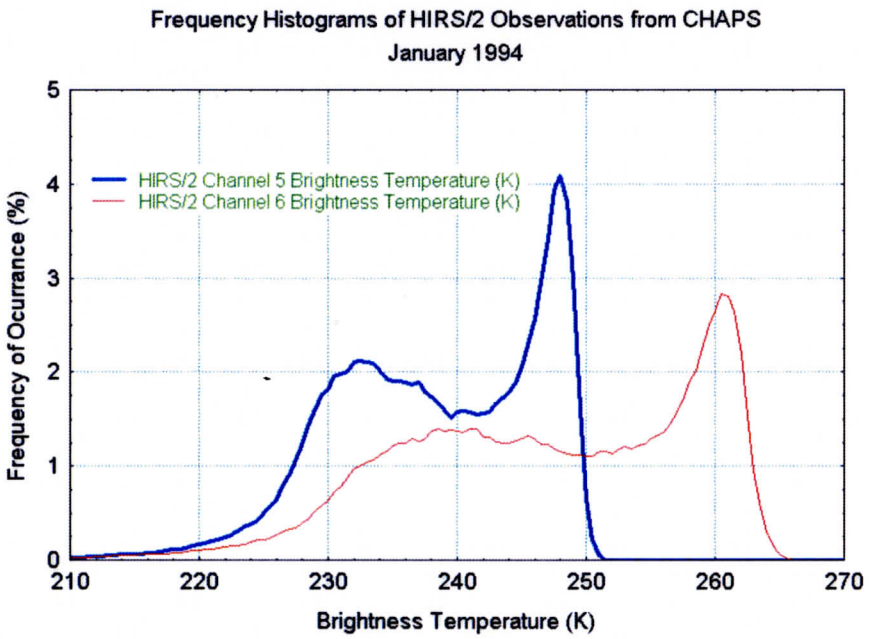

Figure 8. Histogram of BT_{14} and $BT_{13.6}$ HIRS/2 global observations for January 1994, where channel 5 (6) is centered at 14.0 (13.6) μm.

atmosphere. Based on these observations the initial clear-sky threshold is 241 K with low and high confidence thresholds of 239 K and 244 K respectively. These thresholds have been modified for MODIS due to different spectral characteristics of the two instruments. The three thresholds are independent of scene type and are 224, 226 and 228K, respectively. This test is not performed poleward of 60 degrees latitude.

Another test similar to BT_{11} - $BT_{6.7}$ is used for detecting polar inversions at night. $BT_{13.3}$ - BT_{11} is used to identify deep polar inversions likely characterized by clear skies. A pixel is labeled clear if this difference is > 3.0K.

3.2.3 NON-CLOUD OBSTRUCTION FLAG (BIT 8) AND SUSPENDED DUST FLAG (BIT 28)

A heavy aerosol laden atmosphere may result in a low confidence clear scene. Certain simple tests may be constructed that can indicate that the FOV is contaminated with an aerosol and not a cloud. For example, negative values of $BT_{11} - BT_{12}$ are often observed over deserts and can be attributed to the presence of dust storms (Ackerman 1996b). Under such conditions, provided BT_{11} is warm, the non-cloud obstruction bit (Bit 28) is set when $BT11 - BT12$ is < -1. Another part of this test is a smoke and fire test effective over dark, vegetated surfaces. The fire test simply finds hot spots using a 3.75 (band 20) threshold of 350K and a brightness temperature difference between 3.75 and 11 μm which must be > 10K. Smoke is indicated (bit 8 set) when the reflectance in band 7 (2.1 μm) is < .20 and the band 1 (0.66 μm) reflectance is greater than the value of a function based on the 2.1 μm reflectance. Thick smoke is dark at 2.1 μm relative to 0.66 μm. However, this test will give false indications of smoke over some bright land surfaces and should be used with caution. The tri-spectral technique may also be used to flag a region as potentially contaminated with volcanic aerosol. These tests are currently under investigation.

3.2.4 NEAR INFRARED 1.38 μM CIRRUS TEST (BITS 9 AND 16)

MODIS band 26 (1.38 μm) will use reflectance thresholds on a per pixel basis to detect the presence of thin cirrus cloud in the upper troposphere under daytime viewing conditions. The strength of this cloud detection channel lies in the strong water vapor absorption in the 1.38 μm

region (Gao et al., 1993). With sufficient atmospheric water vapor present (estimated to be about 1 cm precipitable water) in the beam path, no upwelling reflected radiance from the earth's surface reaches the satellite. This means that much, but not all, of the earth's surface will be obscured in this channel, precipitable water is often less than 1 cm over polar regions in midlatitude winter regions, and in high elevation regions. With relatively little of the atmosphere's moisture located high in the troposphere, high clouds appear bright; reflectance from low and mid level clouds is partially attenuated by water vapor absorption.

Simple low and high reflectance (normalized by incoming solar at the top of the atmosphere) thresholds are used to separate thin cirrus from clear and thick (near infrared cloud optical depth $> \sim 0.5$) cloud scenes. These thresholds were set initially using a multiple-scattering model with the assumption of no surface reflectance contribution to the satellite observed radiance, i.e., a dark background. Ben-Dor (1994) analyzed a scene from the AVIRIS to demonstrate that thin cirrus detection using 1.38 μm observations may be more difficult for elevated surfaces, dry atmospheric conditions, and high albedo surfaces. New injections of volcanic aerosols into the stratosphere may also impact this test.

If the reflectance lies above the clear-sky threshold and less than a thick cloud, then the thin cirrus bit (bit 9) will be set to 0 (thin cirrus detected). We subjectively define a thin cirrus as a cloud that has a small impact on the visible reflectance, enabling atmospheric correction to be applied to retrieve land surface properties (i.e., NDVI). The 1.38 μm reflectance thresholds are listed in Table 7. The result of the test is reported in bit 16.

Table 7. Thresholds used for $R_{1.3.8}$ test for high thin cirrus cloud in the MODIS cloud mask algorithm. The test is not executed if the surface altitude is above 2000m.

Scene Type	Threshold	High confidence clear	Low confidence clear
Ocean	0.035	0.03	0.040
Land	0.035	0.03	0.040
Snow/ice	0.035	0.03	0.040
Desert	0.035	0.03	0.040
Coastal	0.035	0.03	0.040

3.2.5 INFRARED THIN CIRRUS TEST (BIT 11)

This second thin cirrus bit indicates that IR tests detect a thin cirrus cloud. This test is independent of the thin cirrus flagged by the MODIS 1.38 μm channel. This test applies brightness temperature differences tests to detect the presence of thin cirrus. The APOLLO scheme tests for the presence of thin cirrus using the split window analysis. Analysis of BT_{11}-BT_{12} and BT_8-BT_{11} is also effective in detecting the presence of thin cirrus clouds.

3.2.6 DETECTION OF CLOUD SHADOWS (BIT 10)

The detection of cloud shadows is a problem that has not been addressed adequately in the literature. Clear-sky scenes that are potentially affected by shadows can be theoretically computed given the viewing geometry, solar azimuth and zenith angles, cloud edges distribution and cloud altitude. This approach requires too much CPU to run operationally, and all the information (e.g., cloud altitude) is not available to the cloud mask algorithm. Therefore, as with clouds, solar reflectance tests will be explored for a cloud shadow detection algorithm. Further work in this area has been initiated.

Currently, the cloud masking algorithm checks for shadows whenever a high confident clear scene is identified. Shadow detection is based on reflectance at 1.2, 0.94, 0.87 and 0.66 μm. A shadow is determined present if $R_{0.94} < 0.07$, $R_{0.87}/R_{0.66} > 0.3$, and the 1.2 μm reflectance is < 0.2.

An example result is shown in Figure 9. The left hand panel is a 0.66 μm image, and the right hand panel represents the masking shadow algorithm. Dark regions are shadowed regions; gray, non-shadowed; and white, cloudy scenes.

The MODIS community has also raised the issue of shadows caused by mountainous terrain. These shadows would be directly calculable from digital elevation maps, solar geometry considerations, and the cloud mask. The first two considerations would indicate the FOVs where terrain shadow could occur; the last would determine whether sunlight is available to cause the shadow. The cloud mask will not separate shadows caused by terrain from those caused by

clouds.

Cloud shadow detection has not been fully tested and should be used with caution.

3.2.7 VISIBLE REFLECTANCE TEST (BIT 20)

This is a single channel test whose strength is discriminating bright clouds over dark surfaces (e.g., stratus over ocean) and whose weakness is cloud over bright surfaces (e.g., snow). Two different channels are used depending on the ecosystem (Table 8). The 0.66 μm (band 1) is used over land regions. The 0.87 μm reflectance test is applied over ocean and desert

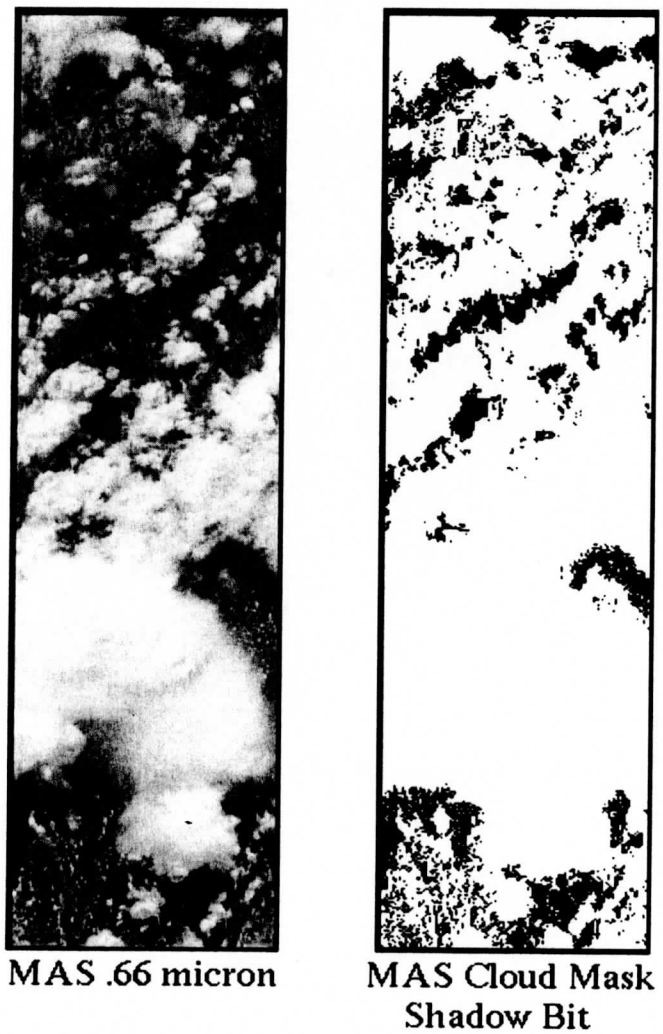

Figure 9. An example of the shadow testing using MAS data over the north slope of Alaska (13 June 1995). The panel to the right demonstrates the results from shadow testing, black regions are shadowed, white areas are cloudy or non-shadowed.

Table 8. Thresholds used for $R_{0.66} - R_{0.87}$ test for the MODIS cloud mask algorithm.

Scene Type	Threshold	High confidence clear	Low confidence clear
$R_{0.66}$			
Land	0.18	0.14	0.22
$R_{0.87}$			
Day Ocean	0.055	0.0 45	0.065
Desert	0.30	0. 26	0.34
Coastal Desert	0 .30	0. 26	0.34

scenes. The nominal thresholds are given in Table 8.

These thresholds were initially set based on observations from AVHRR and MAS. Figure 10 is an example of MAS observations taken over the tropical ocean.

The reflectance test is view-angle dependent when applied in sun glint regions as identified by the sun glint test. Figure 11 demonstrates this angular dependence of the 0.87 μm reflectance test using MODIS observations. The reflectance thresholds in sun-glint regions are therefore a function of θ_r and are divided into three parts. For θ_r from 0-10 degrees, the mid-point threshold

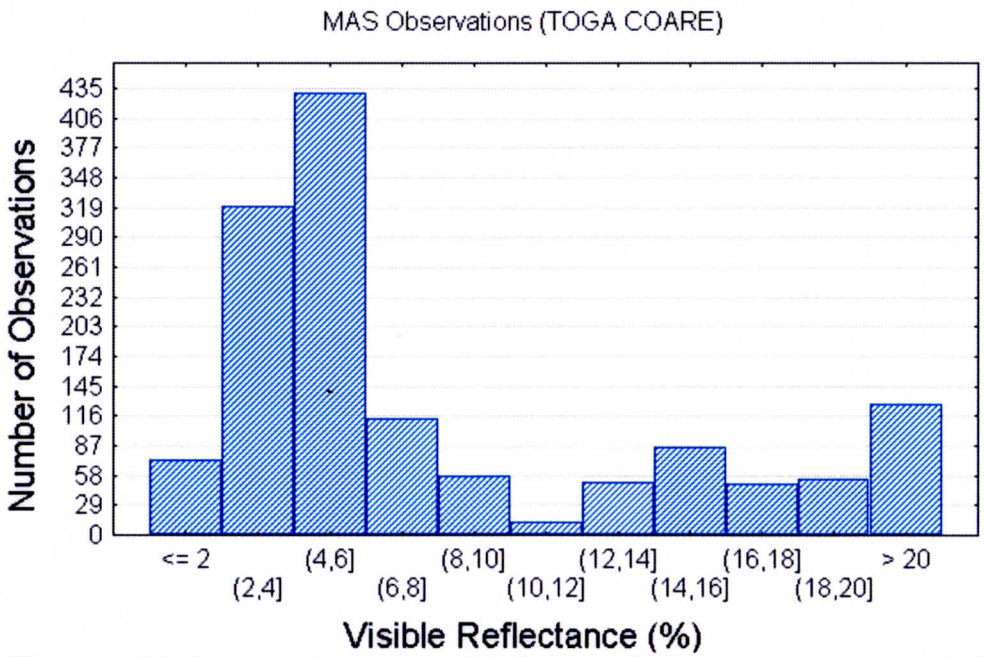

Figure 10. Histogram of the frequency of occurrence of MAS visible reflectance $R_{0.66}$ during part of the TOGA COARE experiment.

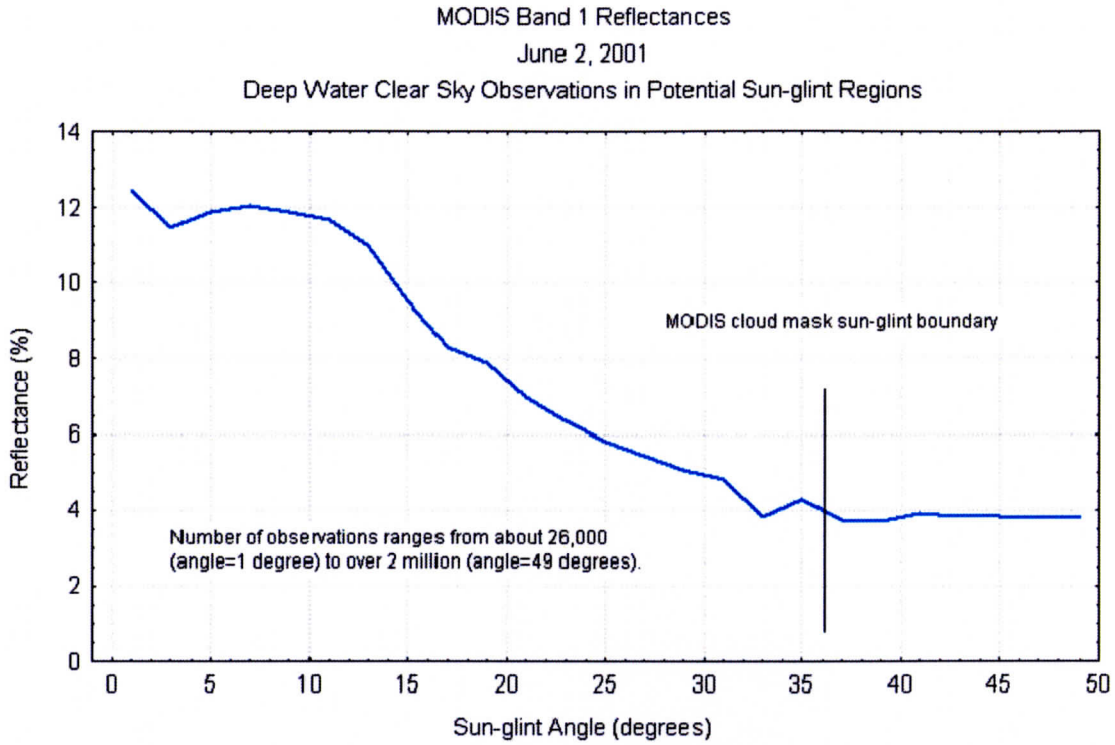

Figure 11. MODIS channel 2 reflectance as a function of reflectance angle, on June 2, 2001 over ocean regions.

is constant at 0.105, for θ_r from 10 to 20 degrees the threshold varies linearly from 0.105 to 0.075, and for θ_r from 20 to 36 degrees it again varies linearly from 0.075 to 0.055. The low and high confidence limits are set to ± 0.01 of the mid-point values.

3.2.8 Reflectance Ratio Test (Bit 21)

The reflectance ratio test uses channel 2 divided by channel 1 ($R_{0.87}/R_{0.66}$). This test makes use of the fact that the spectral reflectance at these two wavelengths is similar over clouds (ratio is near 1) and different over water and vegetation. Using AVHRR data this ratio has been found to be between 0.9 and 1.1 in cloudy regions. If the ratio falls within this range, cloud is indicated. McClain (1993) suggests that the minimum value may need to be lowered to about 0.8, at least for some cases. For cloud-free ocean the ratio is expected to be less than 0.75 (Saunders and Kriebel 1988). This ratio is generally observed to be greater than 1 over vegetation. Table 9 lists the thresholds for the MODIS cloud mask.

Figure 12 illustrates some of the complexities of desert ecosystems as demonstrated by the

Table 9. Thresholds used for $R_{0.66}$ / $R_{0.87}$ test for the MODIS cloud mask algorithm.

Scene Type ($R_{0.87}/R_{0.66}$)	Threshold	High confidence clear	Low confidence clear
Day land	1.90	1.85	1.95
Day ocean	0.90	0.85	0.95

visible reflectance ratio. The observations are from the AVHRR on the NOAA-9 and are over the Arabian Sea, the Arabian Peninsula, and surrounding regions. The figure shows histograms of reflectance ratio values for coastal/water scenes, as well as desert and more densely vegetated areas in the Persian Gulf region from approximately 15-25° N latitude and 50-70° E longitude. Almost all of the observations recorded in the histograms were from clear-sky conditions, as determined by inspection of visible and IR imagery. As suggested by the histograms of $R_{0.87}/R_{0.66}$, clear-sky ocean scenes have a ratio of less than 0.75. The surface type classifications are from the Olson World Ecosystems data set. One can immediately see that clear-sky desert values of the visible reflectance ratio cover a large range of values, including values one might normally associate with cloudy skies over vegetated surfaces. Also note the large amount

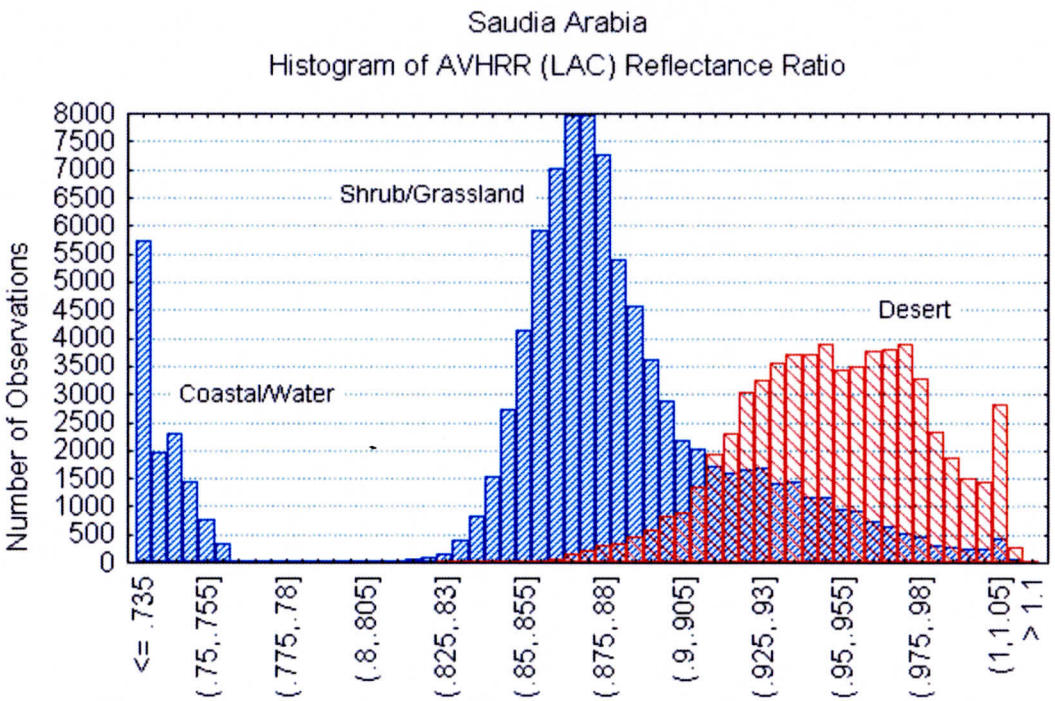

Figure 12. Histogram of the frequency of occurrence of the AVHRR reflectance ratio $R_{0.86}/R_{0.63}$ for a scene over the Arabian peninsula and Arabian Sea.

of overlap between the desert and shrub/grassland categories. This figure shows that clear-sky spectral threshold tests need to be applied very carefully in arid regions and also points out the need for high-resolution ecosystem maps. This test is not performed over desert, semi-desert, snow/ice, or some agricultural ecosystems.

The $R_{1.2}/R_{0.55}$ ratio test is also used to minimize false cloud and uncertain determinations in daytime land situations. If the confidence flag is less than 0.95 and $R_{1.2}/R_{0.55} > 2.0$, and if $BT_{3.7} - BT_{3.9} < 11.0$ and $BT_{3.7}$ $BT_{11} < 15$,the scene is considered probably clear (bit 26 set to 1). The test is designed to identify visibly bright but sparsely or non-vegetated areas.

3.2.9 Night Ocean Spatial Variability Test (bit 27)

The standard deviation of 3x3 arrays of 11 μm brightness temperatures centered on the pixels of interest is calculated for ocean scenes at night. The clear-sky ocean surface is usually very uniform over regions of this size and, in general, the presence of clouds increases the variability. The thresholds are 0.2K, 0.1K, and 0.05K for low, mid-point, and high confidences, respectively. The reader will note that these values are very restrictive, yet some very uniform low clouds are not detected by this test.

3.2.10 Confidence Flags

Each of the tests above returns a confidence level ranging from 1 (high confidence that the pixel is clear) to 0 (high confidence that the pixel is cloudy). The individual confidence levels must be combined to determine a final decision on clear or cloudy. We shall denote the confidence level of an individual test as F_i and the final quality flag as Q. There are different methods of combining these individual tests to yield the final quality flag (bits 1 and 2). We have experimented with a variety of methods of combining the confidence of individual tests. The primary effect occurs on the boundaries of the cloud system.

The final cloud mask confidence could be derived as a product of all the individual tests:

$$Q = \prod_{i=1}^{N} F_i \tag{22}$$

Using this product assures that any test that is high confident cloudy (confidence of 0) will set the final cloud mask as cloudy. This is the proper formulation if all the tests are conditionally independent; however, this is not the case. Different spectral tests are sensitive to the same type of cloud conditions as discussed below. A disadvantage of this product approach is that one cannot improve on the confidence level by increasing the number of tests (N) since $F_i \leq 1$. Thus, if 5 tests have a confidence of 0.95, the final result is $0.95^5 \approx 0.63$.

The final quality flag could also be set to the minimum confidence level of all applied tests:

$$Q = \min[F_i]. \tag{23}$$

This approach would be a clear-sky conservative approach. It makes it insensitive to any test other than the test that produces the minimum. That is, no matter what the other tests are indicating, a single low confidence test will set the quality flag to obstructed. On the other hand, a cloud conservative approach would be to select the maximum confidence level.

$$Q = \max[F_i]. \tag{24}$$

This can be improved upon by the following

$$Q = 1 - \prod_{i=1}^{N}\left[1 \pm F_i\right], \tag{25}$$

a clear-sky conservative case. A test with a high confident clear result sets the bit to clear. Thus, the MODIS cloud masking algorithm is clear-conservative, minimizing clear detection but missing clear regions that spectrally resemble cloud conditions.

Several tests are not independent of one another. For example, consider daytime over oceans in regions without sun glint. If stratocumulus clouds are present, the visible reflectance test, the reflectance ratio test and the $BT_{11} - BT_{3.7}$ will likely detect them. These same tests will likely miss the presence of thin uniform cirrus clouds, which would probably be detected by the tri-spectral tests (combinations of $BT_{8.7}$, BT_{11}, and BT_{12}). Very thin cirrus clouds would best be detected by the 1.38 and 13.9 μm tests, two tests that have difficulty detecting low-level clouds. Because of this overlap in the type of clouds different tests detect, each test is considered in one

of four groups. The five groups are:

Group I (Simple IR threshold test)

BT_{11}

$BT_{13.9}$

$BT_{6.7}$

Group II (Brightness temperature difference)

Tri-spectral test ($BT_{8.6}$ - BT_{11} and BT_{11} - BT_{12})

BT_{11} - BT_{12} thin cirrus test$BT_{7.3}$ - BT_{11}

BT_{11} - $BT_{3.9}$

Group III (Solar reflectance tests)

$R_{0.66}$ or $R_{0.87}$

$R_{0.87}/R_{0.66}$

Group IV (NIR thin cirrus)

$R_{1.38}$

Group V (IR thin cirrus)

$BT_{3.7}$ - BT_{12}

A minimum confidence is determined for each group,

$$G_{i=1,5} = \min[F_i]. \tag{26}$$

The final cloud mask is then determined from the product of the results from each group;

$$Q = \sqrt[N]{\prod_{i=1}^{N} G_i}\,. \tag{27}$$

This approach is still clear-sky conservative. If any test is highly confident that the scene is cloudy ($F_i = 0$), the final cloud mask is $Q = 00$.

The algorithm is divided into seven conceptual domains according to surface type and solar illumination:

1. daytime land,

2. daytime water,
3. nighttime land,
4. nighttime water,
5. daytime desert,
6. daytime snow/ice covered regions, and
7. nighttime snow/ice covered regions.

"Daytime" is defined as a solar zenith angle $\theta_0 < 85°$ (and the instrument is in daytime mode). The "desert" classification is based on the 1-km Olson World Ecosystems data set. A USGS 1 km land/sea tag file is used for land/water discrimination. For all observations within a given domain, it is generally expected that: (i) the same tests may be performed, and (ii) threshold values for each of these tests will not change.

3.2.11 Infrared Window Radiance Spatial Uniformity (Bit 25)

The infrared window spatial uniformity test (applied on 3 by 3 pixel segments) is effective over water and is to be used with caution in other situations. Most ocean regions are well suited for spatial uniformity tests; such tests may be applied with less confidence in coastal regions or regions with large temperature gradients (e.g., the Gulf Stream). Various spatial tests exist such as the spatial coherence and the ISCCP space contrast test.

The spatial coherence test (Coakley and Bretherton 1982) is based on the assumption of a uniform background and single-layered, optically thick cloud systems. The method is based upon the computation of the mean and standard deviation for a group of pixels using 11 μm radiances. When the standard deviation is plotted versus the mean, an arch shaped structure is often observed. The warm pixels with low values of standard deviation are assumed to be clear regions. The clear-sky FOVs can be selected as those within a standard deviation threshold (which is fixed at a small value) of the warm foot of the arch. Note that the derived clear-sky foot of the arch should have a temperature consistent with the thresholds derived using the individual FOV tests.

The ISSCP space contrast (sc) test, described in Rossow and Garder (1993), is similar to that of spatial coherence and is physically based upon the fact that clear pixels tend to be warmer than cloudy pixels and exhibit less spatial variability. First, for a small local region the pixel with the largest brightness temperature (BT_{11}^{max}) is found. All pixels colder than the spatial contrast ($BT_{11}^{max} - \Delta_{sc}$) value are labeled as cloudy; all others, including the warmest pixel are labeled as undecided. The size of the contrast threshold must be larger than the magnitude of natural variation at the surface and smaller than that caused by clouds. Values of Δ_{sc} near 3.5°C are common over ocean regions. It is important that the class of pixels be identical and that the size of the region be chosen carefully. When extending into coastal regions and land regions containing mixed land and water, pixels are excluded from this test since the inherent contrast between land and water surface radiances would dominate the results. For regions that are too large, there is increased likelihood of spatial variations in surface parameters. The shape of the test regions can also be important since meridional gradients in surface temperature generally are larger than zonal gradients.

The MODIS cloud mask currently uses a spatial variability test over oceans and large lakes. The tests are used to modify the confidence of a pixel being clear. If the confidence flag of a pixel is ≤ 0.95 but > 0.05, the variability test is implemented. If the difference between the pixel of interest and any of the surrounding pixel brightness temperatures is ≤ 0.5°C, the scene is considered uniform and the confidence is increased by one output confidence level (i.e., from uncertain to probably clear).

3.2.12 Visible Reflectance Uniformity Test (Bit 25)

The reflectance uniformity test (similar to CLAVR) is applied by computing the maximum and minimum values of MODIS band 1 (0.66 μm) or band 2 (0.87 μm) reflectances within a 3×3 pixel array. Pixel arrays with band 1 reflectance differences greater than threshold 1 (around 9%) over land or band 2 reflectance differences greater than threshold 2 (possibly 0.3%) over ocean are labeled in CLAVR as mixed (Stowe et al. 1995). The value over ocean is low because

a cloud-free ocean is almost uniformly reflective, while non-uniformity is assumed to be caused by cloudiness. This test is only applied to uncertain obstructed FOVs.

3.2.13 250-METER VISIBLE TESTS (BIT 32-47)

The reflectance test (Section 3.2.7) and the reflectance ratio test (Section 3.2.8) are used for clear-sky determination of the 250 m resolution channels. The results are a simple yes/no decision and incorporate the results from the 1 km resolution tests.

3.2.14 CLEAR-SKY RADIANCE COMPOSITE MAPS

Composite maps have been found to be very useful by ISSCP and other cloud detection algorithms. The MODIS cloud mask will eventually rely on composite maps, but to a lesser extent since the advantages of higher spatial resolution and more spectral bands will change the application and the need. Composite clear-sky radiance maps are also useful for quality assessment as demonstrated in Section 4, and are being implemented in the direct-broadcast version of the MODIS cloud mask.

ADDITIONAL CLEAR SKY RESTORAL TESTS (BITS 22 AND 26)

There are additional clear-sky restoral tests not mentioned elsewhere in the test descriptions. A simple NDVI (Normalized Difference Vegetation Index) test is invoked during daylight hours in areas characterized by a land/water mix and also in regions identified as shallow water. Spectral signatures of clear vs. cloudy skies are often convoluted and difficult to separate when land and water surfaces coexist in the same small region. Also, sediments at the bottom of shallow water bodies or suspended in water near river discharges can lead to ambiguous spectral signatures. The NDVI uses ratios of 0.87 and 0.66 μm reflectances (band 2 - band 1 / band 2 + band 1). If no spectral tests found evidence of high cloud and if this value is < -0.18 or > 0.40, then the pixel in question is labeled clear. Low values imply clear water while high values indicate clear land. When the values are between the two thresholds, the initial cloud mask result is not changed. The result is reported in bit 22.

Another test that may "restore" the cloud mask value to clear is performed in sun-glint regions. If the initial result for a given pixel is uncertain or cloudy and if no tests found evidence of high cloud, the following is performed. If the brightness temperature difference between bands 20 and 31 (3.75 and 11 μm) is > 15.0K and the ratio of band 17 to band 18 (0.895 to 0.935 μm) is > 3.0 and also if band 9 (0.443 μm) is *not* saturated, then the pixel is labeled as probably clear. Otherwise, it is called uncertain. These tests are an attempt to discriminate bright, low clouds from almost equally bright sun-glint off of cloud-free water surfaces. The thresholds are based largely on experience with the MODIS data. Thick water clouds often drive the band 17/18 ratio to low values due to lessened differential water vapor absorption and band 9 is often saturated over bright clouds. The brightness temperature difference threshold is set to indicate reflective surfaces so that initial cloud mask results are not modified in an area that is fairly dark and already handled well by other cloud tests.

4.0 Practical Application of Cloud Detection Algorithms

In summary, the cloud mask algorithm is divided into domains according to surface type and solar illumination: daytime land, daytime water, nighttime land, nighttime water, daytime desert, and daytime and nighttime snow or ice surfaces. "Daytime" is defined as a solar zenith angle $\theta_0 < 85°$. The "desert" classification is based on the 10-minute Olson World Ecosystems data set. A USGS 1 km land/sea tag file is used for land/water discrimination. For all observations within a given domain, it is generally expected that: (i) the same tests may be performed, and (ii) threshold values for each of these tests will not change.

Once a pixel has been assigned to a particular domain, MODIS observations for that location are subjected to a series of threshold tests designed to detect the presence of clouds in the instrument FOV. These tests are the heart of the cloud mask algorithm. There are several types of tests, none of which are effective at detecting all cloud types (e.g., low cloud, thin cloud, optically thick cloud). Accordingly, tests are grouped by cloud type to obtain an array of intermediate results that are then combined to form a final cloud mask value. The tests are grouped so that

independence between them is maximized. All tests that detect thin cirrus make up a group, for example, while those which find high, cold clouds form another group, and low-level cloud detection tests make a third group. Of course, few if any spectral tests are completely independent of all other tests.

Within a group the result of each spectral threshold test is expressed as a "confidence" that indicates the strength of the observed radiance signature compared to that which is expected for the cloud type in question. For example, one very fundamental test performed for water surfaces is the "cold cloud test." Over open water any scene with an observed 11 μm brightness temperature colder than ~270 K must be at least partially cloudy. Therefore, the temperature threshold for this test is set at that value. The optimal temperature threshold for any given FOV varies slightly, however, because of differing amounts of atmospheric water vapor attenuation due to changes in actual water vapor content or instrument view angle. Consequently, a "confidence window" is constructed to soften the impact of a floating optimal temperature threshold on the cloud for the result. For the cold cloud test the confidence window has boundaries at 267 and 273 K. Since the ultimate goal of the algorithm is to specify a confidence of clear-sky, an observed brightness temperature of < 267 K is defined to have 0 confidence while a measurement of > 273 K has a confidence of 1. *Note that this confidence does not yet refer to the final cloud mask result, but only to the particular condition tested.* In this case it indicates only the extent of confidence that the FOV did *not* contain significant amounts of opaque, cold clouds. Observations between 267 and 273 K result in confidences ranging linearly between 0 and 1. Figure 4 showed an example of the relationship between test thresholds and confidence boundaries.

When all tests within a group have been performed, the minimum resulting confidence from among them is taken to be representative of that group (i.e., the "group confidence"). Group confidences indicate absence of particular cloud types. A final step is to combine the group confidences, assumed to be independent, by multiplying them together to yield a final confidence of clear-sky conditions.

Using this algorithm, most observations result in confident clear (> 0.95) or very low confi-

dence (< 0.66) of unobstructed view of the surface. There are always those difficult scenes, however, that result in intermediate confidences (i.e., 0.66-0.95). These tend to be found at cloud boundaries, or where low clouds are found over water surfaces at night, or over certain land surfaces such as desert or other sparsely vegetated regions. In these cases, spatial and/or temporal continuity tests are conducted. Currently, only spatial continuity testing has been implemented and this only for water surfaces. The 11 μm brightness temperature differences between the pixel of interest and the surrounding eight are checked for consistency. If all the differences are less than 0.5 K, the confidence is adjusted upward by one "level" (e.g., > 0.66 to > 0.95). We also plan to use a "clear-sky data map" for testing temporal continuity in order to better discriminate clear-sky scenes from any surface type. This processing continues in development.

4.1 Ancillary Data Set Requirements

A number of preprocessing steps are made before the cloud masking algorithm is applied. First, each pixel in the scene is tagged as being land or water, and if land, a land/water percentage is assigned. Second, each land pixel is classified by ecosystem, and its elevation is designated as relatively flat, valley, isolated mountainous region, low mountains or hills, generally mountainous, or extremely rugged mountains. From the MODIS snow mask each pixel will be designated as probably/probably-not snow or ice covered (MOD10 and MOD29).

4.2 Implementation of the Cloud Mask Algorithms

4.2.1 OUTLINE OF CLOUD MASK ALGORITHM

The hierarchical approach used in the cloud mask is:

(1) Determine if the pixel is of a land or water scene.

(2) Determine the ecosystem type.

(3) Determine if pixel is in a sun glint region.

(4) Determine if the pixel is in a day or night regime.

(5) Retrieve information from independent snow cover and ice database.

(6) Update snow cover by implementing simple Normalized Difference Snow Index (NDSI).

(7) Apply appropriate single FOV spectral tests and set initial unobstructed FOV determination for the given domain. Initial confidence flag is assigned for each test result, depending on its relative position to the threshold (see Section 3).

- For daytime testing, solar zenith angles are constrained to be less than 85°.
- Ocean tests are applied between 60°N and 60°S and for large lakes.
- Sun glint occurs when the reflected sun angle lies between 0° and 36°. Reflectance of open water is strongly influenced by illumination and viewing geometry. Sun glint is also a function of surface wind. Wind speed is currently not used in estimating the sun glint area.
- The land algorithm is applied to non-desert and non-water areas between latitudes from 60°N to 60°S, including islands.
- The desert algorithm is applied to desert ecosystems between 60°N and 60°S latitude.
- The polar algorithm is applied to regions poleward of 60°.
- For the single pixel clear-sky determination, 14 single FOV tests are implemented and an obstructed/not obstructed bit set (0 for obstructed, 1 for clear) for each test (bits 8-23).

(8) The single FOV cloud test results are grouped and the group confidence determined.

(9) The group minimums are then multiplied together, and the N^{th} root taken (where N represents the number of groups) to produce the initial cloud mask (Section 3.2.11). If any of the individual tests are high confidence cloudy (clear confidence of 0), the product is zero.

(10) If confidence level is still uncertain ($0.05 < Q < 0.95$), use spatial uniformity tests on 3×3 pixel regions (Currently not implemented over land).

- Spatial IR variability test applied with band 31 using $\Delta_{sv} = 0.50$ K over water.
- Adjust quality flag if appropriate by increasing or decreasing confidence levels.

(11) Check for temporal consistency (currently applied over water).

- Compare with clear-sky composite.

- Adjust quality flag if appropriate by increasing or decreasing confidence levels

(12) Run restoral tests in appropriate cases.

4.2.2 CLOUD MASK EXAMPLES

The cloud mask algorithm has been applied to several data sets selected by the cloud mask group, as well as scenes selected by other science team members. This section includes several examples of the output from the MODIS cloud mask. It is not intended as a validation section, but rather as a visual indication of the success and problems of the current version.

MODIS cloud mask examples

This section demonstrates the results of the cloud mask algorithm applied to the MODIS instrument. In the cloud mask examples, green represents high confidence clear, blue confident clear, red uncertain and white low confident clear.

Figure 13 is an example of the cloud mask results for a scene over Lake Chad. Band 2 (0.87 μm) and Band 31 (11 μm) images are shown in figure 13a and 13b respectively. The Band 31 image demonstrates the influence of a dust storm near the top of the image. Because of its signature in Band 31, most of the dust storm is labeled as cloud or uncertain. The 250-m cloud mask is a yes/no clear-sky decision (gray is clear, white obstructed). Striping in Band 26 (1.38 μm) results in striping of the cloud mask as seen in the 250-m mask. Destriping the 1.38μm image removes the stripes in the cloud mask.

Band 26 (1.38 μm channel) has striping and cross-talk; a correction algorithm developed at the University of Wisconsin is being tested and readied for implementation on MODIS L1B[1]. The impact is demonstrated graphically in Figure 14.

---

[1] C. Moeller, personal communication.

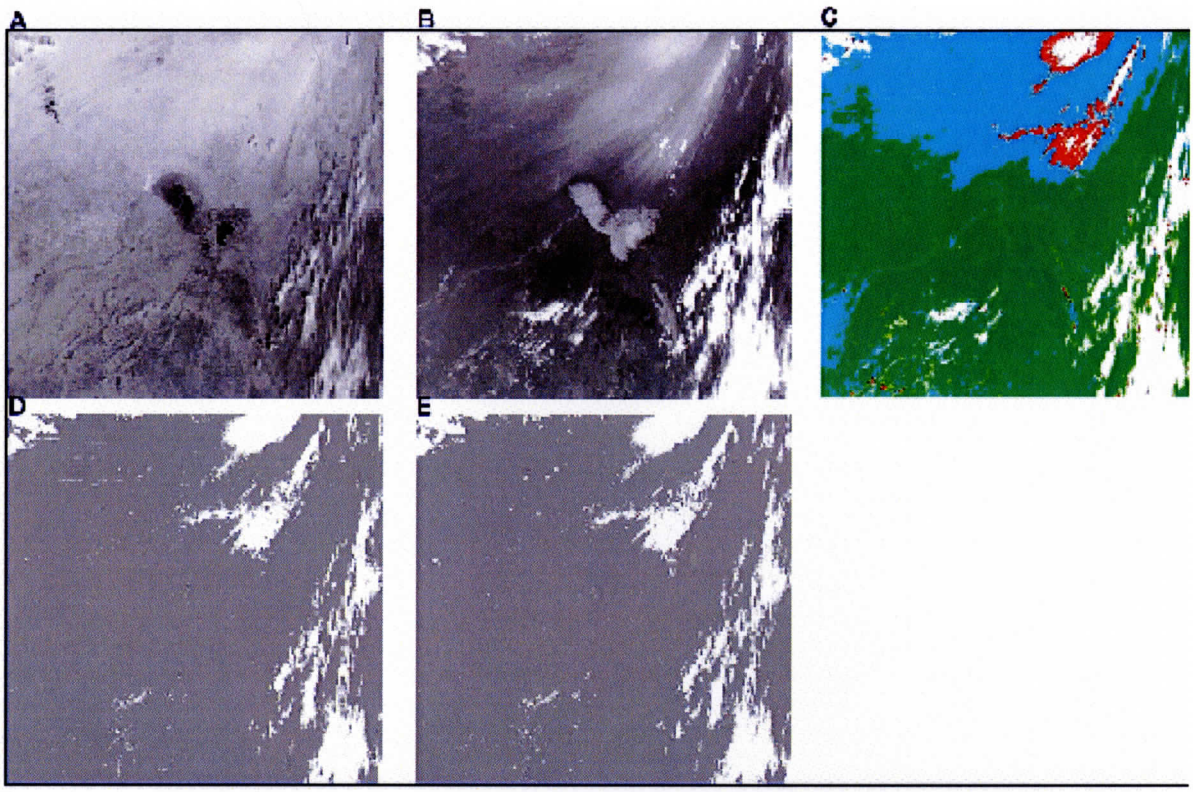

Figure 13. An example cloud mask from a scene over Lake Chad. The upper left-hand figure (A) is the MODIS Band 2, the upper middle image (B) Band 31, and the four-color image (C) is the final cloud mask result. The bottom left (D) is the 250 m cloud mask result, and the image labeled E is the 250 m cloud mask destriped data. A dust storm is observed in (B) and is flagged as cloudy in the cloud mask (C). A comparison of D and E demonstrates the impact of the striping on the cloud mask results.

Figure 15 is a complicated scene on 18:10 UTC December 10, 2000. Surface temperatures are very cold about –28C in North Dakota and southern Manitoba and Saskatchewan. A three-color composite made from MODIS bands 20 (3.9 μm, red), 6 (1.6 μm, green), and 26 (1.38 μm, blue) shows water clouds as green, ice clouds as blue or purple, and snow as red. Note the pale, purple feature extending southeastward from the top left of the image toward the center and terminating in southern North Dakota. This feature is obvious only in Band 26 (see Panels B, C, and D), appearing to be a very thin ice cloud although further analysis indicated a water vapor feature. The corresponding MODIS Band 2 image is shown in Panel B, and Panel C is the destriped 8.5-11 μm brightness temperature differences. Because of a small ($\leq$ 0.2K) scene mirror side influence on Band 31 brightness temperature, a constant multiplier was applied to the radiances of one mirror side leading to the smoothed data shown in Panel C. This 8.5-11 μm dif-

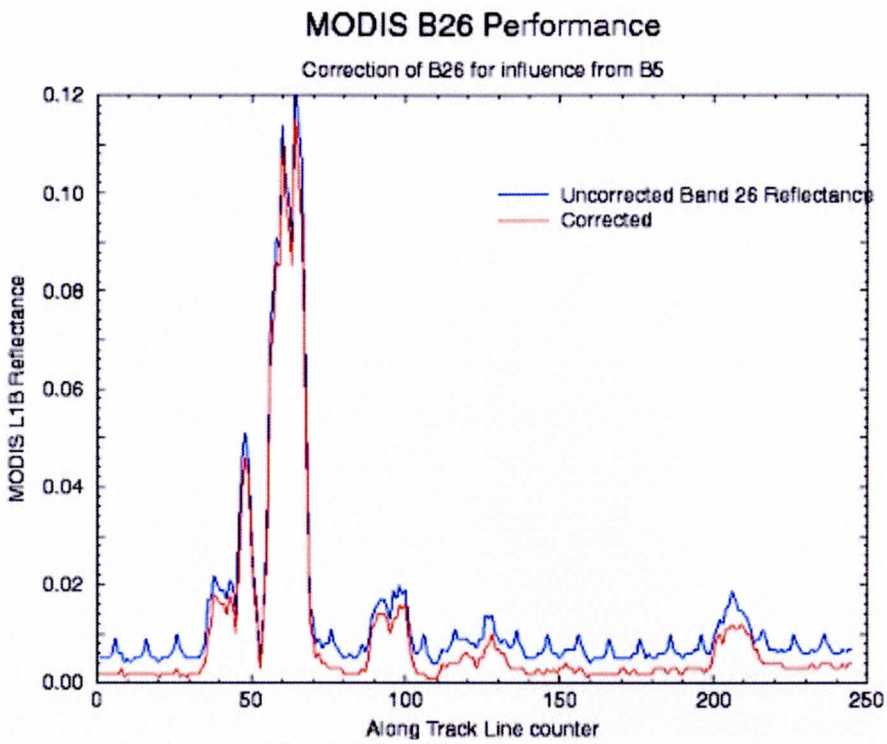

Figure 14. The uncorrected and corrected Level 1b Band 26 reflectance. Detector dependent correction of Terra MODIS Band 26 (1.38 μm) image for striping and out of the band influence, allowing better detection of thin cirrus cloud by the MODIS cloud mask.

ference is used in the snow determination algorithm within the cloud mask. Regions with differences > 0.5K are considered to be ice clouds, not ice cover on the surface. In Panel E, gray indicates snow or ice cover on the surface. The effect on the final cloud mask may be seen in Panel F. Areas not determined to be snow-covered are incorrectly labeled as cloudy.

The corrected image of Band 26 (1.38 μm) reflectance is shown in Panel D. Detector striping and surface reflection have been reduced leading to greater contrast. The detector dependent correction applied to Band 26 is empirically defined from an analysis of Band 5 versus Band 26 radiances. Elimination of detector striping has a positive impact on the final cloud mask as seen in the before (Panel G) and after (Panel F) images. The stripes in Panel G surrounding (what appears to be) the extremely thin cirrus cloud have been eliminated in Panel F. This correction will allow the full use of Band 26 for thin cirrus detection by allowing 1.38 μm cloud test thresholds to be lowered for collection four of MODIS data and products. This image demonstrates an issue in using the 1.38 μm channel over snow with low atmospheric water vapor amounts—the surface

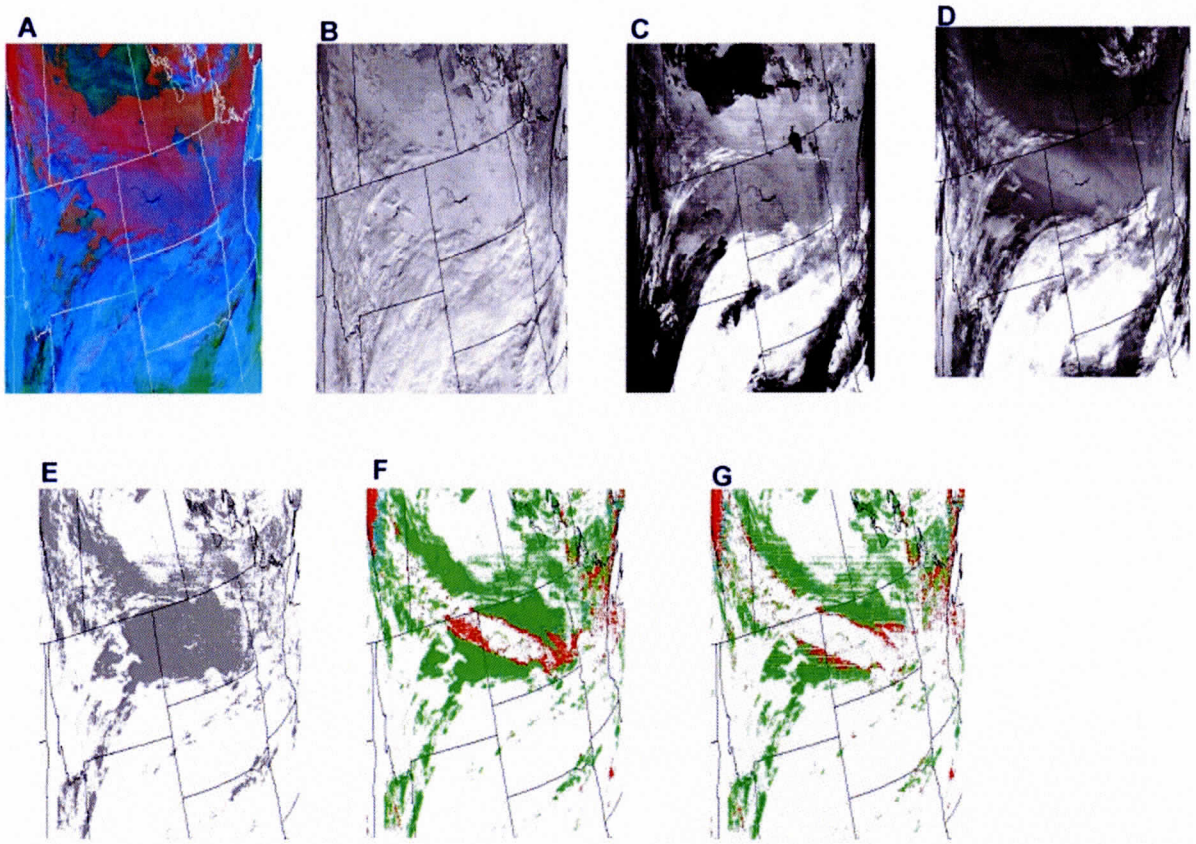

Figure 15. Analysis of a MODIS image over North Dakota and southern Manitoba region on 18:10 UTC December 10, 2000. A) a three-color composite made from MODIS bands 20 (3.9 μm, red), 6 (1.6 μm, green), and 26 (1.38 μm, blue),Water clouds are seen as green, ice clouds are blue or purple, snow is red. B) MODIS Band 2 image, C) the destriped 8.5-11 μm brightness temperature differences, D) destriped MODIS Band 26 image, E) resulting MODIS snowpath bit, F) MODIS cloud mask result, G) MODIS cloud mask result without corrections. (See text for details.

reflected radiance is measured by the detector and in a dry atmosphere results in a false cloud. For this reason, 1.38 μm data is not used for scenes with an altitude greater than 2 km.

4.3 Interpreting the cloud mask

This section provides examples of how to interpret output from the cloud mask algorithm. They are suggested approaches and not strict rules, and recognize that each MODIS science team member will know how to best use the cloud mask for their applications. We are open to working with science team members to develop interpretation procedures similar to those listed below.

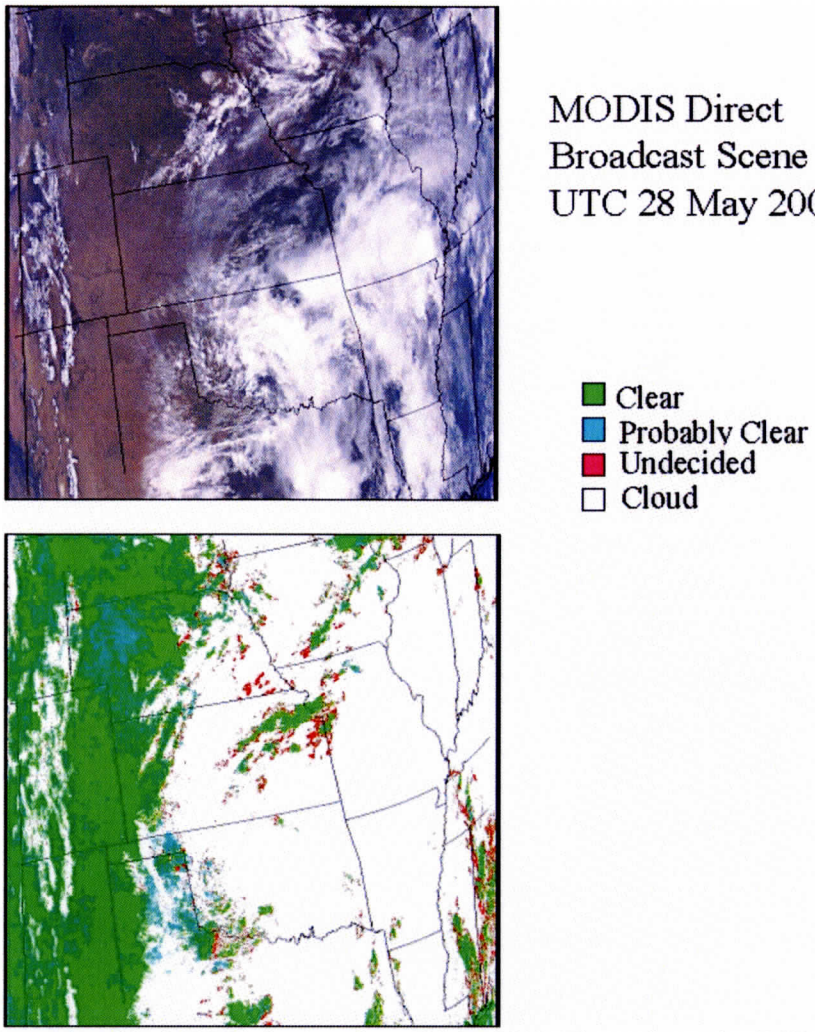

Figure 9. The results of the MODIS cloud mask on 28 May 2002. The top image is a RGB image in the vicinity of the DOE ARM site. The cloud mask result is shown in the bottom image. This MODIS data was collected by the SSEC Direct Broadcast system.

4.3.1 CLEAR SCENES ONLY

Certain applications have little tolerance for cloud contamination. This is an example of how these applications (e.g., bi-directional reflectance models) might interpret the cloud mask output.

1. Read bit 0 to determine if a cloud mask was determined; if this bit is 0 no further processing of the pixel is required.
2. If necessary, read bits 3 through 7 to determine scene domain.

3. Read bits 1 and 2; if both bits are *not* equal to 1, then some tests suggest the presence of cloud, and the pixel is skipped.
4. Read bit 9 to determine if a thin cirrus cloud is present (bit value of 0). An optically thin cirrus cloud may set bit 9 but not be classified as a cloudy scene.
5. Daytime algorithms may (depending on application) read bits 32 through 47 to assess potential subpixel contamination or scene variability.

4.3.2 CLEAR SCENES WITH THIN CLOUD CORRECTION ALGORITHMS

Some algorithms may be insensitive to the presence of thin cloud or may apply appropriate correction algorithms. This is a suggested application; after launch minor modifications may be implemented depending on the performance of the cloud masking algorithm. Two examples are given, one that might be appropriate for Normalized Difference Vegetation Index (NDVI) and the second for sea surface temperature (SST) retrievals.

Interpretation procedure that might be useful for NDVI retrievals:

1. Read bit 0 to determine if a cloud mask was determined; if this bit is 0, no further processing of the pixel is required.
2. Read bits 3 through 7 to determine if scene domain is appropriate (e.g., land and day-time)
3. Read the confidence flag—bits 1 and 2. If high confident cloudy (value of 00), do not process pixel. A value of 01 for bits 1 and 2 (possibly cloudy) often occurs around cloud edges and retrieving NDVI may not be appropriate with this confidence level. If both bits are equal to 1, then most tests are suggesting clear scenes; proceed with steps 4-7. If confidence bits are 10, then detailed checking of bits 13 through 25 may be required to determine NDVI algorithm processing path.
4. Read bit 9 to determine if a thin cirrus cloud is present (bit value of 0). An optically thin cirrus cloud may set bit 9 but not be classified as a cloudy scene. Some of the MODIS solar channels are not as sensitive to thin cirrus as the 1.38 μm band (see

Figure 1 for an example). If thin cirrus is detected, apply appropriate correction algorithms.

5. Check that reflectance tests (bits 20 and 21) did not detect cloud. Note that a value of 0 indicates that either a cloud is present or the test was not run. This test is not run if over snow or solar zenith angles greater than 85°.
6. Read bits 32 through 47 to assess cloud contamination. This would not be recommended if snow were indicated.

Interpretation procedure that might be useful for SST retrievals.

1. Read bit 0 to determine if a cloud mask was determined; if this bit is 0, no further processing of the pixel is required.
2. Read bits 3 through 7 to determine if the scene is water or if sun glint is present.
3. Read the clear confidence flag—bits 1 and 2. If high confident cloudy (value of 00), do not process pixel. A value of 01 for bits 1 and 2 (possibly cloudy) often occurs around cloud edges and retrieving SST may not be appropriate with this confidence level. If both bits are equal to 1, then most tests are suggesting clear scenes; proceed with steps 4-9. If the confidence is 10, then detailed checking of bits 13 through 25 may be required to determine SST algorithm processing path. For example, if confidence bits are 10 and pixel is in a sun glint region, determine how many IR tests are detecting cloud. If all IR tests are passing, then continue with steps 4-8. If the IR tests are failing, then pixel contamination is likely. In this case the SST should either be retrieved with caution, or appropriate corrections to the IR channels should be made.
4. Read bit 9 to determine if a thin cirrus cloud is present (bit value of 0). An optically thin cirrus cloud may set bit 9 but not be classified as a cloudy scene. If thin cirrus is detected, apply appropriate IR correction algorithms. Corrections require other cloud products, such as cloud emissivity and cloud effective temperature (MOD06).
5. Check that IR tests did not detect cloud. The greater the number of IR tests that did

not detect cloud, the more confidence one has in the SST product. Note that a value of 0 indicates that either a cloud is present or the test was not run.

6. Check spatial variability test results. Uniform scenes increase confidence that pixel is clear and improves SST accuracy.
7. Read bits 32 through 47 to assess subpixel cloud contamination. This would not be recommend in sun glint regions.

4.3.3 CLOUDY SCENES

Use of the cloud mask for cloud scene processing may require a more in-depth analysis than clear-sky applications, as the mask is clear-sky conservative in that it minimizes false clear. Here we consider a few approaches to interpret the cloud mask for cloud property retrievals during the day, which are a function of processing path.

Daytime ocean scene, non-sunglint:

1. Read bit 0 to determine if a cloud mask was determined; if this bit is 0, no further processing of the pixel is required.
2. Read bit 3, if this bit is 0 no further processing of the pixel is required (night).
3. Read bits 6 and 7, if 00 then water scene so proceed.
4. Read bit 4, if 0 then sunglint region, may want to place less confidence on product retrieval.
5. Read the confidence flag—bits 1 and 2.
   - If high confident clear (value of 11), Read bit 9 to determine if a thin cirrus cloud is present (bit value of 0). An optically thin cirrus cloud may set bit 9 but not be classified as a cloudy scene. If thin cirrus is detected, apply appropriate algorithms or place less confidence on product retrieval. If bit 9 is 1, it is clear sky and no further processing is required.
   - If both bits are equal to 00, then the scene is cloudy. Check bit 8 for possible heavy aerosol loading. If bit 8 is 0 then pixel may be aerosol contaminated, no

further processing or place less confidence on product retrieval. If bits are 00 then check individual test to determine ice or water phase. For example, if bit 21 is 0 and bit 13 is 1, probably water cloud scene. If bits 16 and 17 are 0, probably an ice cloud.

- If confidence is 10 or 01, then detailed checking of bits 13 through 25 may be required to determine if algorithm should be executed. For example, if confidence bits are 10 and pixel is in a sun glint region, additional testing is advised.

6. Check how many tests detected cloud. The greater the number of tests that detected cloud, the more confidence one has in the cloud property product. Note that a value of 0 indicates that either a cloud is present or the test was not run.
7. Check spatial variability test results.
8. Read bits 32 through 47 to assess subpixel cloud contamination. This would not be recommended for region with sun glint.

Daytime dark vegetated land regions (for example, forests):

1. Read bit 0 to determine if a cloud mask was determined; if this bit is 0, no further processing of the pixel is required.
2. Read bit 3, if this bit is 0 no further processing of the pixel is required (night).
3. Read bits 6 and 7, if 11 then land scene so check ecosystem for correct type.
4. Read bit 4, if 0 then sunglint region, may want to place less confidence on product retrieval.
5. Read the confidence flag—bits 1 and 2.
   - If high confident clear (value of 11), Read bit 9 to determine if a thin cirrus cloud is present (bit value of 0). An optically thin cirrus cloud may set bit 9 but not be classified as a cloudy scene. If thin cirrus is detected, apply appropriate algorithms or place less confidence on product retrieval. If bit 9 is 1, it is clear sky, no further processing is required.
   - If both bits are equal to 00, then the scene is cloudy. Check bit 8 for possible

heavy aerosol loading. If bit 8 is 0 then pixel may be aerosol contaminated, no further processing or place less confidence on product retrieval. If bits are 00 then check individual test to determine ice or water phase. For example, if bit 21 is 0 and bit 13 is 1, probably water cloud scene. If bits 16 and 17 are 0, probably an ice cloud.

- If confidence is 10 or 01, then detailed checking of bits 13 through 25 may be required to determine if algorithm should be executed. For example, if confidence bits are 10 check the number of solar tests passed, if bits 16, 20, 21 and 23 are 1 then IR tests are indicating cloud, probably do not want to process retrieval that depend on solar techniques or place less confidence on product retrieval.

6. Check how many tests detected cloud. The greater the number of tests that detected cloud, the more confidence one has in the cloud property product.
7. Read bits 32 through 47 to assess subpixel cloud contamination. This would not be recommended for region with variable surface reflectance.

Detection of clouds over snow and ice is a difficult problem. One procedure for interpreting the cloud mask output for daytime snow/ice retrieval algorithms follows.

1. Read bit 0 to determine if a cloud mask was determined; if this bit is 0, no further processing of the pixel is required.
2. Read bits 3 through 7 to determine if scene domain is appropriate (e.g., daytime and non-desert).
3. Read bit 5 to determine if snow processing path.
4. Read bits 1 and 2 - the final confidence flag.
    - If high confident cloudy (value of 00) do additional testing. Check bit 19, if cloudy probably low level water cloud.
    - If bits are 10 or 01, check bit 19, if cloudy probably low level water cloud.
    - If high confidant clear (value of 11), check for the possible presence of thin cirrus (bit 9 and bit 11).

An interpretation procedure for application with aerosol retrieval algorithms is:

1. Read bit 0 to determine if a cloud mask was determined; if this bit is 0, no further processing of the pixel is required.
2. Read bits 3 through 7 to determine scene domain is appropriate for aerosol retrieval (e.g., daytime land, daytime water, non-desert processing path)
3. Read bit 4 for sunglint contamination, proceed as appropriate.
4. Read bit 5 for snow/ice contamination.
5. Read bits 1 and 2 - the final confidence flag.
   - If high confident clear (value of 11), search for aerosol. If bit 9 is 0, possible contamination by thin cirrus or high aerosol.
   - If bits 1 and 2 are 00, check bit 8 for heavy aerosol condition. If bit 8 is 0, run aerosol retrieval algorithm.
   - If high confidant clear (value of 11), check for the possible presence of thin cirrus (bit 9 and bit 11).
   - If land bits are 01 or 10, check bit 8 for heavy aerosol, if bit 8 is 0 proceed with retrieval. If bit 8 is 1 (cloud mask aerosol test did not indicate heavy aerosol), check additional bits.
     - check bit 11, if cloudy (bit is 0) cirrus is probably present
     - if bit 19 is 0, probably indicates the presence of a low level cloud, don't process
     - if bit 21 (ratio test) is 0 and appropriate ecosystem (vegetation) probably cloud contaminated scene

4.4 Numerical Programming Considerations

The MODIS cloud mask algorithm runs in production at the Goddard DAAC. The mask was developed at the UW on a SGI with 16 R10000 chip processors. A typical 5 minute MOD35 granule takes anywhere from 350 - 500 seconds (~5-8 minutes) to produce, depending on the

granule time of day (night granules require less processing) and background (more tests are performed over some ecosystems.) The maximum memory usage is 129 MB. The output product is 47.6 MB per granule. A full day (288 granules) volume will be 47.6 MB x 288 granules/day = 13.7 GB/day.

The direct broadcast version of the software has been developed and tested on numerous Unix platforms. This version has been stripped of the SDP toolkit functions. A typical 5 minute granule of data requires ~60 seconds less to process and the max memory usage is 55 MB. The file sizes are about the same. For more information on the direct broadcast cloud mask version and the International MODIS Processing Package please see the UW direct broadcast web page at http://cimss.ssec.wisc.edu/~gumley/IMAPP/.

4.5 Quality Control

An entire document has been written by the atmosphere group relating to Quality Assessment and Quality Control. Please refer to the MODIS Atmosphere Group QA Plan at modis-atmos.gsfc.nasa.gov/_docs/QA_Plan_2000_07.pdf.

4.6 Validation Plan

This section presents some of the strengths and weaknesses of the MODIS cloud mask algorithm. Validating cloud detection is difficult [*Ackerman and Cox* 1981; *Rossow and Garder*, 1993b; *Baum et al.*, 1995, *Ackerman et al*, 1998]. Two important steps in validation are image interpretation and quantitative analysis. In image interpretation, an analyst conducts a validation through visual inspection of the spectral, spatial, and temporal features in a set of composite images. Visual inspection is an important first step in validating any cloud mask algorithm. The analyst uses knowledge of and experience with cloud and surface spectral properties to identify obvious problems. However, visual inspection provides poor quantitative evaluation. More quantitative validation can be attained through direct pixel by pixel comparison with collocated ground or instrument platform based observations, such as lidar. While this approach provides quantitative accuracy, it possesses the problem that the two measurement systems often observe

different cloud properties [*Baum et al.*, 1995]. This section provides some validation examples using image interpretation and quantitative analysis. This section provides examples of the MODIS cloud mask algorithm results.

Comparison of MODIS radiances and products with those from other instruments will be made periodically in different seasons in daytime and nighttime conditions. We anticipate numerous opportunities in which scientists worldwide will compare MODIS-derived data products with local measurements of the geophysical property of interest. This wide-scale synthesis of data sets from scientists from Australia, Japan, China, Europe, South America, and Africa will greatly enhance the confidence that we place in the MODIS-derived products, and will, with time, aid our ability to assess the quality of the data products from a wide variety of climatic conditions and seasons.

4.6.1 AIRCRAFT OBSERVATIONS OF CLOUDS

Key measurements for this validation approach will be MODIS observations collocated with measurements from the ER-2 instruments (MAS, CLS, HIS, passive microwave, multi-angle camera). The major limitation of this approach is establishing statistical significance of the case study samples. The major strength is that it provides a very complete cloud data set. This validation approach relies heavily on the source of data that helped in the algorithm development, primarily the MAS. There have been several field campaigns with the ER-2 carrying the MAS over varying scenes and different ecosystems. These field programs offered opportunities for pre-launch and post-launch MODIS validation through collection and analysis of observations obtained from the MAS and HIS. These field campaigns often include the Cloud and aerosol Lidar System (CLS; Spinhirne et al. 1989) for verifying cloud detection.

The Subsonic Aircraft Contrail and Cloud Effects Special Study (SUCCESS) field experiment was conducted in April-May 1996, with the goal of determining the radiative properties of cirrus contrails, and of contrasting them with naturally occurring cirrus. To assess the radiative impact of these clouds required a well-calibrated set of radiation measurements and "ground (or

in situ) truth" observations. We acquired MAS multispectral observations along with CLS cloud height measurements from the NASA ER-2 aircraft by coordinating over flights of the ER-2 with in situ aircraft and ground based measurements. To quantify the MAS cloud mask algorithm performance, comparisons are made with observations from the Cloud Lidar System (CLS) [*Spinhirne and Hart* 1990]. During the SUCCESS, the MAS flew along with the lidar. The CLS algorithm detects a maximum of five cloud top and cloud bottom altitudes based upon the back-scatter signal. Each collocation consists of the CLS cloud product and approximately 250 to 300 MAS pixels. The percentage of pixels labeled confident clear, probably clear, uncertain, and low confident clear are determined for each collocated scene. The CLS observations are divided into three categories:

Clear—no cloud was detected by the lidar;

Thin cloud—cloud boundary was detected, but a surface return signal was also received;

Thick cloud—cloud boundary was detected with no surface return signal.

Histograms of the percentage of pixels in a given confidence interval are plotted for each CLS cloud type category (see Figure 17). Nearly all of the CLS labeled clear scenes are identified as high confident clear by the MAS cloud mask algorithm. Essentially all of the CLS labeled thick cloud scenes are labeled as cloudy by the MAS cloud mask. A majority of the thin cloud cases are labeled as either confident clear or cloudy by the MAS cloud mask algorithm. Differences between those scenes labeled clear and those classified cloudy are related to the cloud thickness. A more detailed analysis is required for verification of these thin clouds. Such a study is in progress. Also encouraging from this comparison is that few of the scenes are labeled as uncertain. Visualization of the cloud mask indicates that many of these scenes occur near cloud edges.

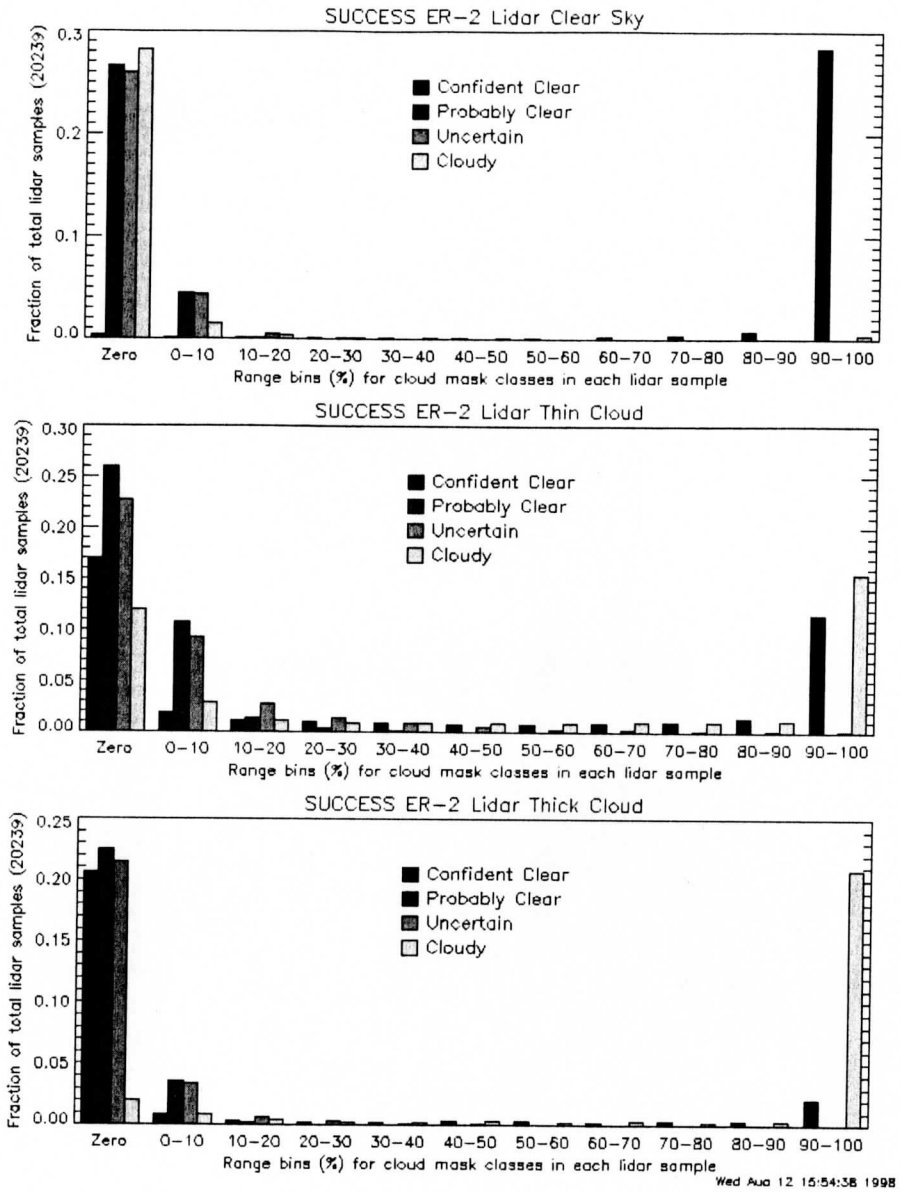

Figure 17. Comparisons between the cloud detection results using MAS and cloud lidar system for five days of the SUCCESS experiment. Cloud mask confidence is compared with three lidar categories: no cloud (top panel), thin cloud (middle panel), and thick cloud (bottom panel).

4.6.2 COMPARISON WITH SURFACE REMOTE SENSING SITES

Figure 18 is a visual analysis of the MODIS cloud mask performance over the DOE Southern Great Plains ARM site. Validation of this scene consists of visual inspection of the imagery. A great many scenes have been evaluated from all regions, surface types, and seasons. For ex-

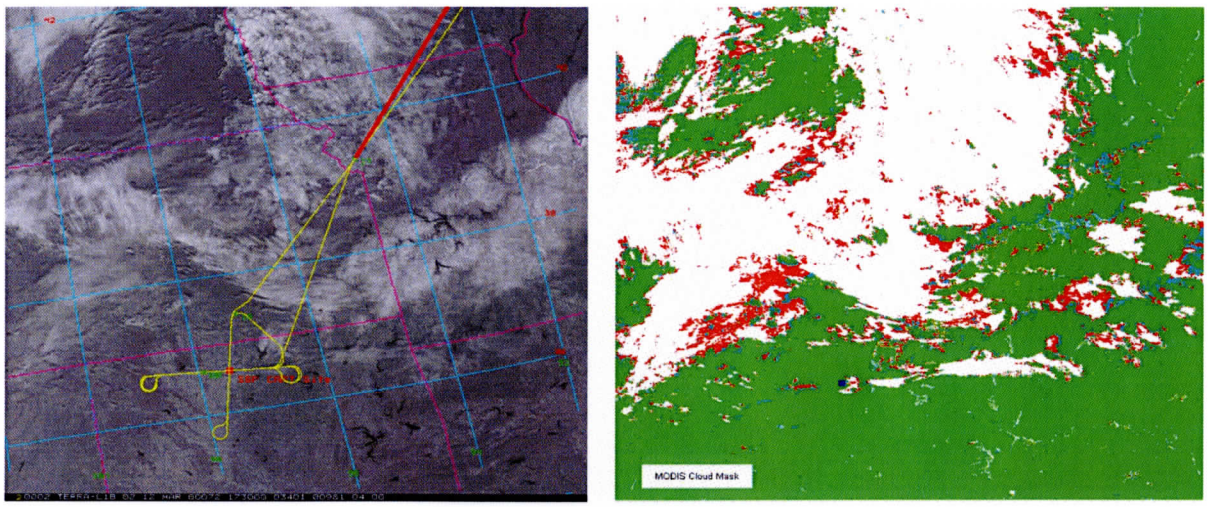

Figure 18. An example cloud mask result over the DOE ARM Southern Great Plains Site. The left image shows the ER-2 flight track (yellow line) superimposed on the MODIS 0.86 μm image from 17:10 UTC March 12, 2000 during WISC-T2000. The cloud mask result is shown at right.

ample, an analysis of multi-spectral MODIS imagery reveals that the cloud mask in the above case properly discriminates cloud from both snow and non-snow covered surfaces. The image on the right shows the cloud mask result. We have compared cloud mask results with ground-based lidar and radar data from the SGP CART Site (red dot on left-hand image).

Results of the cloud mask will be compared to ground based measurements such as lidar, radar, passive microwave and optical radiometers. The advantage is that comparisons will be conducted throughout the lifetime of the MODIS and thus provide proper sampling for statistical analysis. The disadvantage is that the ground-based sites will not represent all climate regimes. There are inherent difficulties in comparing data with vastly different spatial and temporal resolutions and sensitivities.Data used for validation purposes comes from the Department of Energy's (DOE) Atmospheric Radiation Measurement (ARM) program Cloud and Radiation Test bed (CART) site near Lamont, OK. This includes cloud top height derived from a ground-based combination Micropulse Lidar/Millimeter Cloud Radar (MPL/MMCR), which uses an algorithm developed by Clothaiux et al (2000). MPL/MMCR output is every ten seconds during the IOP. Since the MPL/MMCR is subject to attenuation effects and local cloud top height deviations at the single observation point over the CART site, the data need to be adjusted to better match the MODIS observations. This was achieved by using a range binning process which entailed plac-

Table 10. Comparison of scene classifications by the MODIS cloud mask and by coincident ground-based liadar and radar observations at DoE's Southern Great Plains ARM site.

Radar/lidar	MODIS Cloud	MODIS Uncertain	MODIS probably clear	MODIS clear	Total observations
Clear	19	6	85	65	175
Low Cloud	82	0	4	3	89
Middle Cloud	44	3	13	0	60
High Cloud	14	1	6	3	24
	159	10	108	71	

ing every MPL/MMCR observation surrounding the MODIS sounder observation time (five minutes before and after the MODIS observation time was used) into range bins of 250m. Each range bin must have a given number of observations in it to be considered valid, in this case 40% of the observations. A direct comparison was made between the MODIS and MPL/MMCR cloud detection. This is a yes/no comparison; either the instrument is reporting a cloud top height or it is not. For this comparison, the temporal threshold for the MPL/MMCR data set was set to a very low value 16% of observations needed for a valid cloud. The value was set low in order to minimize attenuation effects of the instruments. The MODIS cloud detection algorithm and MPL/MMCR agree on the existence of clear or probably clear 86% of the time (85+65/175), and 92% of the time that a cloud was present.

The ground-based measurements will be obtained on a continuous basis as well as during intensive field experiments. All of these validation opportunities, as well as comparison of data derived from MODIS with other sensors on Terra, Aqua and other spacecraft will be investigated. For example, MODIS cloud retrievals will be compared to analyses of other instruments such as MISR and AIRS. This comparison provides global coverage.

4.6.3 INTERNAL CONSISTENCY TESTS

Figure 19 shows histograms of radiance observations as a function of final clear sky confidences according to the MODIS cloud mask. The top left plot shows how the distribution of visible ratios changes with clear sky confidence. The vertical lines near the center define the threshold interval for this cloud test (confidence of 1.0 at left to 0.0 at the right). One may con-

clude that the thresholds have been chosen properly as very few, if any, clear sky confidences

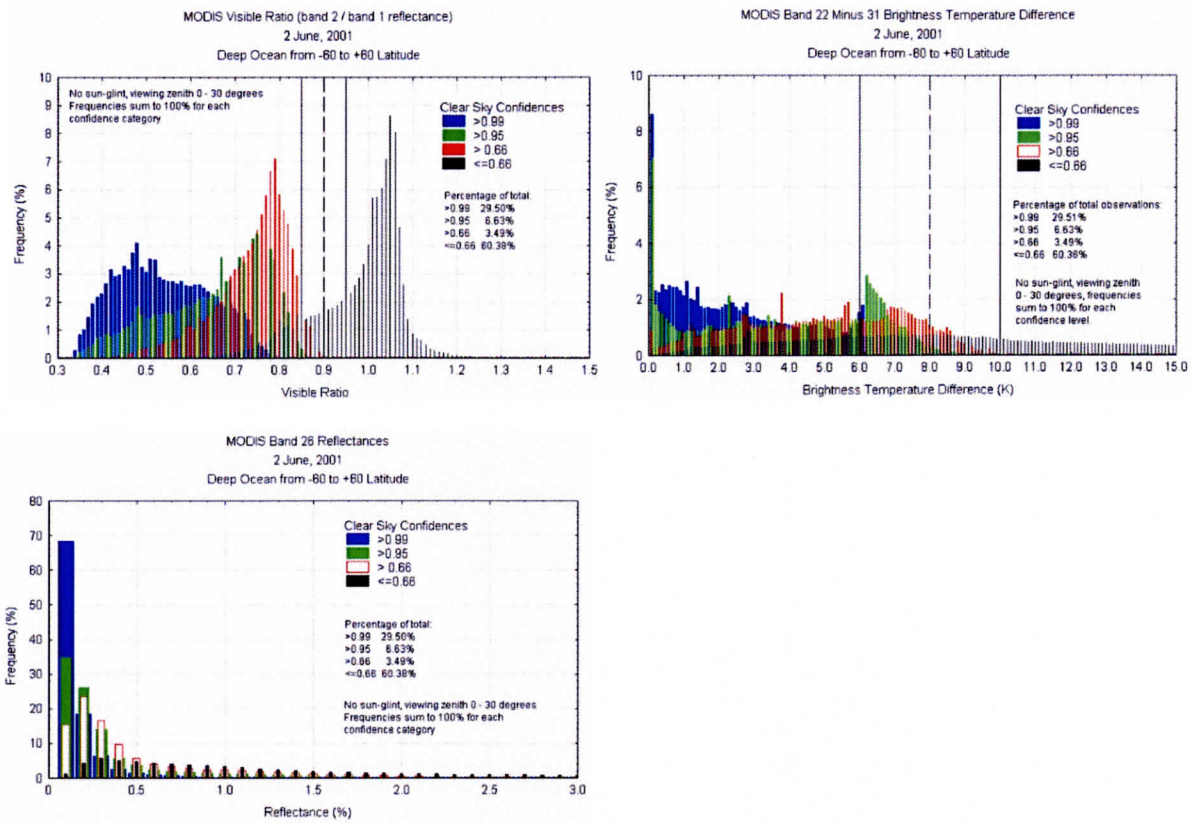

Figure 19. Histograms of MODIS observations on 2 June 2001 over deep ocean regions between 60 degrees North and South latitude as a function of the final cloud mask result. See text for details.

>0.95 fall within the interval. From the figure, however, one sees that part of the distribution of observations denoted as clear (blue) or probably clear (green) falls inside the threshold interval. One could conclude that these thresholds should be reduced (moved left on the graph). Also shown is the distribution of 1.38 μm reflectances (lower right). The threshold interval for this test begins at 3.0% and cannot be shown on the plot. Striping in the (uncorrected) data means that cloud thresholds must be set too high to make optimum use of MODIS band 26. We will also continue with internal consistency checks like the ones shown at left. By compiling statistics from single cloud tests as a function of the final cloud mask results, we can detect thresholds in need of adjustment. In the future, we will generate statistics of single cloud tests and final cloud mask results as functions of land surface type, viewing and solar zenith angles, and season.

In addition, we can compare results from the MODIS instruments on the Aqua and Terra platforms. Figure 20 shows a comparison of the cloud mask from the two instruments over East Africa on July 11, 2002 Terra at 08:05 UTC, Aqua at 11:00 UTC. Results of the cloud detection appear consistent, given the time difference between the two overpasses.

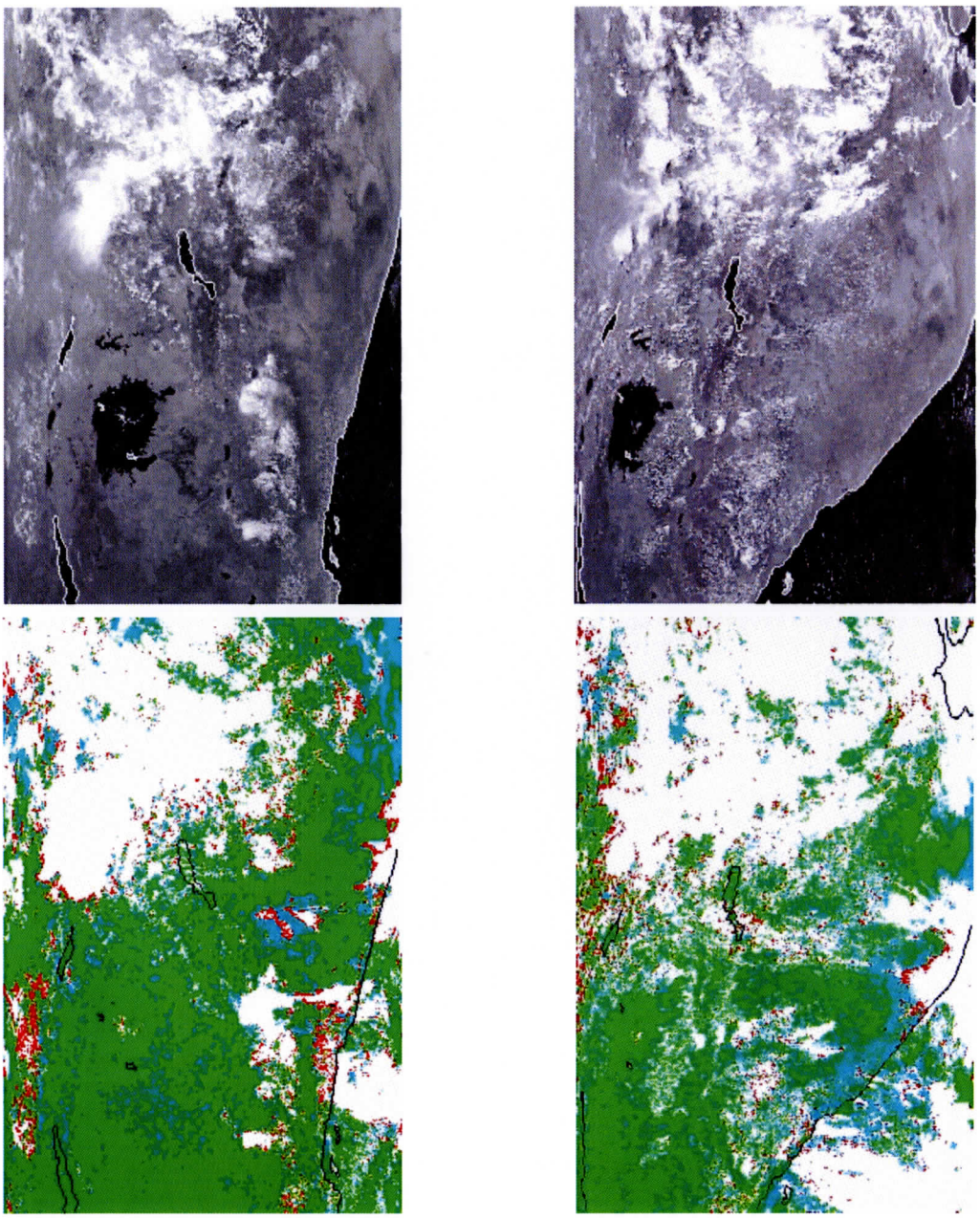

Figure 20. East African scene from July 11, 2002 Terra at 08:05 UTC, Aqua from 11:00 UTC. MODIS Terra (left) and Aqua (right), Band 2 (top) and cloud mask (bottom). Colors: green is confident clear; cyan is probably clear; red is uncertain; white is cloudy.

4.6.4 COMPARISONS WITH OTHER TERRA AND AQUA PLATFORM INSTRUMENTS

Comparisons with products from other platforms are also planned. Cloud masks will be compared with those from ASTER, MISR, and CERES. Timing, coverage and resolution will vary from one instrument to another; for example with ASTER, comparisons will be possible for selected swaths (60 km wide with 30 m resolution) that are available for different (and selected) ecosystems no more than once every 16 days. The ASTER product will include a classification for each pixel poleward of 60°N or 60°S using a bit map with the following bit flags: unknown, ice cloud, water cloud, shadow, land, ice, wet ice, and water. The high spatial resolution of the ASTER data (30 m at nadir) will help to ensure that sub-pixel effects are properly accounted for in the MODIS data.

The MODIS Cloud Mask products will be compared to the MISR Top-of-Atmosphere/Cloud Product. The components of the MISR product that will be used are Reflecting-Level Reference Altitude (retrieved using MISR stereo imagery), Angle-by-angle cloud masks, Cloud shadow mask, and Altitude-binned cloud fraction. The MODIS and MISR Cloud Masks will be compared to ensure consistency of cloud identification, and the MISR stereo cloud heights will be compared with the MODIS cloud top heights to geometrically validate the MODIS radiometrically derived cloud height data.

A comparison of Aqua MODIS cloud mask with AIRS observations has begun. Figure 19 shows a MODIS cloud mask image over the Gulf of Finland. The circles represent the location of the AIRS footprints. A comparison between the AIRS and MODIS cloud detection results is shown in Figure 21.

5.0 Collection 5 updates

Significant improvements have been made to the MODIS cloud mask (MOD35) in preparation for Collection 5 reprocessing and forward stream data production. Most of the modifications are realized for nighttime scenes where polar and oceanic regions will see marked improvement. For polar night scenes, two new spectral tests using the 7.2 μm water vapor absorp-

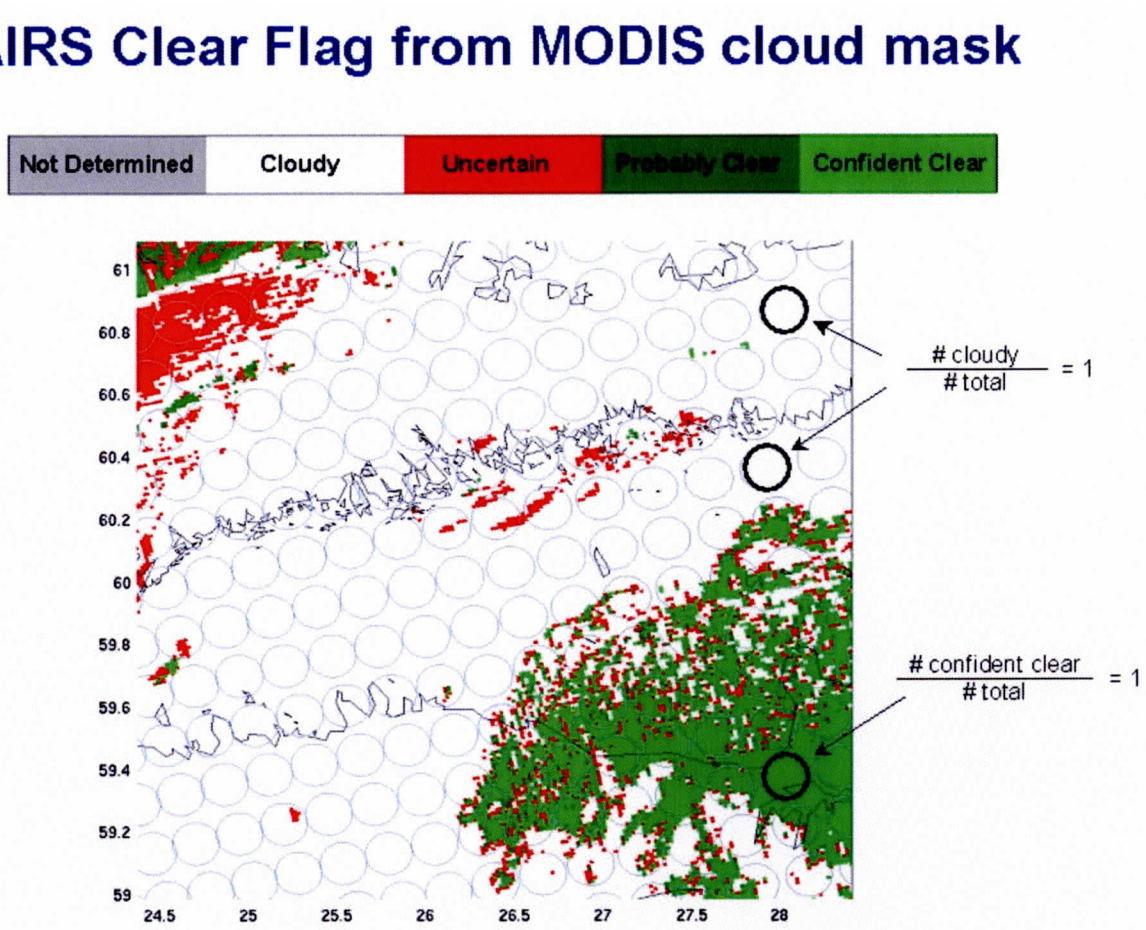

Figure 21. Results for the Aqua MODIS cloud mask for southern Finland. The circles represent the location of the AIRS footprints. A comparison between the AIRS cloud mask algorithm and MODIS has begun.

tion band have been added as well as updates to the 3.9-12 μm and 11-12 μm cloud tests. More non-MODIS ancillary input data has been added. Land and sea surface temperature maps provide crucial information for middle and low-level cloud detection and lessen dependence on ocean brightness temperature variability tests. Sun-glint areas are also improved by use of sea surface temperatures to aid in resolving observations with conflicting cloud vs. clear-sky signals, where visible and NIR reflectances are high, but infrared brightness temperatures are relatively warm. Day vs. night sea surface temperatures derived from MODIS radiances and using only the MODIS cloud mask for cloud screening are contrasted. Frequencies of cloud from sun-glint regions are shown as a function of sun-glint angle to gain a sense of cloud mask quality in those

regions. Continuing validation activities are described.

The 48-bit output structure for each pixel has necessarily changed due to addition of spectral tests. Table 3' and Table 4' are placed at the end of this section and replace the original Tables 3 and 4 found above.

5.1 Algorithm Updates

POLAR NIGHT

Discriminating clear sky from cloudy conditions is nowhere more difficult than in conditions of polar night. Also, verifying cloud detection results in polar night conditions is very difficult without human observations or active sensors to compare with. Both are almost totally absent during polar winter. Figure 22 shows both the underlying problem in cloud detection for polar night and an indication of cloud mask results. It shows a histogram of observed BTs from one MODIS granule (open bars) over frozen ocean near the North Pole. Also shown are the amounts of confident clear and confident cloudy retrievals for each BT class. Instead of clear-sky observations making a distinct peak on the warm end of the histogram as in most Earth scenes, this shows a more Gaussian distribution with most values (both clear and cloudy) somewhere in the middle. However, as shown in the figure, in a given region one expects tempera-

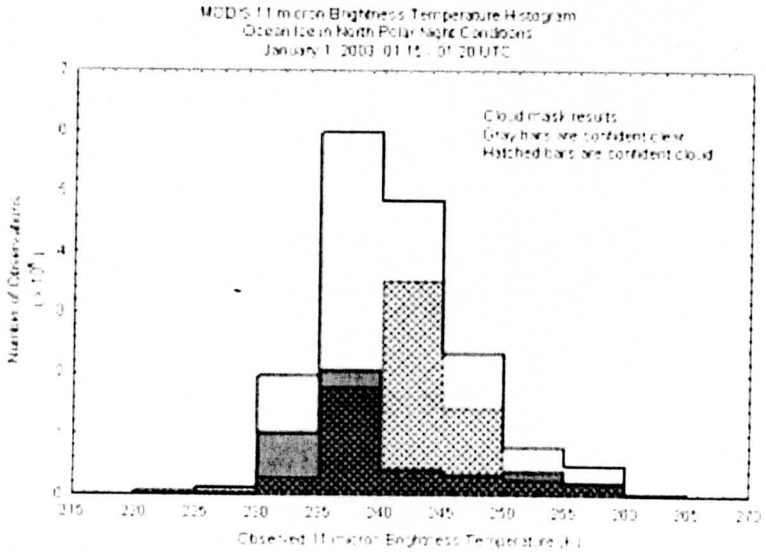

Figure 22. Histogram of 11μm BTs over frozen ocean from January 1, 2003 near the North Pole.

tures and water vapor loading in clear skies over the surface ice to be relatively uniform so that a majority of those BTs will fall in one 5K-wide class. This was verified by inspection of the imagery for this granule. Note that many, if not most of the confident cloudy BTs were in either the same or warmer BT classes as that of the clear-sky peak, indicating the lack of thermal contrast that is the fundamental cloud detection problem for polar night. Liu[1] compared ground-based radar/lidar data to MODIS cloud mask results using the new polar night spectral tests (included in the cloud mask algorithm for Collection 5) and those from Collection 4 (previous operational version) and found that the misidentification rate of cloud as clear decreased from 44.2% to 16.3% in the Arctic. The misidentification of clear as cloud remained at about 8%. In the latest version of the MODIS cloud mask, two spectral cloud tests were modified, one was added, and one clear-sky restoral test was added.

11–3.9 μM BRIGHTNESS TEMPERATURE DIFFERENCE (BTD) LOW CLOUD TEST

The 11–3.9 μm BTD low cloud test is based on the differential absorption between these two wavelengths by both water and ice cloud particles. The nighttime BTD may be either negative or positive depending on cloud optical depth and particle size[1]. The situation becomes more complex in temperature inversions, however, that are frequent in polar night conditions. For a complete discussion of the problem, see Liu[1]. Previous 11-3.9 μm test thresholds did not take temperature inversions into account and were most appropriate for non-polar, thick water clouds. For Collection 5 polar night, the confident cloud thresholds vary linearly from –0.8 to +0.6 as the 11 μm brightness temperature (BT) varies between 235K and 265K. The threshold is constant below 235K and above 265K. This assumes that more inversions are found as surface temperatures decrease. Figure 23b shows an example of test results on April 1, 2003 beginning at 05:05 UTC from northwest Canada. Figure 23a shows imagery of MODIS 11 μm BTs for the same scene. Note that north is at the bottom and west is to the right in these images. In all test result figures, white means cloud indicated, gray means no cloud indicated and black means test not performed.

3.9-12 μM BTD HIGH CLOUD TEST

The 3.9-12 μm BTD high cloud test has been modified for polar night conditions. For reasons not well understood, the thresholds for this test need to be increased with decreasing tem-

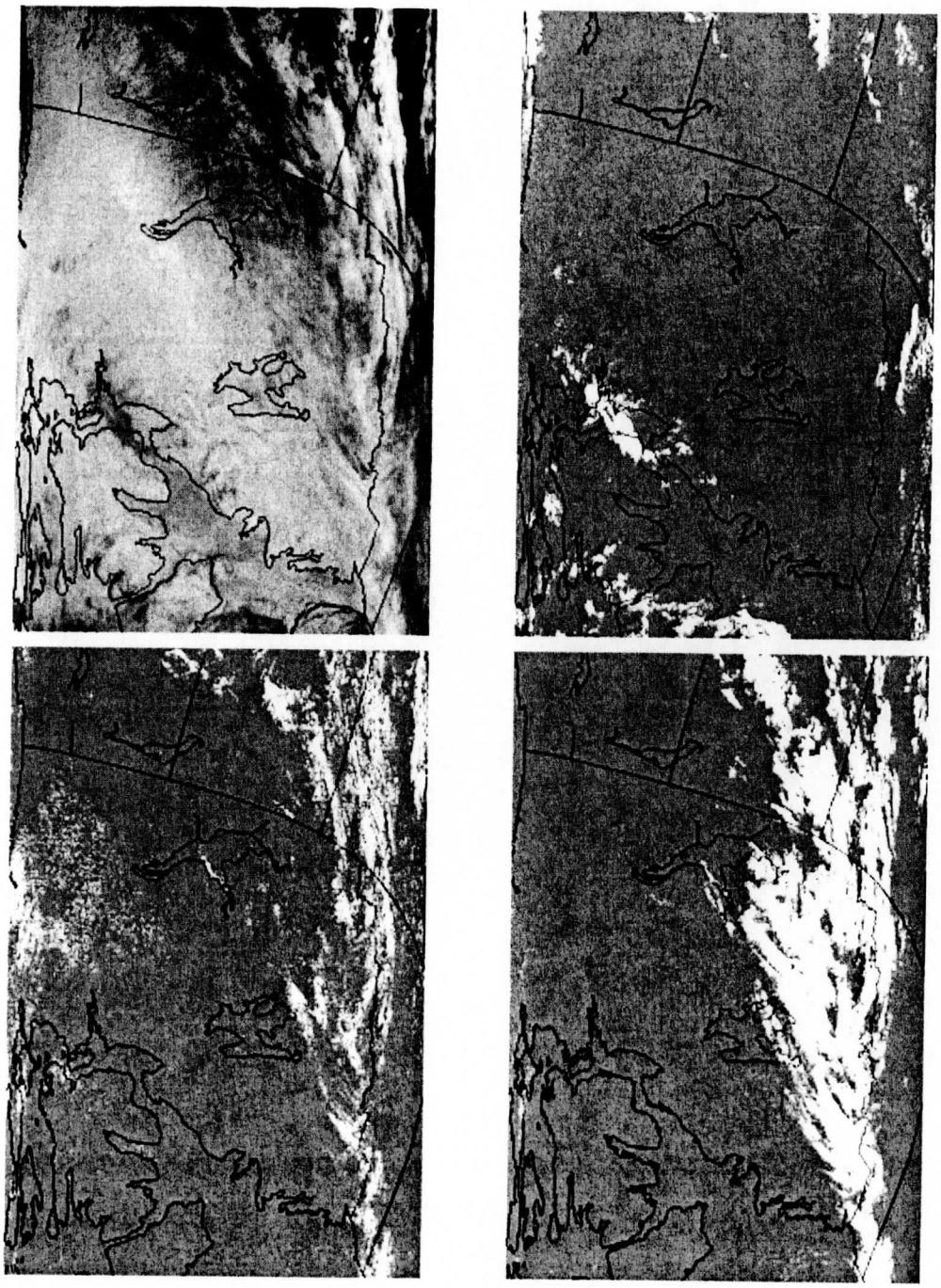

Figure 23a-d. Left to right, top and bottom: MODIS 11 μm BT image (a), 11-3.9 μm BTD test (b), 11-12 μm BTD test (c), and 3.9-12 μm BTD test (d). Scene is from 05:05 UTC, April 1, 2003.

peratures below 265K. This is counter-intuitive from arguments based on atmospheric water vapor loading and absorption at these two wavelengths. Perhaps the calibration of one or both bands is of reduced accuracy at cold temperatures. In addition, the test cannot be used on the very coldest and driest scenes such as are found in Antarctica and Greenland during the winter season. Therefore, the test is not performed in polar night conditions when the elevation exceeds 2000 m. The Collection 5 confident cloud threshold varies linearly from +4.5K to +2.5K as the 11 μm BT varies between 235K and 265K. The threshold is constant below 235K and above 265K. Figure 23d shows an example of test results from the same scene as above.

11-12 μM BTD THIN CIRRUS TEST

Previous versions of the cloud mask algorithm made use of this test only over surfaces not covered by snow or ice. The Collection 5 test makes use of thresholds taken from Key[2] who extended the Saunders and Kriebel[3] values to very low temperatures. The modified test has replaced the original in all processing paths for both day and night processing except for Antarctica. Figure 23c shows example results from the same scene as above. At these very cold scene temperatures, the 11-12 μm BTD starts to become noisy as seen at middle left.

7.2-11 μm BTD Cloud Test

The most significant change to the polar night algorithm is the addition of a new 7.2-11μm BTD cloud test. Since the weighting function of the 7.2 μm band peaks at about 800 hPa, the BTD is related to the temperature difference between the 800 hPa layer and the surface, which the 11 μm band is most sensitive to. In the presence of low clouds under polar night conditions with a temperature inversion, radiation from the 11 μm band comes primarily from the relatively warm cloud top, decreasing the 7.2-11 μm BTD compared to the clear-sky value. For a complete discussion of the theory, see Liu[1]. In conditions of deep polar night, even high clouds may be warmer than the surface and will often be detected with this test. The test as configured in MOD35 is applicable only over nighttime snow and ice surfaces. Because the 7.2 μm band is sensitive to atmospheric water vapor and also because inversion strength tends to increase with

decreasing surface temperatures[1], thresholds for this test are a function of the observed 11 μm BT. The thresholds vary linearly in three ranges: BTD +2K to –4.5K for 11 μm between 220K and 245K, BTD –4.5K to –11.5K for 11 μm between 245 and 255K, and BTD –11.5 to –21K for 11 μm between 255K and 265K. Thresholds are constant for 11 μm below 220K or above 265K. The thresholds are slightly different over ice (frozen water surfaces): BTD +2K to –4.5K for 11 μm between 220K and 245K, BTD –4.5K to –17.5K for 11 μm between 245 and 255K, and BTD –17.5 to –21K for 11 μm between 255K and 265K. These somewhat larger BTDs presumably reflect a lesser tendency for strong inversions and higher water vapor loading over frozen water surfaces as opposed to snow-covered land areas. These thresholds also differ slightly from those reported in Liu[1], a result of extensive testing over many scenes and the necessity of meshing this test with other cloud mask tests and algorithms. Note that this test was also implemented for non-polar (latitude < 60 deg.), nighttime snow-covered land. Figure 23e shows imagery from the 7.2 μm band for this same scene from Canada and 1f shows the results of the test. Note the difference in texture between cloudy and clear on the right in the 7.2 μm BT imagery, even though the gray scale indicates similar temperatures for much of the scene. Clouds indicated on the left are just barely seen in Figure 23a.

7.2-11 μm BTD Clear Sky Test

A 7.2-11 μm BTD test may also be utilized to find clear sky because of the prevalence of polar night temperature inversions. This test works in the same way as the current 6.7-11 μm BTD clear-sky restoral test, where 11 μm BTs are sometimes significantly lower than those measured in the 6.7 μm band because the 6.7 μm weighting function peaks near the top of a warmer inversion layer in some cases. However, since the 7.2 μm band peaks lower in the atmosphere, a 7.2-11 μm BTD test can detect lower and weaker inversions. Pixels are restored to clear if the 7.2-11 μm BTD > 5K.

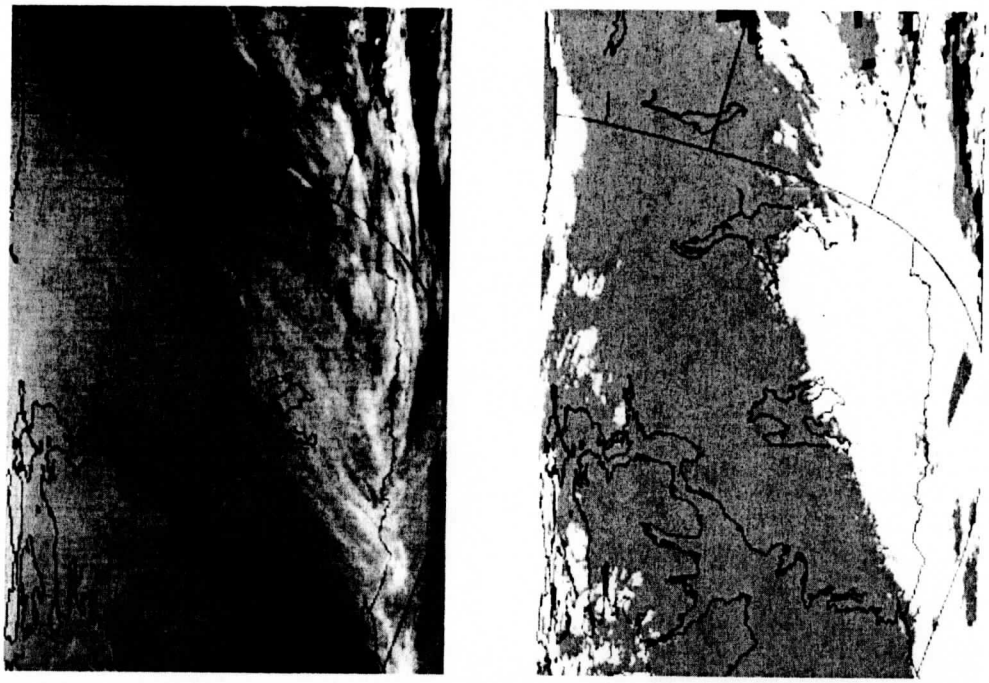

Figure 23 e and f. MODIS 7.2 μm BT image (e) and 7.2-11 μm BTD test (f).

Night Land

The major enhancement to nighttime land processing is the inclusion of a surface temperature (SFCT) test. Gridded surface air temperatures from Global Data Assimilation System[4] (GDAS) model output fields are compared to observed 11 μm BTs. Due to large variations of SFCT in mountainous areas and large diurnal swings in desert regions that are not always well characterized in the gridded data, the test is not performed there. Even with these restrictions, great care must be taken when applying this test. Thresholds of GDAS SFCT-11 μm BT are set at 12K for vegetated areas and 20K for semi-arid lands but are adjusted for viewing zenith angle and water vapor loading based on 11-12 μm BTDs. With threshold values set this high, the test can obviously function only as a gross cloud test. But it is particularly useful for detecting thick mid-level clouds that are surprisingly difficult to detect at night over land. The test is also performed on snow-free polar scenes.

Nighttime Ocean

Nighttime ocean cloud detection has undergone major changes. A sea-surface temperature (SST) test and an 8.6-7.2 μm BTD test have been implemented for the first time. A new 11 μm BT variability test has also been included. The ocean Reynolds[5] SST-11 μm BTD test has the same function as the land surface temperature test, namely as a gross cloud test. Because of the more uniform ocean surface temperatures the threshold can be lowered to a base value of 6K that is adjusted to account for viewing zenith angle and water vapor loading.

An 8.6-7.2 μm BTD test has been added and is designed primarily to detect thick mid-level clouds but can also detect lower clouds in regions of low relative humidity in the middle atmosphere. It is sometimes more effective than the SST test for finding stratocumulus clouds of small horizontal extent. It can also detect high, thick clouds. Both this and the SST test are needed in order to find those clouds that are thick but that also show very small thermal spatial variability. The test thresholds are 16.0K, 17.0K, and 18.0K for 0.0, 0.5, and 1.0 confidence of clear sky, respectively.

The 11 μm variability test has been modified to detect clouds of small spatial extent (a pixel or two) and cloud edges. Most thick clouds are now found by other tests but a variability test is very effective at night for detecting the thinner, warmer cloud edges over the uniform ocean surface. The previous (Collection 4) test determined a standard deviation over the pixel of interest and the eight surrounding. Then, a very stringent threshold was used to determine cloudiness. In the Collection 5 version, the number of differences ≤ 0.5K in 11 μm BT between each surrounding pixel and the center one are counted. The higher the number (8 possible), the more likely the center pixel is clear. The confident cloud and confident clear thresholds are 3 and 7, respectively. Figure 24a-24d shows examples of an ocean scene with widespread stratus clouds in the subtropical southern Pacific west of South America and results of the three tests discussed.

SUN-GLINT AND DAYTIME OCEAN

Improvements have been made to the cloud mask in sun-glint regions and in daytime oceans generally. The SST test has been implemented in the daytime ocean algorithm exactly as in the

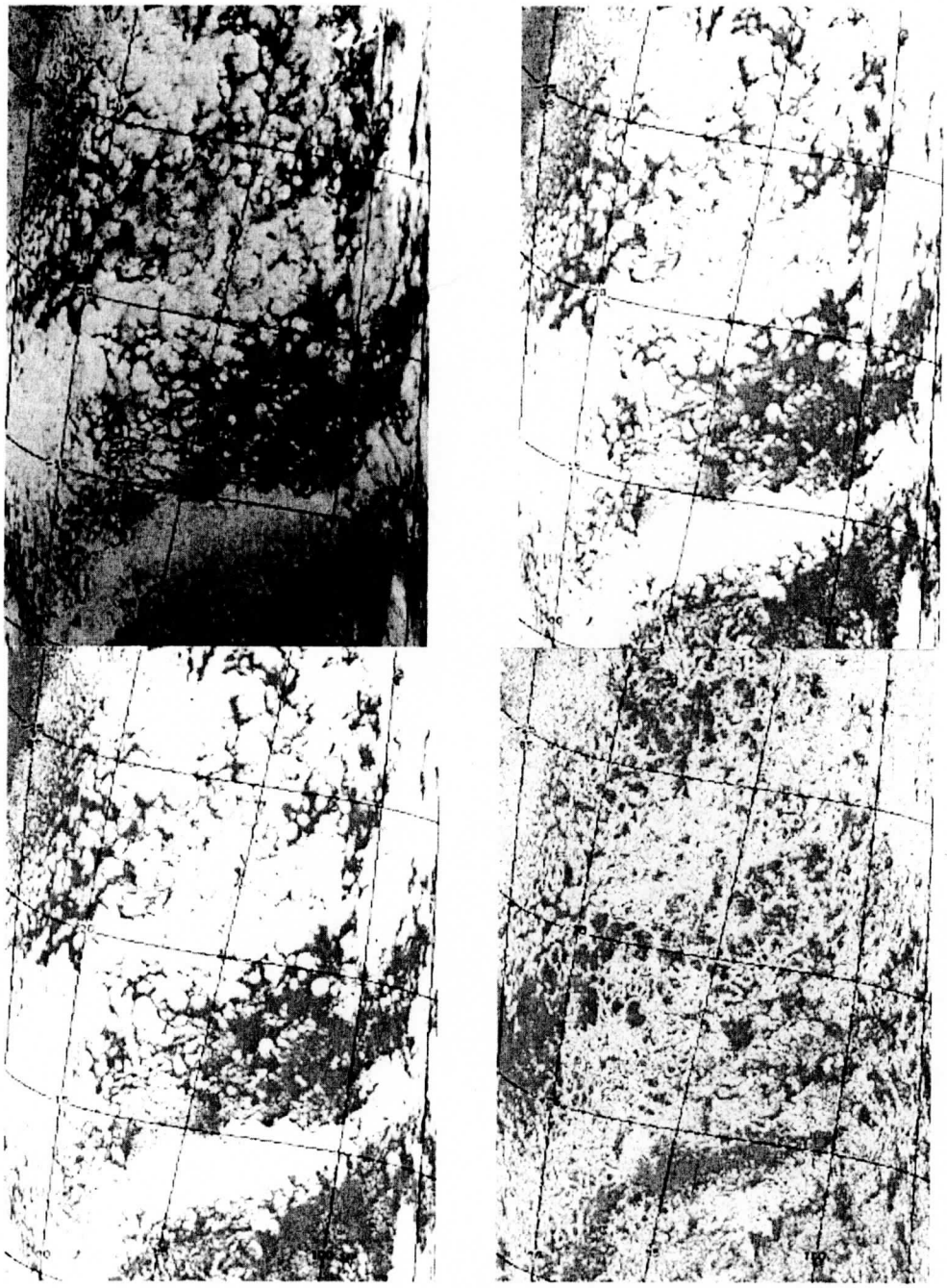

Figure 24. MODIS 3.9 μm BT image (a), and SST test (b) MODIS 8.6-7.2 μm BTD test (c), and 11 μm variability test (d). Scene is from 05:00 UTC, April 6, 2003.

nighttime case. For areas not affected by sun-glint, the improvements are small since the algorithm has already been well developed for some time. The most noticeable change is more confident cloud and less uncertain for scenes containing thin cirrus. The changes are more dramatic

for areas affected by sun-glint. Many low-level clouds with above-freezing cloud top temperatures have been moved from the uncertain to the confident cloud category by use of the SST test. Much of the ambiguity between bright clouds and sometimes equally bright ocean surfaces on the one hand, and between warm clouds and warm ocean surfaces on the other, is ameliorated by knowledge of the SST.

In addition, a new clear-sky restoral test is applied. When no thermal tests indicate the presence of cloud, the mean and standard deviation of 0.86 μm reflectances are computed over the pixel of interest and the eight surrounding. Pixels are declared to be probably clear (confidence 0.96) when the standard deviation multiplied by the mean is < 0.001. This has the effect of restoring to clear many pixels that are bright in the visible and NIR but also very uniform. This test is performed in addition to previously existing restoral tests. Figure 25 shows an example where the new algorithm greatly improves the cloud mask results.

To demonstrate the improvements in the cloud mask sun-glint algorithm and the consistency of results between sun-glint and non sun-glint pixels, a region of the Pacific Ocean between –30 and +45 latitude was chosen for a detailed study. The longitudinal domain was –180 to –130 and

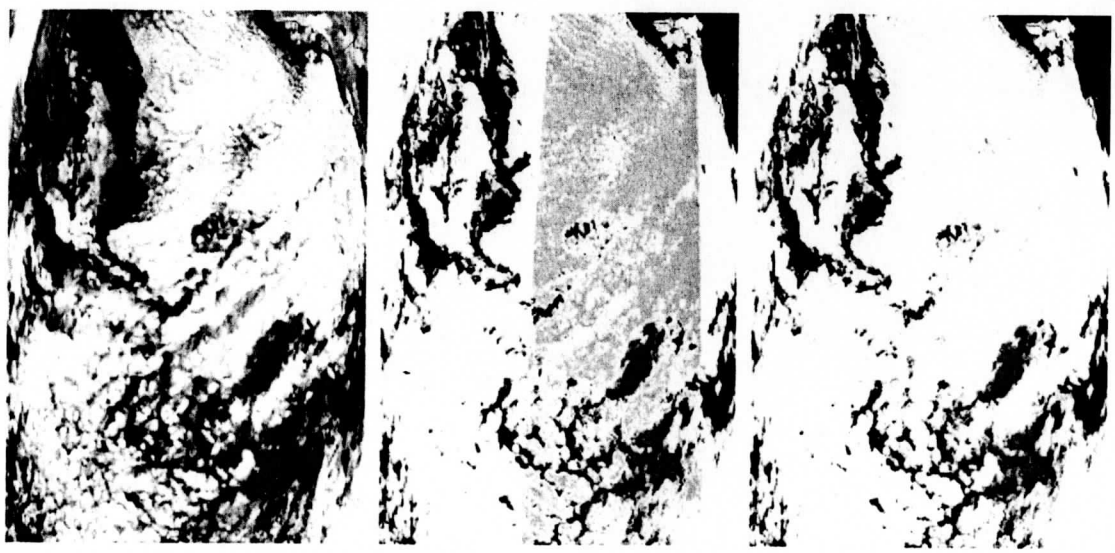

Figure 25. MODIS 0.86 μm image (a), Collection 4 cloud mask (b), and Collection 5 mask result (c). In the mask images, black is confident clear, dark gray is probably clear, light gray is uncertain, and white is confident cloud. Baja California may be seen in (a) in the upper right corner of the image. Scene is from April 6, 2004 at 19:10 UTC.

the temporal range was April 1-8, 2003. Figure 26a shows total cloud amount as a function of glint angle binned in 6-degree increments. Sun-glint is defined in the cloud mask algorithm as glint angles from 0 to 36 degrees, where 0 defines the specular point. Because increasing sun-glint angles on the Earth's surface are characterized by a series of concentric circles, larger glint angles also imply a wider range of latitudes, as well as increasing surface area and viewing zenith angles. At first glance, the total cloud amount from the combined confident cloudy and uncertain decisions from MOD35 (top curve) would appear to be seriously biased in the sun-glint regions, but other indications of cloud (bottom curves) show the same pattern. Sub-freezing observations in the 11 μm band are independent of sun-glint, and thin and thick cirrus as determined by 1.38 μm reflectances, are generally very insensitive to glint especially in moist, tropical regions. The numbers in brackets along the top curve indicate the minimum and maximum latitudes from which the corresponding values originated. Figure 26b shows total cloud frequency from the same region but from non-glint pixels and as a function of latitude. It can be seen from comparing the latitude ranges from the first plot to the cloud frequencies of those latitudes on the second, that the trend toward lower cloud amounts in the latitudes most affected by glint is reasonable. Using the total number of observations from each glint angle bin as a surrogate for areal coverage (not exact), a reasonably accurate weighted average may be obtained over the entire region. The non-glint cloud amount was 70.8% while the cloud percentage from the

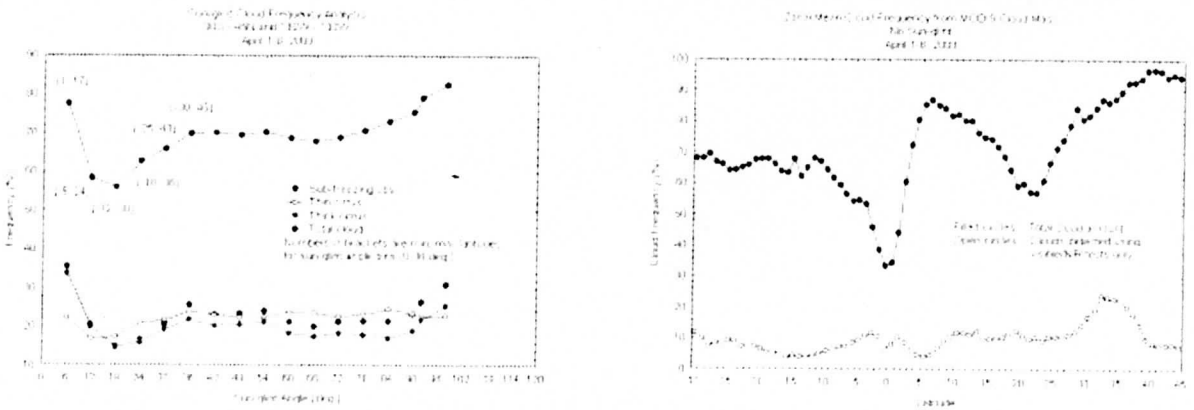

Figure 26. Cloud frequencies as a function of sun-glint angle (a) and as a function of latitude (b). The cloud frequencies in (b) do not contain any observations from sun-glint conditions. Data is from April 1-8, 2003.

glint region was 64.5%, a difference of 6.3%. Although not proven by this analysis, we suspect that the majority of missed cloudy pixels in glint areas are those warm clouds of small extent that are detected only by visible and NIR cloud tests. In areas affected by glint, the background ocean reflectance is often about the same or greater than that from these clouds, rendering them invisible. The bottom curve on Figure 26b shows zonal means of the frequencies of these clouds as defined by the cloud mask from non-glint regions.

POLAR DAYTIME SNOW

A new version of the 3.9-11 μm test has been developed for polar, daytime conditions. The test thresholds are now dependent on the observed 11 μm BT when that BT is lower than 245K. Also, the test will no longer be performed at all when the 11 μm BT is below 230K. During Arctic and Antarctic spring and autumn seasons, the sun is above the horizon but surface temperatures and hence clear-sky observed BTs are still very low, sometimes < 200K at 11 μm on the Antarctic plateau near the South Pole. Under these conditions, and adding just a small amount of solar insulation, the extreme nonlinearity of the Planck function at 3.9 μm makes the 3.9-11 μm BTD higher than one would expect for clear-sky observations at warmer temperatures. This effect, along with the use of static test thresholds was leading to false cloud determinations in Antarctica and Greenland. The new thresholds will vary between 7.0K and 14.5K as 11 μm BTs vary between 245K and 230K at the 0.5 clear-sky confidence level. Above 245K, the threshold will remain as before, at 7K.

SUMMARY

Changes for Collection 5 reprocessing in the MODIS cloud mask (MOD35) are described in this paper. They include changes in the polar night, ocean and land night, polar day snow, and sun-glint processing paths. Including tests for thin cirrus clouds (11-12 μm and 7.2-11 μm BTDs) will enhance the cloud detection capability in polar night conditions, while a new clear-sky restoral test (also 7.2-11 μm BTD) will allow more surface temperature inversions to be located that are normally cloud-free. Users of the cloud mask will see an increase in the number of

pixels flagged as cloudy under polar night conditions. The nighttime ocean algorithm has been reworked so that a more realistic amount of clouds are detected. Night ocean cloud amounts now compare well with those from daytime data. An analysis of SST using only MOD35 for cloud screening shows that a product that is very sensitive to small amounts of cloud contamination generates reasonable results from both the day and night algorithms. It is not apparent that the nighttime SSTs show more cloud contamination than the daytime ones above that which may be expected due to lack of visible and NIR data. Zonal mean SST differences between day and night range from 0.25K in the warmest regions to about 1K in colder, cloudier areas. Both day and night distributions of Reynolds SSTs vs. SSTs using MOD35 peak at –0.25K (Reynolds warmer). A study of cloud amount as a function of sun-glint angle reveals that the cloud mask does a reasonable job in the difficult glint regions. An 8-day, area-weighted average of cloud amounts between glint and non-glint areas shows a deficit of 6.3% from glint regions. We suspect this difference is due to warm clouds of small areal extent that cannot be reliably detected by IR tests and that fade into the visible and NIR glint background reflectances. Users will see a marked decrease in false cloud determinations in daylight conditions during the spring and fall seasons in Greenland and Antarctica. This is due to a modification in the 3.9-11 μm BTD test.

5.2 Validation Activities

The performance of the MODIS cloud mask has been addressed in several recent papers (Lee et al, Li et al,). In this section we compare 3 years (2003 through 2005) of the Collection-5 cloud mask algorithm to cloud detection from the Active Remotely Sensed Cloud (ARSCL) product algorithm, which utilizes combined observations from a micropulse lidar (MPL) and a millimeter-wavelength cloud radar (MMCR) to determine cloud presence and cloud-top height from the ground at the Department of Energy (DOE) Atmospheric Radiation Measurement (ARM) program Southern Great Plains (SGP) site in Lamont, Oklahoma (Clothiaux et al., 2000).

The ARSCL algorithm (Clothiaux et al, 2000) processes and combines data from the MPL and MMCR to determine objectively cloud-base and cloud-top altitude at a vertical spatial reso-

lution of forty-five meters and a temporal resolution of ten seconds. The ARSCL algorithm processes the four modes of MMCR operational output and merges the MMCR output with the output of the MPL to produce cloud-top height retrievals. The paper focuses on cloud detection of this algorithm, using cloud height retrieval only as an analysis tool. Problems in the ARSCL product can be due to a number of factors, including ARSCL beam attenuation (e.g., rain), excessive ground clutter or equipment failure

A cloud is an ambiguous quantity, as there can be many different ways to define a cloud – visual estimates, radiative and physical properties. Comparing cloud detection methods from two independent sources that retrieve cloud properties based on different physical principles over different spatial and temporal scales makes for a difficult process. Since the resolution of the MODIS data is fixed (later we discuss the impact of varying the spatial resolution on clear-sky detection), the ARSCL data are averaged temporally to explore the impact on this comparison. ARSCL cloud detection was averaged over 10, 30 and 60 minute time periods, and histogram of the cloud fraction is shown in Figure 27 for the three-years. The 10-minute data set has more clear-sky scenes and overcast scenes than the longer time periods. Because of the large frequen-

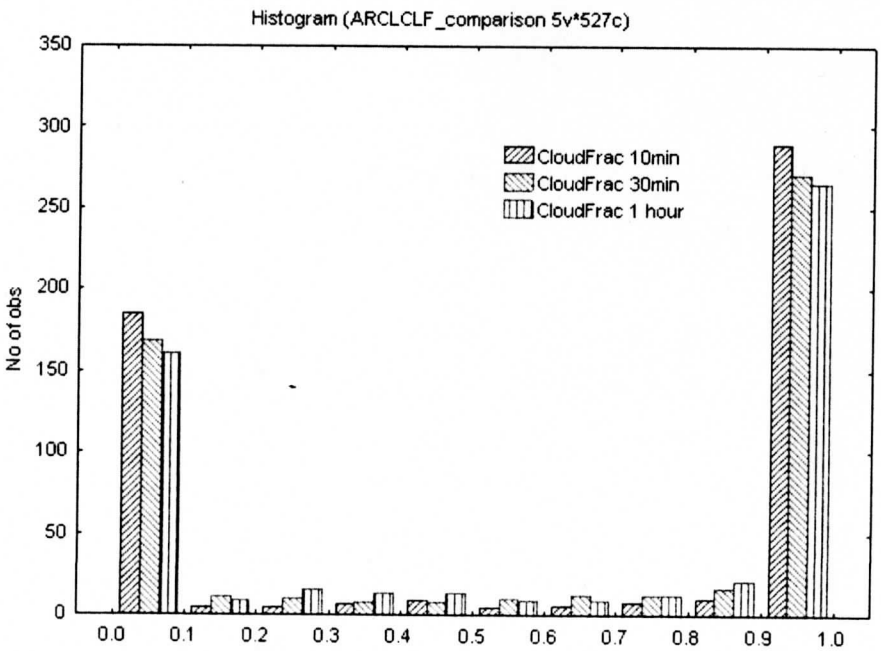

Figure 27. Histogram of cloud fraction from the ARCL data set for three averaging periods.

Table 10. Comparison of MODIS cloud detection with the ARCL over the ARM site of the Southern Great Plains.

	ARCL clear	ARCL cloudy
MODIS clear	Terra: 146	Terra: 45
	Aqua: 117	Aqua: 58
MODIS cloudy	Terra: 38	Terra: 298
	Aqua: 12	Aqua: 185

cies of both total clear or total cloudy in the distribution, the differences in a annual histogram of this data sets is not statistically different. A group of 5×5 MODIS observations centered on the ARM site are used in the comparison, averaging the final cloud mask confidences and assuming a value of greater than 0.95 represents a clear scene. The radiances were collected from the MODIS direct broadcast system and run through the MODIS cloud mask, collection-5.

Table 10 lists the comparison between the MODIS cloud mask and the ARCL data set for both the Terra and Aqua data set. There is agreement for more than 80% of the observations. There is little difference in the skill score with season. Those observations that are determined by MODIS as cloudy while ARCL is indicating clear are mostly associated with the average MODIS confidence flag of 0.90 (Figure 28), where we have defined a value of greater than 0.95 as clear. Those cases in which MODIS defines clear and ARCL cloudy occur primarily for

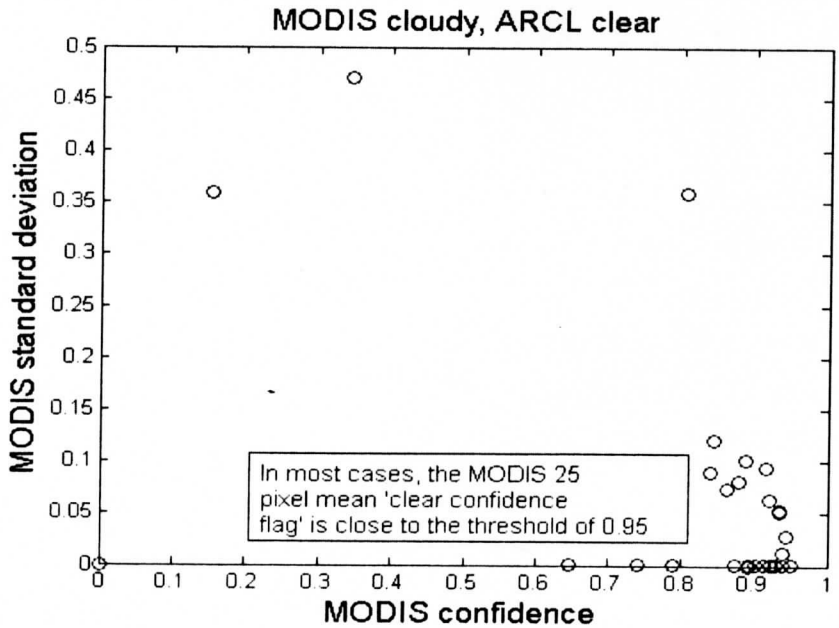

Figure 28. MODIS average confidence versus standard deviation for cases labeled by MODIS as cloudy and by the ARCL algorithm as clear. The clear-sky threshold is 0.95.

cloud tops altitudes greater than 8 km.

Table 3'. File specification for the 48-bit MODIS cloud mask. A '0' for bits 8-47 may mean the test was not run.

BIT FIELD	DESCRIPTION KEY	RESULT
0	Cloud Mask Flag	0 = not determined 1 = determined
1-2	Unobstructed FOV Confidence Flag	00 = cloudy 01 = uncertain 10 = probably clear 11 = confident clear
PROCESSING PATH FLAGS		
3	Day / Night Flag	0 = Night / 1 = Day
4	Sun glint Flag	0 = Yes / 1 = No
5	Snow / Ice Background Flag	0 = Yes/ 1 = No
6-7	Land / Water Flag	00 = Water 01 = Coastal 10 = Desert 11 = Land
ADDITIONAL INFORMATION		
8	Non-cloud obstruction Flag (heavy aerosol)	0 = Yes / 1 = No
9	Thin Cirrus Detected (solar)	0 = Yes / 1 = No
10	Shadow Found	0 = Yes / 1 = No
11	Thin Cirrus Detected (infrared)	0 = Yes / 1 = No
12	Spare	
	1-km CLOUD FLAGS	
13	Cloud Flag - Ocean 11 μm BT Threshold Test	0 = Yes / 1 = No
14	High Cloud Flag - 13.9 μm BT Threshold Test	0 = Yes / 1 = No
15	High Cloud Flag – 6.7 μm BT Threshold Test	0 = Yes / 1 = No
16	High Cloud Flag – 1.38 μm Refl. Threshold Test	0 = Yes / 1 = No
17	High Cloud Flag – 3.9-12 μm BTD Threshold Test	0 = Yes / 1 = No
18	Cloud Flag - IR BTD Threshold Tests	0 = Yes / 1 = No
19	Cloud Flag - 3.9-11 μm BTD Threshold Test	0 = Yes / 1 = No
20	Cloud Flag - Vis/NIR Refl. Threshold Test	0 = Yes / 1 = No
21	Cloud Flag - Vis/NIR Refl. Ratio Threshold Test	0 = Yes / 1 = No
22	Clear-sky Restoral Test - NDVI in Coastal Areas	0 = Yes / 1 = No
23	Cloud Flag - 7.3-11 μm BTD Threshold Test	0 = Yes / 1 = No
24	Spare	
25	Clear-sky Restoral Test - Ocean 11 μm Spatial Consistency	0 = Yes / 1 = No
26	Clear-sky Restoral Tests - Land and Sun-glint	0 = Yes / 1 = No
27	Cloud Flag - Surface Temperature Tests	0 = Yes / 1 = No
28	Suspended Dust Flag	0 = Yes / 1 = No
29	Cloud Flag - Night Ocean 8.6-7.3 μm BTD Test	0 = Yes / 1 = No
30	Cloud Flag – Night Ocean 11 μm Variability Test	0 = Yes / 1 = No
31	Spare	
	250-m CLOUD FLAG - AISIBLE TESTS	
32	Element (1,1)	0 = Yes / 1 = No
33	Element (1,2)	0 = Yes / 1 = No
34	Element (1,3)	0 = Yes / 1 = No
35	Element (1,4)	0 = Yes / 1 = No
36	Element (2,1)	0 = Yes / 1 = No
37	Element (2,2)	0 = Yes / 1 = No
38	Element (2,3)	0 = Yes / 1 = No
39	Element (2,4)	0 = Yes / 1 = No
40	Element (3,1)	0 = Yes / 1 = No
41	Element (3,2)	0 = Yes / 1 = No
42	Element (3,3)	0 = Yes / 1 = No
43	Element (3,4)	0 = Yes / 1 = No
44	Element (4,1)	0 = Yes / 1 = No
45	Element (4,2)	0 = Yes / 1 = No
46	Element (4,3)	0 = Yes / 1 = No
47	Element (4,4)	0 = Yes / 1 = No

Table 4'. MODIS cloud tests executed for a given processing path.

	Daytime Ocean	Nighttime Ocean	Daytime Land	Nighttime Land	Daytime Snow/ice	Nighttime Snow/ice	Daytime Coastline	Daytime Desert	Polar Day	Polar Night
BT_{11} (Bit 13)	✓	✓								
$BT_{13.9}$ (Bit 14)	✓	✓	✓	✓	✓	✓	✓	✓		
$BT_{6.7}$ (Bit 15)	✓	✓	✓	✓	✓	✓	✓	✓	✓	✓
$R_{1.38}$ (Bit 16)	✓		✓		✓		✓		✓	
$BT_{3.9} - BT_{12}$ (Bit 17)				✓		✓				✓
$BT_{8.6} - BT_{11}$ *and/or* $BT_{11} - BT_{12}$ (Bit 18)	✓	✓	✓	✓	✓	✓	✓	✓	✓	✓
$BT_{11} - BT_{3.9}$ (Bit 19)	✓	✓	✓	✓	✓	✓	✓	✓	✓	✓
$R_{0.66}$ or $R_{0.87}$ (Bit 20)	✓		✓				✓	✓		
$R_{0.87}/R_{0.66}$ (Bit 21)	✓		✓							
$BT_{7.3} - BT_{11}$ (Bit 23)				✓		✓				✓
Surface Temperature Test (Bit 27)	✓	✓		✓						
$BT_{8.6} - BT_{7.3}$ (Bit 29)		✓								
BT_{11} *Variability Test* (Bit 30)		✓								

6.0 References

Ackerman, S. A., W. L. Smith and H. E. Revercomb, 1990: The 27-28 October 1986 FIRE IFO cirrus case study: Spectral properties of cirrus clouds in the 8-12 μm window. *Mon. Wea. Rev.*, **118**, 2377-2388.

Ackerman, S. A., W. L. Smith, A. D. Collard, X. L. Ma, H. E. Revercomb, and R. O. Knuteson, 1995: Cirrus cloud properties derived from high-spectral resolution infrared spectrometry during FIRE II. Part II: Aircraft HIS results. *J. Atmos. Sci.*, **52**, 4246-4263.

Ackerman, S. A., 1996: Global satellite observations of negative brightness temperature difference between 11 and 6.7 μm. *J. Atmos. Sci.*, **53**, 2803-2812.

Ackerman, S. A., 1997: Remote sensing aerosols using satellite infrared observations. *J. Geophys. Res.*, **102**, 17069-17079.

Ackerman, S. A., K. I. Strabala, W. P. Menzel, R. A. Frey, C. C. Moeller, and L. E. Gumley, 1998: Discriminating clear sky from clouds with MODIS. *J. Geophys. Res.*, **103**, 32141-32157.

Baum, B. A., P. F. Soulen, K. I. Strabala, M. D. King, S. A. Ackerman, and W. P. Menzel, 2000: Remote sensing of cloud properties using MODIS Airborne Simulator imagery during SUCCESS. II. Cloud thermodynamic phase. *J. Geophys. Res.*, **105**, 11781-11792

Ben-Dor, E., 1994: A precaution regarding cirrus cloud detection from airborne imaging spectrometer data using the 1.38 μm water vapor band. *Remote Sens. Environ.*, **50**, 346-350.

Chung, S., S. A. Ackerman, P. F. v. Delst and W. P. Menzel, 2000: Model calculations and interferometer measurements of ice cloud characteristics. *J. Appl. Meteor.*, **39**, 634-644.

Clothiaux, E. E., T. P. Ackerman, G. G. Mace, K. P. Moran, R. T. Marchand, M. A. Miller and B. E. Martner, 2000: Objective determination of cloud heights and radar reflectivities using a combination of active remote sensors at the ARM CART sites. *J. Appl. Meteor.*, **39**, 645-665.

Coakley, J. A., Jr., and F. P. Bretherton, 1982: Cloud cover from high-resolution scanner data: Detecting and allowing for partially filled fields of view. *J. Geophys. Res.*, **87**, 4917-4932.

Collard, A. D., S. A. Ackerman, W. L. Smith, X. L. Ma, H. E. Revercomb, R. O. Knuteson, and S. C. Lee, 1995: Cirrus cloud properties derived from high-spectral resolution infrared spectrometry during FIRE II. Part III: Ground-based results. *J. Atmos. Sci.*, **52**, 4264-4275.

DeSlover, D. H., W. L. Smith, P. K. Piironen, and E. W. Eloranta, 1999: A methodology for measuring cirrus cloud visible to infrared optical depth ratios. *J. Atmos. Oceanic Technol.*, **16**, 251-262.

Duda, D. P., and J. D. Spinhirne, 1996: Split-window retrieval of particle size and optical depth in contrails located above horizontally inhomogeneous ice clouds. *Geophys. Res. Lett.*, **23**, 3711-3714.

Frey, R. A., S. A. Ackerman, and B. J. Soden, 1995: Climate parameters from satellite spectral measurements. Part I: Collocated AVHRR and HIRS/2 observations of the spectral greenhouse parameter. *J. Climate*, **9**, 327-344.

Frey, R. A., B. A. Baum, W. P. Menzel, S. A. Ackerman, C. C. Moeller, and J. D. Spinhirne, 1999: A comparison of cloud top heights computed from airborne lidar and MAS radiacne data using CO_2 slicing. *J. Geophys. Res.*, **104**, 24547-24555.

Gao, B. C., and A. F. H. Goetz, 1991: Cloud area determination from AVIRIS data using water vapor channels near 1 μm. *J. Geophys. Res.*, **96**, 2857-2864.

Gao, B. C., A. F. H. Goetz, and W. J. Wiscombe, 1993: Cirrus cloud detection from airborne im-

aging spectrometer data using the 1.38 μm water vapor band. *Geophys. Res. Lett.*, **20**, 301-304.

Gesell, G., 1989: An algorithm for snow and ice detection using AVHRR data: An extension to the APOLLO software package. *Int. J. Remote Sens.*, **10**, 897-905.

Hall, D. K., G. A. Riggs, and V. V. Salomonson, 1995: Development of methods for mapping global snow cover using Moderate Resolution Imaging Spectroradiometer data. *Remote Sens. Environ.*, **54**, 127-140.

Hawkinson, J., W. Feltz, A. J. Schreiner, and T. Schmit, 2001: A validation study of the GOES sounder cloud top pressure product. *Proc. 11th Conference on Satellite Meteorology*, Amer. Meteor. Soc., Madison WI.

Hutchison, K. D., and K. R. Hardy, 1995: Threshold functions for automated cloud analyses of global meteorological satellite imagery. *Int. J. Remote Sens.*, **16**, 3665-3680.

Inoue, T., 1987: A cloud type classification with NOAA 7 split window measurements. *J. Geophys. Res.*, **92**, 3991-4000.

Key, J., and R. G. Barry, 1989: Cloud cover analysis with Arctic AVHRR data. 1: Cloud detection. *J. Geophys. Res.*, **94** (D15), 18521-18535.

Key, J., 2000: The Cloud and Surface Parameter Retrieval (CASPR) System for Polar AVHRR Data User's Guide. Cooperative Institute for Meteorological Satellite Studies, Madison, WI, 32 pp.

Kim, D. S., and S. G. Benjamin, 2000: Assimilation of cloud-top pressure derived from GOES sounder data into MAPS/RUC. *Proc. 10th Conference on Satellite Meteorology*, Amer. Meteor. Soc., Long Beach, CA, 110-113.

King, M. D., M. G. Strange, P. Leone, and L. R. Blaine, 1986: Multiwavelength scanning radiometer for airborne measurements of scattered radiation within clouds. *J. Atmos. Oceanic Technol.*, **3**, 513-522.

King, M. D., W. P. Menzel, P. S. Grant, J. S. Myers, G. T. Arnold, S. E. Platnick, L. E. Gumley, S. C. Tsay, C. C. Moeller, M. Fitzgerald, K. S. Brown, and F. G. Osterwisch, 1996: Airborne scanning spectrometer for remote sensing of cloud, aerosol, water vapor and surface properties. *J. Atmos. Oceanic Technol.*, **13**, 777-794.

King, M. D., W. P. Menzel, Y. J. Kaufman, D. Tanré, B. C. Gao, S. Platnick, S. A. Ackerman, L. A. Remer, R. Pincus, and P. A. Hubanks, 2003: Cloud and aerosol properties, precipitable water, and profiles of temperature and humidity from MODIS. *IEEE Trans. Geosci. Remote Sens.*, **41**, 442-458.

King, M. D., S. Platnick, P. Yang, G. T. Arnold, M. A. Gray, J. C. Riédi, S. A. Ackerman and K.-N Liou, 2004: Remote Sensing of Liquid Water and Ice Cloud Optical Thickness and Effective Radius in the Arctic: Application of Airborne Multispectral MAS Data. *J. Atmos. Oceanic Tech.* **21**, 857-875.

Kriebel, K. T., 1978: Measured spectral bidirectional reflection properties of four vegetated surfaces. *Appl. Opt.*, **17**, 253-259.

Kriebel, K. T., R. W. Saunders, and G. Gesell, 1989: Optical properties of clouds derived from fully cloudy pixels. *Beitr. Phys. Atmos.*, **62**, 165-171.

Lee, Y., G. Wahba, and S. A. Ackerman, 2004: Cloud classification of satellite radiance data by multicategory support vector machines. *J. Atmos. Oceanic Technol.*, **21**, 159-169.

Leprieur, C., Y. H. Kerr, and J. M. Pichon, 1996: Critical assessment of vegetation indices from AVHRR in a semi-arid environment. *Int. J. Remote Sens.*, **17**, 2549-2563.

Li, J., W. P. Menzel, and A. J. Schriener, 2001: Variational retrieval of cloud parameters from

GOES sounder longwave cloudy radiance measurements. *J. Appl. Meteor.*, **40**, 312-330.

Li, J., W. P. Menzel, Z. Yang, R. A. Frey, and S. A. Ackerman, 2002: High-spatial-resolution surface and cloud-type classification from MODIS multispectral band measurements. *J. Appl. Meteor.*, **42**, 204-226.

Liu, Y. H., J. R. Key, R. A. Frey, S. A. Ackerman, and W. P. Menzel, 2004: Nighttime polar cloud detection with MODIS. *Remote Sens. Environ.*, **92**, 181-194.

Liou, K. N., 1973: A numerical experiment on Chandrasekhar's discrete-ordinate method for radiative transfer: Applications to cloudy and hazy atmospheres. *J. Atmos. Sci.*, **30**, 1303-1326.

Mace, G. G., T. P. Ackerman, P. Minnis, and D. F. Young, 1998: Cirrus layer microphysical properties derived from surface-based millimeter radar and infrared interferometer data. *J. Geophys. Res.*, **103**(D18), 23207-23216

Matthews, E., and W. B. Rossow, 1987: Regional and seasonal variations of surface reflectance from satellite observations at 0.6 μm. *J. Climate Appl. Meteor.*, **26**, 170-202.

McClain, E. P., 1993: Evaluation of CLAVR Phase-I algorithm performance. Final Report 201-424.

Menzel, W. P., D. P. Wylie, and K. I. Strabala, 1992: Seasonal and diurnal changes in cirrus clouds as seen in four years of observations with the VAS. *J. Appl. Meteor*, **31**, 370-385.

Menzel, W. P., D. P. Wylie, and K. I. Strabala, 1993: Trends in global cirrus inferred from four years of HIRS data. *Tech. Proc. 7th Inter. TOVS Study Conf.*, Igls, Austria.

Minnis, P., and E. F. Harrison, 1984a: Diurnal variability of regional cloud and clear sky radiative parameters derived from GOES data: Part I: Analysis method. *J. Climate Appl. Meteor.*, **23**, 993-1011.

Minnis, P., and E. F. Harrison, 1984b: Diurnal variability of regional cloud and clear sky radiative parameters derived from GOES data: Part III: November 1978 radiative parameters. *J. Climate Appl. Meteor.*, **23**, 1032-1051.

Minnis, P., J. W. L. Smith, Jr., D. P. Garber, J. K. Ayers, and D. R. Doelling, 1995: *Cloud Properties derived from GOES-7 for the Spring 1994 ARM Intensive Observing Period using Version 1.0.0 of the ARM Satellite Data Analysis Program.* NASA Reference Publication 1366, 59 pp.

Minnis, P., D. P. Garber, D. F. Young, R. F. Arduini, and Y. Takano, 1998: Parameterization of reflectance and effective emittance for satellite remote sensing of cloud preperties. *J. Atmos.*, **55**, 3313-3339.

Moeller, C., S. A. Ackerman, K. I. Strabala, W. P. Menzel, and W. L. Smith, 1996: Negative 11 μm minus12 μm brightness temperature differences: A second look. *Proc. 8th Conf. Satellite Meteor. Ocean.*, Amer. Meteor. Soc., Atlanta, GA, 313-316.

Penaloza, M. A., and R. M. Welch, 1996: Feature selection for classification of polar regions using a fuzzy expert system. *Remote Sens. Environ.*, **58**, 81-100.

Pinty, B., and M. M. Verstraete, 1992: GEMI: A non-linear index to monitor global vegetation from satellites. *Vegetatio*, **101**, 15-20.

Platnick, S., M. D. King, S. A. Ackerman, W. P. Menzel, B. A. Baum, J. C. Riédi, and R. A. Frey, 2003: The MODIS cloud products: Algorithms and examples from Terra. *IEEE Trans. Geosci. Remote Sens.*, **41**, 459-473.

Prabhakara, C., J. M. Yoo, D. P. Kratz, and G. Dalu, 1993: Coundary layer stratus clouds: Inferred from satellite infrared spectral measurements over oceans. *J. Quant. Spectrosc. Radiat. Transfer*, **49**, 559-607.

Prata, A. J., 1989: Infrared radiative transfer calculations for volcanic ash clouds. *Geophys. Res. Lett.*, **16**, 1293-1296.

Rizzi, R., C. Serio, G. Kelly, V. Tramutoli, A. McNally, and V. Cuomo, 1994: Cloud clearing of infrared sounder radiances. *J. Appl. Meteor.*, **33**, 179-194.

Rossow, W. B., 1989: Measuring cloud properties from space: A review. *J. Climate*, **2**, 201-213.

Rossow, W. B., L. C. Garder, and A. A. Lacis, 1989: Global, seasonal cloud variations from satellite radiance measurements. Part I: Sensitivity of analysis. *J. Climate*, **2**, 419-458.

Rossow, W. B., and L. C. Garder, 1993: Cloud detection using satellite measurements of infrared and visible radiances for ISCCP. *J. Climate*, **6**, 2341-2369.

Rossow, W. B., A. W. Walker, and L. C. Garder, 1993: Comparison of ISCCP and other cloud amounts. *J. Climate*, **6**, 2394-2418.

Saunders, R. W., and K. T. Kriebel, 1988: An improved method for detecting clear sky and cloudy radiances from AVHRR data. *Int. J. Remote Sens.*, **9**, 123-150.

Schreiner, A. J., T. J. Schmit and W. P. Menzel, 2001: Observations and trends of clouds based on GOES Sounder data. *J. Geophys. Res.*, **106**(D17), 20349-20363.

Sèze, G., and W. B. Rossow, 1991a: Time-cumulated visible and infrared radiance histograms used as descriptors of surface and cloud variations. *Int. J. Remote Sens.*, **12**, 877-920.

Sèze, G., and W. B. Rossow, 1991b: Effects of satellite data resolution on measuring the space-time variations of surfaces and clouds. *Int. J. Remote Sens.*, **12**, 921-952.

Simpson, J. J., 1992: Image masking using polygon fill and morphological operations. *Remote Sens. Environ.*, **40**, 161-183.

Simpson, J. J., and R. H. Keller, 1996: An improved fuzzy logic segmentation of sea ice, clouds, and ocean in remotely sensed artic imagery. *Remote Sens. Environ.*, **54**, 290-312.

Smith, W. L., 1968: An improved method for calculating tropospheric temperature and moisture profiles from satellite radiometer measurements. *Mon. Wea. Rev.*, **96**, 387-396.

Smith, W. L., and C. M. R. Platt, 1978: Comparison of satellite-deduced cloud heights with indications from radiosonde and ground-based laser measurements. *J. Appl. Meteor.*, **17**, 1796-1802.

Smith, W. L., and R. A. Frey, 1990: On cloud altitude determinations from High Resolution Interferometer Sounder (HIS) observations. *J. Appl. Meteor.*, **29**, 658-662.

Smith, W. L., X. L. Ma, S. A. Ackerman, H. E. Revercomb, and R. O. Knuteson, 1993: Remote sensing cloud properties from High Spectral Resolution Infrared observations. *J. Atmos. Sci.*, **50**, 1708-1720.

Smith, W. L., H. E. Revercomb, R. O. Knuteson, F. A. Best, R. Dedecker, H. B. Howell and H. M. Woolf, 1995: Cirrus cloud properties derived from high spectral resolution infrared spectrometry during FIRE II. Part I: The high resolution interferometer sounder (HIS) systems. *J. Atmos. Sci.*, **52**, 4238-4245.

Smith, W. L., S. Ackerman, H. Revercomb, H. Huang, D. H. DeSlover, W. Feltz, L. Gumley, and A. Collard, 1998: Infrared spectral absorption of nearly invisible cirrus clouds. *Geophys. Res. Lett.*, **25**, 1137-1140.

Soden, B. J., and F. P. Bretherton, 1993: Upper tropospheric relative humidity from the GOES 6.7 μm channel: Method and climatology for July 1987. *J. Geophys. Res.*, **98**, 16669-16688.

Spinhirne, J. D., R. Boers, and W. D. Hart, 1989: Cloud top liquid water from lidar observations of marine stratocumulus. *J. Appl. Meteor.*, **28**, 81-90

Spinhirne, J. D., and W. D. Hart, 1990: Cirrus structure and radiative parameters from airborne

lidar and spectral radiometer observations—The 28 October 1986 FIRE study. *Mon. Wea. Rev.*, **118**, 2329-2343.

Spinhirne, J. D., and T. Nakajima, 1994: Glory of clouds in the near infrared. *Appl. Opt.*, **33**, 4652-4662.

Spinhirne, J. D., W. D. Hart, and D. L. Hlavka, 1996: Cirrus infrared parameters and shortwave reflectance relations from observations. *J. Atmos. Sci.*, **53**, 1438-1458.

Stackhouse, P. W., and G. L. Stephens, 1991: A theoretical and observational study of the radiative properties of cirrus: Results from FIRE 1986. *J. Atmos. Sci.*, **48**, 2044-2059.

Stamnes, K., and R. A. Swanson, 1981: A new look at the discrete ordinate method for radiative transfer calculations in the anisotropically scattering atmospheres. *J. Atmos. Sci.*, **38**, 387-399.

Stearns, C. R., R. H. Keller, G. A. Weidner and M. Sievers, 1993: Monthly mean climatic data for Antarctic automatic weather stations. *Antarctic Meteorology and Climatology: Studies Based on Automatic Weather Stations*, D. H. Bromwich and C. R. Stearns, Eds., Antarctic Research Series, **6**, 11-21.

Stowe, L. L., E. P. McClain, R. Carey, P. Pellegrino, G. Gutman, P. Davis, C. Long, and S. Hart, 1991: Global distribution of cloud cover derived from NOAA/AVHRR operational satellite data. *Adv. Space Res.*, **11**, 51-54.

Stowe, L. L., S. K. Vemury, and A. V. Rao, 1994: AVHRR clear sky radiation data sets at NOAA/NESDIS. *Adv. Space Res.*, **14**, 113-116.

Strabala, K. I., S. A. Ackerman, and W. P. Menzel, 1994: Cloud properties inferred from 8-12 μm data. *J. Appl. Meteor.*, **33**, 212-229.

Suttles, J. T., R. N. Green, P. Minnis, G. L. Smith, W. F. Staylor, B. A. Wielicki, I. J. Walker, D. F. Young, V. R. Taylor, and L. L. Stowe, 1988: Angular radiation models for Earth-atmosphere system: Volume I - Shortwave radiation. NASA Reference Report 1184, 144 pp.

Tanamachi, R. L., 2001: Data quality control and preliminary data analysis from the Interferometric Monitor for Greenhouse Gases data set. Madison, 31.

Tarpley, J. D., 1979: Estimating incident solar radiation at the surface from geostationary satellite data. *J. Appl. Meteor.*, **18**, 1172-1181.

Tsonis, A. A., 1984: On the separability of various classes from GOES visible and infrared data. *J. Climate Appl. Meteor.*, **23**, 1393-1410.

Vane, G., R. O. Green, T. G. Chrien, H. T. Enmark, E. G. Hansen and W. M. Porter, 1993: The Airborne Visible/Infrared Imaging Spectrometer (AVIRIS). *Remote Sens. Environ.*, **44**, 127-143.

Walden, V. P., D. C. Tobin, and H. E. Revercomb, 1998: Creation of a Web-Based Archive of IMG Data Over the Arctic.

Wang, J. R., P. Racette, J. D. Spinhirne, K. F. Evans, and W. D. Hart, 1998: Observations of cirrus clouds with airborne MIR, CLS, and MAS during SUCCESS. *Geophys. Res. Lett.*, **25**, 1145-1148.

Wielicki, B. A., J. T. Suttles, A. J. Heymsfield, R. W. Welch, J. D. Spinhirne, M. L. Wu, D. O. C. Starr, L. Parker, and R. F. Arduini, 1990: The 27-28 October 1986 FIRE cirrus case study: Comparison of radiative transfer theory with observations by satellite and aircraft. *Mon. Wea. Rev.*, **118**, 2356-2376

Wu, X. Q., J. J. Bates and S. J. S. Khalsa, 1993: A climatology of the water vapor band brightness temperatures for NOAA operational satellites. *J. Climate*, **7**, 1282-1300.

Wylie, D. P., and W. P. Menzel, 1989: Two years of cloud cover statistics using VAS. *J. Climate*, **2**, 380-392.

Wylie, D. P., W. P. Menzel, H. M. Woolf, and K. I. Strabala1, 1994: Four years of global cirrus cloud statistics using HIRS. *J. Climate*, **7**, 1972-1986.

Yamanouchi, T., K. Suzuki, and S. Kawaguci, 1987: Detection of clouds in Antarctica from infrared multispectral data of AVHRR. *J. Meteor. Soc. Japan*, **65**, 949-962.

Yang, P., B. C. Gao, B. A. Baum, Y. X. Hu, W. J. Wiscombe, M. I. Mishchenko, D. M. Winker, and S. L. Nasiri, 2001: Asymptotic solutions of optical properties of large particles with strong absorption. *Appl. Opt.*, **40**, 1532-1547.

Yang, P., B. C. Gao, B. A. Baum, Y. X. Hu, W. J. Wiscombe, S. C. Tsay, D. M. Winker, and S. L. Nasiri, 2000: Radiative properties of cirrus clouds in the infrared (8-13 μm) spectral region. *J. Quant. Spectrosc. Radiat. Transfer*, **70**, 473-504.

Appendix A. Example Code for reading Cloud Mask Output

This is an example FORTRAN program to read the MODIS cloud mask. The code picks out the first byte of data from the six byte product, and returns -1 in the CldMsk data array (one scan cube) if the product is not defined at a certain pixel, a 1 if it is clear and a 0 if cloudy. This particular version just passes a binary (0 or 1) value for cloud or clear, where clear is defined by this user to be anything greater than 66% probability of clear. It also returns the value of the land sea flag from the 2 bit product in the cloud mask product (0-3) to the LandSea_Flag variable. This is a good example of how a user can design what they extract out of the cloud mask file based upon their needs. It also includes the appropriate MAPI and SDP toolkit calls used in Version 1.

========== Begin Example Cloud Mask Reader ==========

```
      INTEGER FUNCTION ReadCldMsk_MOD05(Modfil,Scan_No,Buf_Size1,
           &                  Buf_Size2,Data_Size,CldMsk,LandSea_Flag)
      IMPLICIT NONE
            INCLUDE 'mapi.inc'
            INCLUDE 'hdf.inc'
            INCLUDE 'PGS_SMF.f'
            INCLUDE 'PGS_MODIS_39500.f'
      C-----------------------------------------------------------------------
      C !F77
      C
      C !DESCRIPTION: Retrieves one scan cube of MODIS Cloud Mask data from
      C               an HDF target array of 100 scan cubes (a granule).
      C
      C !INPUT PARAMETERS:
      C     INTEGER  Modfil(3)     File handle structure for HDF files
      C     INTEGER  Scan_No       Scan Number
      C     INTEGER  Buf_Size1/2   Size of dimension 1/2 of 'Cloud Mask' output
      C                            buffer as dimensioned in calling program
      C
      C !OUTPUT PARAMETERS:
      C     INTEGER  Data_Size(2) Array specifying the size of 'Cloud Mask'
      C                           data block within output buffer.
      C             In definitions below, x = Buf_Size1
```

```
C                                       y = Buf_Size2
C     INTEGER  CldMsk(x,y)  Buffer storing Cloud Mask.
C     INTEGER  LandSea_Flag(x,y)  Buffer storing LandSea_Flag.
C
C !TEAM-UNIQUE HEADER:
C
C     This software is developed by the MODIS Science Data Support
C     Team for the National Aeronautics and Space Administration,
C     Goddard Space Flight Center, under contract NAS5-32373.
C
C !REFERENCES AND CREDITS
C
C     WRITTEN BY:
C     Xiao-Yang Ding                    09/12/95
C     Research and Data systems Corporation
C     SAIC/GSC MODIS Science Data Support Office
C     7501 Forbes Blvd, Seabrook MD 20706
C
C !DESIGN NOTES:
C
C     ReadCldMsk_MOD05 checks the return status of all MODIS Application
C     Program Interface (M-API) function calls.  A successful M-API
C     call is indicated by a return value of MAPIOK (0).  If unsuccessful,
C     a warning error message (i.e., type .._W_..) is written to the
C     LogStatus file, and control reverts back to the calling routine.
C     Subroutine MODIS_SMF_SETDYNAMICMSG is used for message passing to
C     the LogStatus file.
C
C    Externals:
C
C       Function:
C         GMAR                          (libmapi.a)
C         GMARDM                        (libmapi.a)
C
C       Subroutines:
C         MODIS_SMF_SETDYNAMICMSG
C         CONCATENATE
C
C       Named Constant:
C         DFACC_READ                    (hdf.inc)
```

```
C         MAPIOK                        (mapi.inc)
C         MODIS_W_GENERIC               (MODIS_39500.f)
C
C    Internals Variables:
C         arrnam       Name of the SDS array.
C         grpnm        Name of the data group containing the target
C         data_type    String describing the data type of the array.
C         Edge(3)      Array specifying the number of data value to read.
C         Start(3)     Array specifying the starting location of data.
C         Fmax         Maximum frame number per scan line.
C         Lmax         Maximum line number per scan cube.
C         Rank         The number of dimensions in an array
C         ReadCldMsk_MOD05 The function return value
C         MaxScan_No   Total Swath Number.
C         count(15000) A temporary buffer for data of the target array
C         LinesPerScan The number of lines per scan cube
C
C !END
C-------------------------------------------------------------------------

C Declarations
      CHARACTER*80 arrnm,grpnm,data_type,msgbuf,msgbuf1
      INTEGER      Scan_No,LinesPerScan,Rank,I,j,k,L,Fmax,
     2             Lmax,MaxScan_No,No_Bytes
      LOGICAL      error_flag
      PARAMETER    (No_Bytes=6,Fmax=1500,Lmax=10)
      BYTE         count(No_Bytes*Fmax*Lmax)
      INTEGER      Temp1,Temp2,Start(3),Edge(3),Data_Size(2),
     2             Dim_Size(3),Buf_Size1,Buf_Size2,Modfil(3),
     3             CldMsk(Buf_Size1,Buf_Size2),
     4             LandSea_Flag(Buf_Size1,Buf_Size2)

C Initialization
      grpnm = ' '
      arrnm = 'Cloud_Mask'
      error_flag = .false.
      ReadCldMsk_MOD05 = -1
      LinesPerScan = 10
      Rank  =  3
      Start(1) = 0
```

```
      Start(2) = 0
      Start(3) = (Scan_No-1)*LinesPerScan

C Check for valid file and band numbers
      IF (Modfil(1).le.0 .or. Modfil(3).ne.DFACC_READ) THEN
          CALL MODIS_SMF_SETDYNAMICMSG(MODIS_W_GENERIC,
     &    'Invalid SD_ID or invalid file access type','ReadCldMsk_MOD05')
          error_flag = .true.
      End If

C Retrieve the rank, dimensions and data type of SDS data.
      IF (GMARDM(Modfil, arrnm, grpnm, data_type, Rank, Dim_Size)
     &  .ne.MAPIOK) THEN
          CALL MODIS_SMF_SETDYNAMICMSG(MODIS_W_GENERIC,
     &  'GMARDM failed','ReadCldMsk_MOD05')
          error_flag = .true.
      End If

C  Additional input check of Scan_No and buffer size
      MaxScan_No=Dim_Size(3)/LinesPerScan

      IF (Scan_No.lt.1 .or. Scan_No.gt.MaxScan_No) THEN
         write(msgbuf,'(i4)') MaxScan_No
         call Concatenate('Scan_No out of bounds; range 1 -',
     &   msgbuf, msgbuf1)
         CALL MODIS_SMF_SETDYNAMICMSG(MODIS_W_GENERIC,
     &   msgbuf1,'ReadCldMsk_MOD05')
         error_flag = .true.
      End If

      IF (Buf_Size1 .lt. Dim_Size(2)) THEN
         CALL MODIS_SMF_SETDYNAMICMSG
     2   (MODIS_W_GENERIC,'Buffer size too small','ReadCldMsk_MOD05')
         error_flag = .true.
      END IF

C Get Cloud MASK data
      Edge(1) = Dim_Size(1)
      Edge(2) = Dim_Size(2)
      Edge(3) = LinesPerScan
```

```
C Read HDF target array into 'count' buffer
      IF (GMAR(Modfil,arrnm,grpnm,Start,Edge,count).ne.MAPIOK) THEN
         CALL MODIS_SMF_SETDYNAMICMSG(MODIS_W_GENERIC,'GMAR failed',
     &   'ReadCldMsk_MOD05')
         error_flag = .true.
      END IF

      IF (.not.error_flag) THEN

C Set size of output data.  Note Data_Size(1) set in previous call
C to GMARDM.
         Data_Size(1) = Dim_Size(2)
         Data_Size(2) = LinesPerScan
         L = -5

         Do 30 k=1,Edge(3)
         Do 40 j=1,Edge(2)

C The Cloud mask consists of 6 separate 1-byte words.
C Increment memory buffer index by 6 for each successive pixel.
           L = L + 6

C Examine first byte of cloud mask at each pixel.
C First, find out whether cloud mask for pixel was determined.
C Zero-based bit 0 is 1 for determined, 0 for not determined.
C If cloud mask not determined, set CldMsk(j,k) to -1.
C In Version 1, LandSea_Flag takes 5 values:  0 (water), 1 coastal,
C 2 (wetland), 3 (land), and -1(invalid data marker).

           Temp1 = ibits(count(L),0,1)

           if (Temp1 .EQ. 0) then
              CldMsk(j,k) = -1
              LandSea_Flag(j,k) = -1
           else

C Go to clear/cloud confidence level bits (zero-based bits 1 and 2)
C Note: We treat the clear confidence levels of 66%, 95%, and 99% as
C all clear.  Modifications are expected if the Cloud MASK data are
```

```
C used as more than a simple switch.  Set default Cloud value to
C clear (1).  If cloud is found, re-assign Cloud value to 0.

              CldMsk(j,k) = 1
              Temp2 = ibits(count(L),1,2)
              if (Temp2 .EQ. 0) CldMsk(j,k) = 0

C Go to bits 6 and 7 to set Version 1 land/sea flag, 0 for water;
C 1 coastal, 2 wetland, 3 land.
              Temp2 = ibits(count(L),6,2)
              LandSea_Flag(j,k) = Temp2
           end if

   40     continue
   30     continue
          ReadCldMsk_MOD05 = 0
      END IF

      RETURN
      END
```

========== End Example Cloud Mask Reader ==========

This is an example MATLAB program to read the MODIS cloud mask.

```
function cloudmask = readModisCloudMask(maskFilename, byteList, area)

% function cloudmask = readModisCloudMask(maskFilename, byteList)
%
% DESCRIPTION:
% Reads the mask product information from a MODIS MOD35 HDF file
%
% REQUIRED INPUT:
%   maskFilename (string)       Name of MODIS MOD35 HDF file
%
% ---------------------------------------------------------------------
%
% OPTIONAL INPUT:
%   byteList      Byte numbers of data to return.  If this argument is
%           specified, all bits of the selected byte are
%           returned.  If this argument is not specified, ONLY
%           bits 1 & 2 of byte 1 (cloud mask probability of clear,
%           with QA) is returned.
%
%           byteList can be either an array of byte #s
%           (1 through 6) or the string 'all' to return all
%           bytes.  Note that to get the 250m cloud mask, only
%           byte 5 or 6 (not both) needs to be requested.
%
%           See list below (under "Output") for a description of the
%           bits in each byte.
%
%           For each byte requested, QA information is also read in
%           A separate QA array is not returned, instead this information
%           is incorporated into the cloud mask fields that are returned.
%           The cloud mask values corresponding to QA "not useful" or
%           "not applied" are set to -1.
%
% ---------------------------------------------------------------------
%
% OUTPUT:
%   cloudmask (struct) with contents determined by the byte
%   numbers selected in byteList:
%
%   BYTE 1
%    cloudmask.flag (bit 0)
%                   0 = Not determined
%                   1 = Determined
%          .mask (bits 1 & 2)
```

```
%                -1 = Not Useful (from QA)
%                 0 = Cloud
%                 1 = 66% Probability of clear
%                 2 = 95% Probability of clear
%                 3 = 99% Probability of clear
%          .confidenceQA (QA byte 1, bits 1,2,3)
%               0 - 7 confidence level for cloudmask.mask
%        .dayOrNight (bit 3)
%               0 = Night   1 = Day  -1 = Not Useful (from QA)
%        .sunglint (bit 4)
%               0 = Yes     1 = No   -1 = Not Useful (from QA)
%        .snowIce (bit 5)
%               0 = Yes     1 = No   -1 = Not Useful (from QA)
%        .landWater (bits 6 & 7)
%              -1 = Not Useful (from QA)
%               0 = Water
%               1 = Coastal
%               2 = Desert
%               3 = Land
%
%  BYTE 2 (0 = Yes;  1 = No; -1 = Not Applied, from QA)
%   cloudmask.bit0 (Non-cloud obstruction flag)
%        .bit1 (Thin cirrus detected, solar)
%        .bit2 (Shadow found)
%        .bit3 (Thin cirrus detected, IR)
%        .bit4 (Adjacent cloud detected -- implemented
%             post-launch to indicate cloud found within
%             surrounding 1km pixels)
%        .bit5 (Cloud Flag, IR threshold)
%        .bit6 (High cloud flag, CO2 test)
%        .bit7 (High cloud flag, 6.7 micron test)
%
%  BYTE 3 (0 = Yes;  1 = No; -1 = Not Applied, from QA)
%   cloudmask.bit0 (High cloud flag, 1.38 micron test)
%        .bit1 (High cloud flag, 3.7-12 micron test)
%        .bit2 (Cloud flag, IR temperature difference)
%        .bit3 (Cloud flag, 3.7-11 micron test)
%        .bit4 (Cloud flag, visible reflectance test)
%        .bit5 (Cloud flag, visible reflectance ratio test)
%        .bit6 (0.935/0.87 reflectance test)
%        .bit7 (3.7-3.9 micron test)
%
%  BYTE 4 (0 = Yes;  1 = No; -1 = Not Applied, from QA)
%   cloudmask.bit0 (Cloud flag, temporal consistency)
%        .bit1 (Cloud flag, spatial variability)
%        .bit2 (Final confidence confirmation test)
```

```
%          .bit3 (Cloud flag, night water spatial variability)
%          .bit4 (Suspended dust flag)
%
%   BYTES 5 & 6 250m Cloud Flag Visible Tests
%            (0 = Yes;  1 = No; -1 = Not Applied, from QA)
%     cloudmask.visibleTest250m        250m resolution array
%
%
%  24 April: removed this field, it is memory intensive and not
%          too useful so far.
%                    .sumVisibleTest250m          1km resolution, sum of all
%                              16 elements in each 1km grid
%
% ------------------------------------------------------------------
%
% Time to run this code for:   Byte 1       1 minute
%                              Bytes 1-4    1.5 minutes
%                              Bytes 5 & 6  3.3 minutes
%
% Note: With 1G of RAM, I run out of memory if I try to read all bytes at
%       once.  Instead, I read bytes 1-4, then 5-6 separately.
%
% ------------------------------------------------------------------
%
% Written By:
%   Suzanne Wetzel Seemann
%   swetzel@ssec.wisc.edu
%   April 2001
%
% update 23 April 2001 -- added QA for bytes 5 & 6
% update 24 April 2001 -- removed .sumVisibleTest250m field because it
%                    is memory intensive and not very useful so far
%
% Code History: Based on a code by Shaima Nasiri (modis_mask_read.m) that
%             reads Byte 1 of the cloud mask.
%
% RESTRICTIONS:
%   Only tested on Matlab version 5.3.1 (R11.1) - performance under
%   other versions of Matlab is unknown
%
% ------------------------------------------------------------------
%
% SAMPLE RUN STATEMENTS:
%  dataPath = '/home/swetzel/data/gomo310/';
%
%  readModisCloudMask([dataPath
```

```
'MOD35_L2.A2000310.1750.002.2000332030507.hdf'], ...
    %              [1 4]);
    % readModisCloudMask([dataPath
'MOD35_L2.A2000310.1750.002.2000332030507.hdf'], ...
    %              5);
    % readModisCloudMask([dataPath
'MOD35_L2.A2000310.1750.002.2000332030507.hdf'], ...
    %              1,'all');

    %%%%%%%%%%%%%%%%%%%%%%%%%%%%%%%%%%%%%%%%%%%%%%%%%%%%%%%%%%%%%%%%%%%%%%%%%%%%%%%
%%%%%%%%%%%%%%%%%%%%%%%%%%%%%%%%
    % Error check inputs
    %%%%%%%%%%%%%%%%%%%%%%%%%%%%%%%%%%%%%%%%%%%%%%%%%%%%%%%%%%%%%%%%%%%%%%%%%%%%%%%
%%%%%%%%%%%%%%%%%%%%%%%%%%%%%%%%
    onlyBits1and2 = 0;

    if nargin < 1
      error(['readModisCloudMask requires at least one input: maskFilename']);
    elseif nargin == 1
      byteList = 1;
      onlyBits1and2 = 1;
    elseif nargin > 1
      if ischar(byteList)
        if strcmp(byteList,'all')
            byteList = [1:6];
        else
            error(['Second input argument, byteList must either ' ...
              'be an array of integers 1-6 or the string "all"']);
        end
      else
        if any(byteList > 6) | any(byteList < 1)
            error(['Second input argument, byteList must either ' ...
              'be an array of integers 1-6 or the string "all"']);
        end
      end
    end

    % Check for valid MOD35 HDF file
    if (~exist(maskFilename,'file'))
      error(['Filename : ' maskFilename ' was not found']);
    end

    len_filename = length(maskFilename);
    if (~strcmp( maskFilename(len_filename-3:len_filename), '.hdf'))
      error(['Filename: ' maskFilename ' is not an HDF file']);
    end
```

```
%% Add byte 5 to byteList if byte 6 was given or add
%% byte 6 to byteList if byte 5 was given

 if ismember(5,byteList) & ~ismember(6,byteList)
    byteList = [byteList 6];
 elseif ~ismember(5,byteList) & ismember(6,byteList)
    byteList = [byteList 5];
 end

%% Find the largest cloud mask and QA byte number, to minimize
%% the amount of data we need to read in.

 minBytes = min(byteList);
 maxBytes = max(byteList);
 cloudMaskDataByteList = [minBytes:1:maxBytes];

%%%%%%%%%%%%%%%%%%%%%%%%%%%%%%%%%%%%%%%%%%%%%%%%%%%%%%%%%%%%%%%%%%%%%%%%%%%%%%%%%%
% Open cloud mask file and read data, dimensions, and attributes
%%%%%%%%%%%%%%%%%%%%%%%%%%%%%%%%%%%%%%%%%%%%%%%%%%%%%%%%%%%%%%%%%%%%%%%%%%%%%%%%%%
SD_id = hdfsd( 'start', maskFilename, 'read' );
if (SD_id < 0)
  error(['HDF file' maskFilename ' was not opened.']);
end

% data we want is 'Cloud_Mask'
mask_ex = hdfsd('nametoindex', SD_id, 'Cloud_Mask');
mask_id = hdfsd('select',SD_id, mask_ex);
[name,rank,dimsizes,data_type,nattrs,status(1)] = hdfsd('getinfo',mask_id );

nbytes = dimsizes(1);
npixels_across =  dimsizes(2);
npixels_along = dimsizes(3);

start = [minBytes-1; 0 ; 0];
count = [1 ; 1 ; 1];
edge = [1 ; npixels_across ;  npixels_along];


if (nargin == 3)
  start(2) = min( [max([area(1) 0]) (npixels_across - 1)] );
  start(3) = min( [max([area(2) 0]) (npixels_along - 1)] );
  edge(2) = min( [max([area(3) 0]) (npixels_across - start(2))] );
  edge(3) = min( [max([area(4) 0]) (npixels_along - start(3))] );
```

```
end

% if maxBytes <= nbytes
%   edge = [maxBytes-minBytes+1; npixels_along; npixels_across];
% else
%   error(['maxBytes cannot be greater than the number of bytes in the file']);
% end

[cloudMaskData,status(2)] = hdfsd('readdata',mask_id,start,count,edge);
cloudMaskData  = double(cloudMaskData);
attr_ex = hdfsd('findattr', mask_id, 'scale_factor');
[scale, status(3)] = hdfsd('readattr', mask_id,attr_ex) ;

attr_ex = hdfsd('findattr', mask_id, 'long_name');
[longname, status(4)] = hdfsd('readattr', mask_id,attr_ex) ;

attr_ex = hdfsd('findattr', mask_id, 'Cell_Along_Swath_Sampling');
[sampling, status(5)] = hdfsd('readattr', mask_id,attr_ex) ;

attr_ex = hdfsd('findattr', mask_id, 'add_offset');
[offset, status(6)] = hdfsd('readattr', mask_id,attr_ex) ;
if offset ~= 0 | scale ~= 1
  error(['Cloud_Mask offset ~= 0 or slope ~= 1']);
end

% stop accessing data
status(7) = hdfsd('endaccess',mask_id);

if any(status == -1)
  error('Trouble reading Cloud_Mask data, dimensions, or attributes');
end

clear status

% close HDF file
status = hdfsd('end', SD_id);
if (status < 0)
  warning(['HDF file' maskFilename ' was not closed.']);
end

%%%%%%%%%%%%%%%%%%%%%%%%%%%%%%%%%%%%%%%%%%%%%%%%%%%%%%%%%%%%%%%%%%%%%%%%%%%%%%%%%%%%%%%%%%%%%%%%%%%%%%%%%%%%%%%%%%%%%%%%%%%%%%%%%%%%%%%%%%%%%%%%%%%%%%%%%%%%%%%%%%
%% Read all bits from the selected bytes
%%%%%%%%%%%%%%%%%%%%%%%%%%%%%%%%%%%%%%%%%%%%%%%%%%%%%%%%%%%%%%%%%%%%%%%%%%%%%%%%%%%%%%%%%%%%%%%%%%%%%%%%%%%%%%%%%%%%%%%%%%%%%%%%%%%%%%%%%%%%%%%%%%%%%%%%%%%%%%%%%%
```

```
%% For each byte, before reading the bits, we must separate
%% the bytes and adjust image array for use in Matlab :
%%        convert values to double precision
%%        rotate and flip the image
%%        convert from MOD35's signed integers to Matlab's unsigned
%%        integers where [0:127 -128:-1] is mapped to [0:1:255]

 clear cloudmask
 cloudmask.filename = maskFilename;


%%%%%%%%%%%%%%%%%%%%%%%%%%%%%%%%%%%%%%%%%%%%%%%%%%%%%%%%%%%%%%
%%%%%%%%%%%%%%%%%%%%%%%%%%%%%%%%%%%%%%%%%%%%%%%%%%%%%%%%%%
    %% Cloud_Mask: BYTE 1

%%%%%%%%%%%%%%%%%%%%%%%%%%%%%%%%%%%%%%%%%%%%%%%%%%%%%%%%%%%%%%
%%%%%%%%%%%%%%%%%%%%%%%%%%%%%%%%%%%%%%%%%%%%%%%%%%%%%%%%%%
    if any(byteList == 1)

      byteInd = find(1 == cloudMaskDataByteList);
      byte1 = flipud(rot90(squeeze(cloudMaskData(:,:,byteInd)) ));
      % find negative integers and remap them
      ind = find(byte1 < 0);
      byte1(ind) = 256 + byte1(ind);
      clear ind

      %% BITS 1,2 - Unobstructed FOV Quality Flag
      %%   0 = Cloud
      %%   1 = 66% Probability of clear
      %%   2 = 95% Probability of clear
      %%   3 = 99% Probability of clear

      bit3 = bitget(byte1,3);
      bit2 = bitget(byte1, 2);
      clear99prob_ind = find(bit3 & bit2);
      clear95prob_ind = find(bit3 & ~bit2);
      clear66prob_ind = find(~bit3 & bit2);
      cloud_ind = find(~bit3 & ~bit2);

      cloudmask.byte1.mask = NaN * ones(size(byte1));
      cloudmask.byte1.mask(clear99prob_ind) = 3;
      cloudmask.byte1.mask(clear95prob_ind) = 2;
      cloudmask.byte1.mask(clear66prob_ind) = 1;
      cloudmask.byte1.mask(cloud_ind) = 0;

      clear bit3 bit2 clear99prob_ind clear95prob_ind clear66prob_ind cloud_ind
```

```
      if onlyBits1and2 == 0
        %% BIT 0 - CloudMask Flag
        %%   0 = Not determined
        %%   1 = Determined
        cloudmask.byte1.flag = bitget(byte1, 1);

        %% BIT 3 - Day or Night Path
        %%   0 = Night   1 = Day
        cloudmask.byte1.dayOrNight = bitget(byte1,4);

        %% BIT 4 - Sunglint Path
        %%   0 = Yes     1 = No
        cloudmask.byte1.sunglint = bitget(byte1,5);

        %% BIT 5 - Snow/Ice Background Path
        %%   0 = Yes     1 = No
        cloudmask.byte1.snowIce = bitget(byte1,6);

        %% BITS 6,7 - Land or Water Path
        %%   0 = Water
        %%   1 = Coastal
        %%   2 = Desert
        %%   3 = Land
        cloudmask.byte1.landWater = NaN * ones(size(byte1));

        bit7 = bitget(byte1,7); bit8 = bitget(byte1,8);
        land_ind  = find(bit8 & bit7);
        desert_ind = find(bit8 & ~bit7);
        coastal_ind = find(~bit8 & bit7);
        water_ind = find(~bit8 & ~bit7);

        cloudmask.byte1.landWater(land_ind) = 3;
        cloudmask.byte1.landWater(desert_ind) = 2;
        cloudmask.byte1.landWater(coastal_ind) = 1;
        cloudmask.byte1.landWater(water_ind) = 0;

        clear bit7 bit8 land_ind desert_ind coastal_ind water_ind
      end
      clear byte1
    end % byte 1


%%%%%%%%%%%%%%%%%%%%%%%%%%%%%%%%%%%%%%%%%%%%%%%%%%%%%%%%%%%%%%%%%%%%%%%%%%%%%%%%
%%%%%%%%%%%%%%%%%%%%%%%%%
    %% Cloud_Mask: BYTES 2-4
```

```
    %%  0 = Yes    1 = No

%%%%%%%%%%%%%%%%%%%%%%%%%%%%%%%%%%%%%%%%%%%%
%%%%%%%%%%%%%%%

    if any(byteList == 2 | byteList == 3 | byteList == 4)
      indBytes234 = find(byteList == 2 | byteList == 3 | byteList == 4);
      for j = 1:length(indBytes234)

        byteInd = find(byteList(indBytes234(j)) == cloudMaskDataByteList);
        byteData = flipud(rot90(squeeze(cloudMaskData(:,:,byteInd)) ));
      clear byteInd

        % find negative integers and remap them
        ind = find(byteData < 0);
        byteData(ind) = 256 + byteData(ind);
        clear ind

        if byteList(indBytes234(j)) < 4
          %% 8 bits (0-7) in bytes 2 and 3
          numBits = 8;
        else
          %% 5 bits (0-4) in byte 4
          numBits = 5;
        end

        % assign data to cloudmask structure: cloudmask.byte#.bit#
        for k = 1:numBits
          eval(['cloudmask.byte' num2str(byteList(indBytes234(j))) ...
            '.bit' num2str(k-1) ' = bitget(byteData,k);']);
        end
        clear byteData

      end %% for
    end  %% bytes 2, 3, 4


%%%%%%%%%%%%%%%%%%%%%%%%%%%%%%%%%%%%%%%%%%%%
%%%%%%%%%%%%%%%
    %% Cloud_Mask: BYTES 5 & 6: 250-m Cloud Flag, Visible Tests
    %%  0 = Yes    1 = No

%%%%%%%%%%%%%%%%%%%%%%%%%%%%%%%%%%%%%%%%%%%%
%%%%%%%%%%%%%%%
    if any(byteList == 5) | any(byteList == 6)
```

```
%% BYTE 5

  byteInd = find(5 == cloudMaskDataByteList);
  byte5 = flipud(rot90(squeeze(cloudMaskData(:,:,byteInd)) ));
  clear byteInd

  % find negative integers and remap them
  ind = find(byte5 < 0);
  byte5(ind) = 256 + byte5(ind);
  clear ind

  %% create an array of all NaNs 4x the size of one element
  %% repmat is faster than ones*NaN
  elementSize = size(bitget(byte5,1));
  cloudmask.visibleTest250m = repmat(0,elementSize*4);

  xStartInds = [1 1 1 1 2 2 2 2];
  yStartInds = [1 2 3 4 1 2 3 4];

  %% insert each element into the array of NaNs.
  for j = 1:8
    %allbits(j,:,:) = bitget(byte5,j);
    cloudmask.visibleTest250m([xStartInds(j):4:elementSize(1)*4], ...
            [yStartInds(j):4:elementSize(2)*4]) = bitget(byte5,j);
  end

  clear byte5

%% BYTE 6

  byteInd = find(6 == cloudMaskDataByteList);
  byte6 = flipud(rot90(squeeze(cloudMaskData(:,:,byteInd)) ));
  clear byteInd

  % find negative integers and remap them
  ind = find(byte6 < 0);
  byte6(ind) = 256 + byte6(ind);
  clear ind

  byte6bits = [9:16];
  xStartInds = [3 3 3 3 4 4 4 4];
  yStartInds = [1 2 3 4 1 2 3 4];

  %% insert each element into the array of NaNs.
  for j = 1:8
    %allbits(byte6bits(j),:,:) = bitget(byte6,j);
```

```
        cloudmask.visibleTest250m([xStartInds(j):4:elementSize(1)*4], ...
            [yStartInds(j):4:elementSize(2)*4]) = bitget(byte6,j);

      end
      clear byte6

      %cloudmask.sumVisibleTest250m = squeeze(sum(allbits,1));

    end  %% byte 5,6

    clear cloudMaskData

  %%%%%%%%%%%%%%%%%%%%%%%%%%%%%%%%%%%%%%%%%%%%%%%%%%%
%%%%%%%%%%%%%%%%%%%%%%%%%%%
  % QA: Open cloud mask file and read QA data, dimensions, and attributes
  %
  % NOTE: It is repetitive to do QA separately after all of the 'Cloud_Mask'
  %       data, however it would take too much memory to keep
  %       'Quality_Assurance' and 'Cloud_Mask' (qaData and cloudMaskData)
  %       arrays around simultaneously
  %%%%%%%%%%%%%%%%%%%%%%%%%%%%%%%%%%%%%%%%%%%%%%%%%%%
%%%%%%%%%%%%%%%%%%%%%%%%%%%

  SD_id = hdfsd( 'start', maskFilename, 'read' );
  if (SD_id < 0)
    error(['HDF file' maskFilename ' was not opened.']);
  end

  % data we want is 'Quality_Assurance'
  mask_ex = hdfsd('nametoindex', SD_id, 'Quality_Assurance');
  mask_id = hdfsd('select',SD_id, mask_ex);
  [name,rank,dimsizes,data_type,nattrs,status(1)] = hdfsd('getinfo',mask_id );

  % npixels_along = dimsizes(1);
  % npixels_across = dimsizes(2);
  % nbytes = dimsizes(3);
   start = [0 ; 0 ; minBytes-1];
   count = [1 ; 1 ; 1];
  %
  % if maxBytes <= nbytes
  %   edge = [npixels_along; npixels_across; maxBytes-minBytes+1];
  % else
  %   error(['maxBytes cannot be greater than the number of bytes in the file']);
  % end

  edge = [npixels_across ;  npixels_along; maxBytes-minBytes+1];
```

```
if (nargin == 3)
   start(1) = min( [max([area(1) 0]) (npixels_across - 1)] );
   start(2) = min( [max([area(2) 0]) (npixels_along - 1)] );
   edge(1) = min( [max([area(3) 0]) (npixels_across - start(2))] );
   edge(2) = min( [max([area(4) 0]) (npixels_along - start(3))] );
end

 [qaData,status(2)] = hdfsd('readdata',mask_id,start,count,edge);

 qaData  = double(qaData);

 attr_ex = hdfsd('findattr', mask_id, 'scale_factor');
 [qascale, status(3)] = hdfsd('readattr', mask_id,attr_ex) ;

 attr_ex = hdfsd('findattr', mask_id, 'long_name');
 [qalongname, status(4)] = hdfsd('readattr', mask_id,attr_ex) ;

 attr_ex = hdfsd('findattr', mask_id, 'Cell_Along_Swath_Sampling');
 [qasampling, status(5)] = hdfsd('readattr', mask_id,attr_ex) ;

 attr_ex = hdfsd('findattr', mask_id, 'add_offset');
 [qaoffset, status(6)] = hdfsd('readattr', mask_id,attr_ex) ;
 if qaoffset ~= 0 | qascale ~= 1
   error(['Quality_Assurance offset ~= 0 or slope ~= 1']);
 end

% stop accessing data
 status(7) = hdfsd('endaccess',mask_id);

 if any(status == -1)
  error('Trouble reading Quality_Assurance data, dimensions, or attributes');
 end

 clear status

% close HDF file
 status = hdfsd('end', SD_id);
 if (status < 0)
   warning(['HDF file' maskFilename ' was not closed.']);
 end

 if any(byteList == 1)

%%%%%%%%%%%%%%%%%%%%%%%%%%%%%%%%%%%%%%%%%%%%%%%
```

```
%%%%%%%%
        %% 'Quality_Assurance': BYTE 1

%%%%%%%%%%%%%%%%%%%%%%%%%%%%%%%%%%%%%%%%%%%%%%%%%%%%%%
%%%%%%%%
        byteInd = find(1 == cloudMaskDataByteList);
        qabyte1 = flipud(rot90(squeeze(qaData(byteInd,:,:)) ));
        % find negative integers and remap them
        ind = find(qabyte1 < 0);
        qabyte1(ind) = 256 + qabyte1(ind);
        clear ind

        %% BIT 0 - Cloud Mask QA
        %% 0 = not useful    1 = useful
        %% Assign all not useful values to -1 byte1 fields
        notUsefulInds = find(~bitget(qabyte1,1));
        cloudmask.byte1.mask(notUsefulInds) = -1;

        if onlyBits1and2 == 0
          cloudmask.byte1.dayOrNight(notUsefulInds) = -1;
          cloudmask.byte1.sunglint(notUsefulInds) = -1;
          cloudmask.byte1.snowIce(notUsefulInds) = -1;
          cloudmask.byte1.landWater(notUsefulInds) = -1;

          %% BITS 1,2,3 - Cloud Mask Confidence
          bit2 = bitget(qabyte1,2);
          bit3 = bitget(qabyte1,3);
          bit4 = bitget(qabyte1,4);
          ind0 = find(~bit4 & ~bit3 & ~bit2);
          ind1 = find(~bit4 & ~bit3 & bit2);
          ind2 = find(~bit4 & bit3 & ~bit2);
          ind3 = find(~bit4 & bit3  & bit2);
          ind4 = find(bit4 & ~bit3 & ~bit2);
          ind5 = find(bit4 & ~bit3 & bit2);
          ind6 = find(bit4 & bit3 & ~bit2);
          ind7 = find(bit4 & bit3 & bit2);
          clear bit2 bit3 bit4

          cloudmask.byte1.confidenceQA = NaN * ones(size(qabyte1));
          cloudmask.byte1.confidenceQA(ind0) = 0;
          cloudmask.byte1.confidenceQA(ind1) = 1;
          cloudmask.byte1.confidenceQA(ind2) = 2;
          cloudmask.byte1.confidenceQA(ind3) = 3;
          cloudmask.byte1.confidenceQA(ind4) = 4;
          cloudmask.byte1.confidenceQA(ind5) = 5;
          cloudmask.byte1.confidenceQA(ind6) = 6;
```

```
      cloudmask.byte1.confidenceQA(ind7) = 7;

      clear ind0 ind1 ind2 ind3 ind4 ind5 ind6 ind7
    end
    clear qabyte1 notUsefulInds

  end  %% qa byte 1

  if any(byteList == 2 | byteList == 3 | byteList == 4)

%%%%%%%%%%%%%%%%%%%%%%%%%%%%%%%%%%%%%%%%%%%%%%%%%%%%%%%%%
%%%%%%%%
    %% Quality_Assurance: BYTES 2-4
    %%
    %% 0 = Not Applied   1 = Applied

%%%%%%%%%%%%%%%%%%%%%%%%%%%%%%%%%%%%%%%%%%%%%%%%%%%%%%%%%
%%%%%%%%

    indBytes234 = find(byteList == 2 | byteList == 3 | byteList == 4);
    for j = 1:length(indBytes234)

      qaByteInd = find(byteList(indBytes234(j)) == cloudMaskDataByteList);
      qaByteData = flipud(rot90(squeeze(qaData(qaByteInd,:,:)) ));
    clear qaByteInd

      % find negative integers and remap them
      ind = find(qaByteData < 0);
      qaByteData(ind) = 256 + qaByteData(ind);
      clear ind

      if byteList(indBytes234(j)) < 4
        %% 8 qa bits (0-7) in qa bytes 2 and 3
        numBits = 8;
      else
        %% 5 qa bits (0-4) in qa byte 4
        numBits = 5;
      end

      %% For QA "not applied", set corresponding value in
      %% cloudmask.byte#.bit# to -1
      for k = 1:numBits
        eval(['cloudmask.byte' num2str(byteList(indBytes234(j))) ...
          '.bit' num2str(k-1) '(find(~bitget(qaByteData,k))) = -1;']);
      end % for k
```

```
        clear qaByteData

      end %% for j
    end  %% bytes 2, 3, 4

%%%%%%%%%%%%%%%%%%%%%%%%%%%%%%%%%%%%%%%%%%%%%%%%%%%%%%%%%%%%%%%%%%%%%%%%%%%%%%%%%%%%%%%%%%%%%%%%%%%%%%%%%%%%%%%%
%%%%%%%%%%%%%%%%%%%%%%%%%%%%
    %% Quality_Assurance: BYTES 5 & 6: 250-m Cloud Flag, Visible Tests
    %%   0 = Not Applied     1 = Applied

%%%%%%%%%%%%%%%%%%%%%%%%%%%%%%%%%%%%%%%%%%%%%%%%%%%%%%%%%%%%%%%%%%%%%%%%%%%%%%%%%%%%%%%%%%%%%%%%%%%%%%%%%%%%%%%%
%%%%%%%%%%%%%%%%%%%%%%%%%%%%
    if any(byteList == 5) | any(byteList == 6)

    save tempCMdata
    keep2 cloudMaskDataByteList qaData
    clear cloudmask

    %% BYTE 5

     qaByteInd = find(5 == cloudMaskDataByteList);
     qaByteData = flipud(rot90(squeeze(qaData(qaByteInd,:,:)) ));
     clear qaByteInd

     % find negative integers and remap them
     ind = find(qaByteData < 0);
     qaByteData(ind) = 256 + qaByteData(ind);
     clear ind

     %% create an array of all NaNs 4x the size of one element
     %% repmat is faster than ones*NaN
     elementSize = size(bitget(qaByteData,1));
     temporaryQA = repmat(0,elementSize*4);

     xStartInds = [1 1 1 1 2 2 2 2];
     yStartInds = [1 2 3 4 1 2 3 4];

     %% insert each element into the array of NaNs.
     for j = 1:8
       temporaryQA([xStartInds(j):4:elementSize(1)*4], ...
                [yStartInds(j):4:elementSize(2)*4]) = bitget(qaByteData,j);
     end

     clear qaByteData
```

```
%% BYTE 6

  qaByteInd = find(6 == cloudMaskDataByteList);
  qaByteData = flipud(rot90(squeeze(qaData(qaByteInd,:,:)) ));
  clear qaByteInd

  % find negative integers and remap them
  ind = find(qaByteData < 0);
  qaByteData(ind) = 256 + qaByteData(ind);
  clear ind

  xStartInds = [3 3 3 3 4 4 4 4];
  yStartInds = [1 2 3 4 1 2 3 4];

  %% insert each element into the array of NaNs.
  for j = 1:8
    temporaryQA([xStartInds(j):4:elementSize(1)*4], ...
          [yStartInds(j):4:elementSize(2)*4]) = bitget(qaByteData,j);
  end

  clear qaByteData qaData

  notAppliedInds = find(~temporaryQA);

  load tempCMdata
  cloudmask.visibleTest250m(notAppliedInds) = -1;

  clear notAppliedInds temporaryQA

end  %% byte 5,6
```

Appendix B. Acronyms

ACARS	ARINC (Aeronautical Radio Inc.) Communications, Addressing and Reporting System
AERI	Atmospheric Emitted Radiation Interferometer
AEROCE	Aerosol/Ocean Chemistry Experiment
AERONET	Aerosol Robotic Network
AirMISR	Airborne MISR
AIRS	Atmospheric Infrared Sounder
AMSU	Advanced Microwave Sounding Unit
APOLLO	AVHRR (Advanced Very High Resolution Radiometer) Processing scheme Over cLoud Land and Ocean
ARM	Atmospheric Radiation Measurement Program
ARMCAS	Arctic Radiation Measurements in Column Atmosphere-surface System (Beaufort Sea, Alaska, June 1995)
ASTEX	Atlantic Stratocumulus Transition Experiment (Azores, June 1992)
ASTER	Advanced Spaceborne Thermal Emission and Reflection radiometer
AVHRR	Advanced Very High Resolution Radiometer
AVIRIS	Airborne Visible/Infrared Imaging Spectrometer
BRDF	Bi-directional Reflectance Distribution Function
CAR	Cloud Absorption Radiometer
CART	Clouds and Radiation Testbed
CEPEX	Central Equatorial Pacific Experiment (Fiji, February-March 1993)
CERES	Clouds and the Earth's Radiant Energy System
CHAPS	Collocated HIRS/2 and AVHRR Processing Scheme
CLAVR	Cloud Advanced Very High Resolution Radiometer
CLS	Cloud Lidar System
COARE	Coupled Ocean-Atmosphere Response Experiment

DAO	Data Assimilation Office (Goddard Space Flight Center)
EOS	Earth Observing System
EOSDIS	EOS Data and Information System
FIRE	First ISCCP Regional Experiment (California, June-July 1987, Beaufort Sea, Alaska, April-June, August 1998)
FOV	Field of View
GAC	Global Area Coverage
GLAS	Geoscience Laser Altimeter System
GLI	Global Imager
GOES	Geostationary Operational Environmental Satellite
HIS	High-spectral resolution Interferometer Sounder
HIRS	High Resolution Infrared Radiation Sounder
HSB	Humidity Sounder from Brazil
ILAS	Improved Limb Atmospheric Spectrometer
ISCCP	International Satellite Cloud Climatology Project
LASE	Lidar Atmospheric Sensing Experiment
LBA	Large Scale Biosphere-Atmosphere Experiment in Amazonia
M-AERI	Marine-Atmospheric Emitted Radiation Interferometer
MAS	MODIS Airborne Simulator
MAST	Monterey Area Ship Tracks Experiment (Monterey and nearby Pacific Ocean, June 1994)
McIDAS	Man-computer Interactive Data Access System
MISR	Multi-angle Imaging Spectro-Radiometer
MOBY	Marine Optical Buoy
MODIS	Moderate Resolution Imaging Spectroradiometer
NAST	NPOESS Aircraft Sounding Testbed
NCAR	National Center for Atmospheric Research

NDSI	Normalized Difference Snow Index
NDVI	Normalized Difference Vegetation Index
NPOESS	National Polar Orbiting Environmental Satellite System
NSA	North Slope of Alaska
POLDER	Polarization and Directionality of Earth's Reflectances
RAMS	Radiation Measurement System (NASA Ames Research Center and Scripps Institution of Oceanography)
SCAR-A	Sulfate, Clouds and Radiation–Atlantic (Delmarva Peninsula and near-by Atlantic Ocean, July 1993)
SCAR-B	Smoke, Clouds and Radiation–Brazil (Brazil, August-September 1995)
SCAR-C	Smoke, Clouds and Radiation–California (Pacific Northwest, September 1994)
SCF	Science Computing Facility
SeaWiFS	Sea-viewing Wide Field-of-view Sensor
SGP	Southern Great Plains
SHEBA	Surface Heat Budget of the Arctic Ocean
SSFR	Spectral Solar Flux Radiometer (NASA Ames Research Center)
SST	Sea Surface Temperature
SUCCESS	Subsonic Aircraft Contrail and Cloud Effects Special Study (April-May 1996)
TARFOX	Tropospheric Aerosol Radiative Forcing Observational Experiment (Delmarva Peninsula and near-by Atlantic Ocean, July 1996)
TIROS	Television and Infrared Observation Satellite
TLCF	Team Leader Computing Facility
TM	Thematic Mapper
TOGA	Tropical Ocean Global Atmosphere
TOMS	Total Ozone Mapping Spectrometer
TOVS	TIROS-N Operational Vertical Sounder

WINCE	Winter Cloud Experiment
WMO	World Meteorological Organization